REPORT DOCUMENTATION PAGE

AFRL-SR-BL-TR-00-

0296

1. AGENCY USE ONLY *(Leave blank)*	2. REPORT DATE	3. REPORT TYPE AND DATES COVERED
		Final - January 1, 1998 - 30 November 1998

4. TITLE AND SUBTITLE
Effects of the Mutation on Circadian Organization

5. FUNDING NUMBERS
F49620-98-1-0174

6. AUTHOR(S)
Dr. Michael Menaker
Department of Biology

7. PERFORMING ORGANIZATION NAME(S) AND ADDRESS(ES)
University of Virginia
Charlottesville, VA 22903

8. PERFORMING ORGANIZATION REPORT NUMBER

9. SPONSORING/MONITORING AGENCY NAME(S) AND ADDRESS(ES)
AFOSR/NL
801 North Randolph Street
Arlington, VA 22203-1977

10. SPONSORING/MONITORING AGENCY REPORT NUMBER

11. SUPPLEMENTARY NOTES

12a. DISTRIBUTION AVAILABILITY STATEMENT
APPROVED FOR PUBLIC RELEASE: DISTRIBUTION UNLIMITED

12b. DISTRIBUTION CODE

13. ABSTRACT *(Maximum 200 words)*

As a consequence of the abbreviated grant period (11 months), we did not make as much progress as we anticipated in our original 3-year proposal. We finished and published a study on c-fos expression in the SCN of tau mutant hamsters. We demonstrated a correlation between phase-shifting and Fos induction thresholds under conditions where both responses are dramatically altered by the previous light history, suggesting a casual association between changes in behavioral phase shifting and c-fos in the SCN. We finished and published a lengthy study of multiunit electrical activity (MUA) rhythms recorded from the SCN and other brain areas of awake, behaving hamsters. Ths study was something of a technical tour-de-force. There are only one or two others like it in the circadian literature. We modeled the pacemaker system of the tau mutant hamster using computer simulation. These simulations led to two primary conjectures: (1) the total amplitude of the pacemaker system in tau mutant hamsters is less than in wild type animals, and (2) the coupling between the unit E and M oscillators is weakened during continuous exposure of hamsters to DD.

14. SUBJECT TERMS	15. NUMBER OF PAGES
Circadian, mutation	36
	16. PRICE CODE

17. SECURITY CLASSIFICATION OF REPORT	18. SECURITY CLASSIFICATION OF THIS PAGE	19. SECURITY CLASSIFICATION OF ABSTRACT	20. LIMITATION OF ABSTRACT
Unclas	Unclas	Unclas	

FINAL TECHNICAL REPORT

January 1, 1998-November 30, 1998

EFFECTS OF THE *TAU* MUTATION ON CIRCADIAN ORGANIZATION

AFOSR GRANT F49620-98-1-0174

Principal Investigator: Michael Menaker
Department of Biology
Gilmer Hall
University of Virginia
Charlottesville, VA 22903

REPORT DOCUMENTATION PAGE

AFRL-SR-BL-TR-00-

0296

1. AGENCY USE ONLY *(Leave blank)*	2. REPORT DATE	3. REPORT TYPE AND DATES COVERED
		Final - January 1, 1998 - 30 November 1998

4. TITLE AND SUBTITLE
Effects of the Mutation on Circadian Organization

5. FUNDING NUMBERS
F49620-98-1-0174

6. AUTHOR(S)
Dr. Michael Menaker
Department of Biology

7. PERFORMING ORGANIZATION NAME(S) AND ADDRESS(ES)
University of Virginia
Charlottesville, VA 22903

8. PERFORMING ORGANIZATION REPORT NUMBER

9. SPONSORING/MONITORING AGENCY NAME(S) AND ADDRESS(ES)
AFOSR/NL
801 North Randolph Street
Arlington, VA 22203-1977

10. SPONSORING/MONITORING AGENCY REPORT NUMBER

11. SUPPLEMENTARY NOTES

12a. DISTRIBUTION AVAILABILITY STATEMENT
APPROVED FOR PUBLIC RELEASE: DISTRIBUTION UNLIMITED

12b. DISTRIBUTION CODE

13. ABSTRACT *(Maximum 200 words)*

As a consequence of the abbreviated grant period (11 months), we did not make as much progress as we anticipated in our original 3-year proposal. We finished and published a study on c-fos expression in the SCN of tau mutant hamsters. We demonstrated a correlation between phase-shifting and Fos induction thresholds under conditions where both responses are dramatically altered by the previous light history, suggesting a casual association between changes in behavioral phase shifting and c-fos in the SCN. We finished and published a lengthy study of multiunit electrical activity (MUA) rhythms recorded from the SCN and other brain areas of awake, behaving hamsters. Ths study was something of a technical tour-de-force. There are only one or two others like it in the circadian literature. We modeled the pacemaker system of the tau mutant hamster using computer simulation. These simulations led to two primary conjectures: (1) the total amplitude of the pacemaker system in tau mutant hamsters is less than in wild type animals, and (2) the coupling between the unit E and M oscillators is weakened during continuous exposure of hamsters to DD.

14. SUBJECT TERMS	15. NUMBER OF PAGES
Circadian, mutation	36
	16. PRICE CODE

17. SECURITY CLASSIFICATION OF REPORT	18. SECURITY CLASSIFICATION OF THIS PAGE	19. SECURITY CLASSIFICATION OF ABSTRACT	20. LIMITATION OF ABSTRACT
Unclas	Unclas	Unclas	

EXECUTIVE SUMMARY

— As a consequence of the abbreviated grant period (11 months), we did not make as much progress as we anticipated in our original 3-year proposal.

● We finished and published a study on c-*fos* expression in the SCN of *tau* mutant hamsters. We demonstrated a correlation between phase-shifting and *Fos* induction thresholds under conditions where both responses are dramatically altered by the previous light history, suggesting a causal association between changes in behavioral phase shifting and c-*fos* in the SCN.

● We finished and published a lengthy study of multiunit electrical activity (MUA) rhythms recorded from the SCN and other brain areas of awake, behaving hamsters. This study was something of a technical *tour-de-force.* There are only one or two others like it in the circadian literature (none as thorough). The conclusions were as follows:

- Circadian MUA rhythms in the SCN had periods that reflected the genotype of the subject.
- Circadian MUA rhythms in most other brain areas were 180° out of phase with those in the SCN.
- Circadian MUA rhythms in the bed nucleus were in phase with those in the SCN.
- Ultradian rhythms with 2 periods were measured (80 minutes &14 minutes). In contrast to the circadian rhythms, these were not affected by the *tau* mutation.

● We modeled the pacemaker system of the *tau* mutant hamster using computer simulation. These simulations led to two primary conjectures: (1) the total amplitude of the pacemaker system in *tau* mutant hamsters is less than in wild type animals, and (2) the coupling between the unit *E* and *M* oscillators is weakened during continuous exposure of hamsters to DD.

PERSONNEL SUPPORTED

Michael Menaker, Ph.D.	Principal Investigator
Shin Yamazaki, Ph.D.	Research Associate
Naomi Ihara	Lab Specialist Advanced
Vinessa Alones	Lab Specialist Senior
Wendy Irelan	Lab Specialist
Denise Holmes	Lab Tech Senior

PUBLICATIONS

Shimomura K, Kornhauser JM, Wisor JP, Umezu T, Yamazaki S, Ihara NL, Takahashi JS and Menaker M (1998) Circadian behavior and plasticity of light-induced *c-fos* expression in SCN of *tau* mutant hamsters. *J Biol Rhythms* **13**(4): 305-314.

Yamazaki S, Kerbeshian MC, Hocker CG, Block GD, Menaker M (1998) Rhythmic properties of the hamster suprachiasmatic nucleus *in vivo*. *J Neurosci* **18**(24): 10709-10723

Oda GA, Menaker M, Friesen WO (2000) Modeling the dual pacemaker system of the *tau* mutant hamster *J Biol Rhythms* **15**(3): 1-19.

CIRCADIAN BEHAVIOR AND *C-FOS* EXPRESSION

In hamsters homozygous for the circadian clock mutation *tau*, the photic history dramatically affects the magnitude of light-induced circadian phase shifts. The maximum amplitude of phase shifts produced by one-hour light pulses presented at circadian time 14 was less than 2 hours in animals that had been in constant darkness (DD) for 2 days, while animals that had been kept in DD for 49 days could be shifted by more than 8 hours.

In this study, we compared the effect of previous light history on the amplitude of circadian phase shifts and on c-*fos* expression in the suprachiasmatic nucleus (SCN) of *tau* mutant hamsters. Although the maximum amplitude of behavioral phase shifts was drastically different between animals that had been held for either 2 or 49 days in DD, maximal *fos* induction was not significantly different in these two groups. However, photic thresholds for light-induced behavioral phase shifts, c-*fos* mRNA, and Fos immunoreactivity were closely correlated within both groups, and these thresholds were lower (more sensitive to light) after 49 than after 2 days in DD. The correlation between phase shifting and Fos induction thresholds, under conditions where both responses are dramatically altered by the previous light history, demonstrates an association between changes in circadian behavioral phase shifting responses of *tau* mutant hamsters and plasticity of light-induced c-*fos* expression in suprachiasmatic nucleus. However, because the maximum amplitudes of Fos induction and phase shifting were not correlated in animals that had been in DD for 2 days, we speculate that the level of c-*fos* expression does not directly determine phase shift amplitude.

IN VIVO RECORDING OF RHYTHMIC MULTIUNIT ACTIVITY

We recorded multiple unit neural activity [multiunit activity (MUA)] from inside and outside of the suprachiasmatic nucleus (SCN) in freely moving male golden hamsters housed in running-wheel cages under both light./dark cycles and constant darkness. The circadian period of MUA in the SCN matched the period of locomotor activity: it was ~24 hr in wild-type and 20 hr in homozygous *tau* mutant hamsters. The peak of MUA in the SCN always occurred in the middle of the day or, in constant darkness, the subjective day. There were circadian rhythms of MUA outside of the SCN in the ventrolateral thalamic nucleus, the caudate putamen, the accumbens nucleus, the medial septum, the lateral septum, the ventromedial hypothalamic nucleus, the medial preoptic regions, and the stria medullaris. The rhythms were out of phase with the electrical rhythm in the SCN but in phase with the rhythm of locomotor activity, peaking during the night or subjective night. In addition to circadian rhythms, there were significant ultradian rhythms present; one, with a period of ~80 min, was in antiphase between the SCN and other brain areas, and another, with a period of ~14 min, was in phase between the SCN and other brain areas. The periods of these ultradian rhythms were not significantly different in wild-type and *tau* mutant hamsters. Of particular interest was the unique phase relationship between the MUA in the bed nucleus of the stria terminalis (BNST) and the SCN: in these two areas, both circadian and ultradian components were always in phase. This suggests that the BNST is strongly coupled to the SCN and may be one of its major output pathways. In addition to circadian and ultradian rhythms of MUA, neural activity both within and outside the SCN was acutely affected by locomotor activity. Whenever a hamster ran on its wheel, MUA in the SCN and the BNST was suppressed, and MUA in other areas was enhanced.

MODELING THE PACEMAKER OF THE *TAU* MUTANT HAMSTER

Circadian pacemakers in many animals are compound. In rodents, a two-oscillator model of the pacemaker comprising an evening (*E*) and a morning (*M*) oscillator has been proposed based on the phenomenon of "splitting" and bimodal activity peaks. For our computer simulations, we viewed the hamster pacemaker as a system of mutually coupled *E* and *M* oscillators. *Tau* mutant animals exhibit normal type-1 phase-response curves (PRCs) when released into DD, but make a transition to a type-0 PRC when held for many weeks in DD. The two-oscillator model describes particularly well some behavioral experiments on these hamsters. We tried to determine the relationships between oscillator amplitude, period, PRC, and activity duration through computer simulations. Two complementary approaches proved useful for analyzing weakly coupled oscillator systems. We adopted a "distinct oscillators" view when considering the component *E* and *M* oscillators and a "system" view when considering the system as a whole. For strongly coupled systems, only the system view is appropriate. The simulations lead us to two primary conjectures: (1) the total amplitude of the pacemaker system in *tau* mutant hamsters is less than in the wild-type animals, and (2) the coupling between the unit *E* and *M* oscillators is weakened during continuous exposure of hamsters to DD. As coupling strength decreases, activity duration (α) increases due to a greater phase difference between *E* and *M*. At the same time, the total amplitude of the system decreases, causing an increase in observable PRC amplitudes. Reduced coupling also increases the relative autonomy of the unit oscillators. The relatively autonomous phase shifts of *E* and *M* oscillators can account for both immediate compression and expansion of activity bands in *tau* mutant and wild-type hamsters subjected to light pulses.

Circadian Behavior and Plasticity of Light-Induced c-*fos* Expression in SCN of *tau* Mutant Hamsters

Kazuhiro Shimomura[*,†] Jon M. Kornhauser,[†,§] Jonathan P. Wisor,[†,#] Toyoshi Umezu,[**]
Shin Yamazaki,[*] Naomi L. Ihara,[*] Joseph S. Takahashi,[‡] and Michael Menaker[*,1]

[*]*NSF Center for Biological Timing and Department of Biology, Gilmer Hall, University of Virginia, Charlottesville, VA 22903, USA;*
[†]*NSF Center for Biological Timing and Department of Neurobiology & Physiology, Northwestern University, Evanston, IL 60208, USA;*
[‡]*Howard Hughes Medical Institute, NSF Center for Biological Timing and Department of Neurobiology & Physiology, Northwestern University, Evanston, IL 60208, USA;*
§Current address: Division of Neuroscience, Children's Hospital, and Department of Neurobiology, Harvard Medical School, Boston, MA 02115, USA;
#Current address: Sleep Research Center, Stanford University, Palo Alto, CA 94304, USA;
***Current address: Environment Health Science Division, National Institute for Environmental Studies, Tsukuba, Ibaraki, Japan*

Abstract In hamsters homozygous for the circadian clock mutation *tau*, the photic history dramatically affects the magnitude of light-induced circadian phase shifts. The maximum amplitude of phase shifts produced by 1-h light pulses presented at CT 14 was less than 2 h in animals that had been in DD for 2 days, whereas animals that had been kept in DD for 49 days could be shifted by more than 8 h. In this study, the authors compared the effect of previous light history on the amplitude of circadian phase shifts and on c-*fos* expression in the SCN of *tau* mutant hamsters. Although the maximum amplitude of behavioral phase shifts was drastically different between animals that had been held for either 2 or 49 days in DD, maximal *fos* induction was not significantly different in these two groups. However, photic thresholds for light-induced behavioral phase shifts, c-*fos* mRNA, and Fos immunoreactivity were closely correlated within both groups, and these thresholds were lower (more sensitive to light) after 49 than after 2 days in DD. The correlation between phase shifting and Fos induction thresholds, under conditions where both responses are dramatically altered by the previous light history, demonstrates an association between changes in circadian behavioral phase-shifting responses of *tau* mutant hamsters and plasticity of light-induced c-*fos* expression in SCN. However, because the maximum amplitudes of Fos induction and phase shifting were not correlated in animals that had been in DD for 2 days, we speculate that the level of c-*fos* expression does not directly determine phase shift amplitude.

Key words c-*fos*, *tau* mutant, phase shift, light, circadian, SCN

1. To whom all correspondence should be addressed.

INTRODUCTION

A variety of evidence indicates that circadian pacemakers are located within the SCN of the hypothalamus in mammals (Moore, 1995). Entrainment of circadian rhythms by light in mammals is mediated by retinal photoreceptors that project to the SCN via a direct retinohypothalamic tract. Recent studies have shown that the proto-oncogenes c-*fos* and *jun*-B are induced in the rodent SCN in response to light (Aronin et al., 1990; Earnest et al., 1990; Kornhauser et al., 1990, 1992; Rea, 1989; Rusak et al., 1990, 1992; Takeuchi et al., 1993). Fos and Jun family proteins appear to function in cellular signal transduction by coupling transient stimuli to gene regulation in the nucleus (Muller et al., 1984; Greenberg and Ziff, 1984; Lau and Nathans, 1987). The Fos protein dimerizes with Jun family proteins to form a complex, AP-1 (Lee et al., 1987; Bohmann et al., 1987; Rauscher et al., 1988; Curran and Franza, 1988; Sassone-Corsi et al., 1988), which regulates the transcription of target genes (Curran et al., 1988). Castel et al. (1997) have recently estimated that light pulses which produced saturating phase shifts of the circadian locomotor rhythm of Sabra mice induce c-*fos* expression in a heterogeneous population of SCN cells comprising about one fifth of the total number of cells in the SCN.

The characteristics of the photic induction of c-*fos* and *jun*-B in the SCN are correlated in several respects with behavioral phase-shifting responses (Kornhauser et al., 1996). First, the induction of c-*fos* and *jun*-B is limited to the retinorecipient area of the SCN. Second, the light sensitivities of the behavioral phase-shifting response and of the induction of c-*fos* mRNA are quantitatively correlated. Third, c-*fos* and *jun*-B are induced by light only during the subjective night, a time when light pulses cause phase shifts in circadian rhythms. Fourth, injection of antisense oligonucleotides into the third ventricle (which block the translation of c-*fos* and *jun*-B in the SCN) before a light pulse prevents light-induced phase delays in rats. These results suggest that the light-induced expression of these two genes may be causally involved in photic entrainment of circadian rhythms.

The circadian period mutation, *tau*, affects both the free-running period and the shape of the phase response curve in the golden hamster (Ralph and Menaker, 1988; Shimomura and Menaker, 1994). *tau* mutant hamsters regularly exhibit high-amplitude phase resetting (*type 0* resetting) (Winfree, 1980) under certain circumstances, but it is rare to find *type 0* resetting in wild type hamsters. The magnitude of light-induced phase shifts in homozygous *tau* mutant hamsters is dramatically affected by the animal's light history prior to receiving a light pulse. For example, after short durations (2 or 7 days) in DD, the phase response curve is *type 1* (maximum amplitude about 2-3 h), phase resetting does not resemble *type 0*, even in response to a bright light pulse, whereas after long durations in DD (e.g., 49 days), it becomes *type 0* (maximum amplitude about 8-10 h). Grosse et al. (1995) found that although the magnitude of phase advances produced by saturating light pulses was much larger in homozygous *tau* mutant hamsters than wild types, the number of Fos immunoreactive (IR) cells in the SCN was similar between the two genotypes. Their study suggests that Fos may not determine the amplitude of light-induced phase shifts directly.

We report here the results of experiments designed to determine whether change in circadian behavioral responses between 2 and 49 days in DD in *tau* mutant hamsters is accompanied by differences in photic sensitivity and, if so, whether the differences in both sensitivity and maximum response are correlated with c-*fos* expression in the SCN.

METHODS

Animals and Housing

Homozygous *tau* mutant hamsters were bred from homozygous parents at the University of Virginia. All animals in these experiments were raised on a 20-h LD cycle (L:D = 11.7:8.3, which has the same L:D ratio as L:D = 14:10) since birth. After weaning, they were group housed (1-3 animals per cage). At 5-12 weeks of age, they were transferred to individual cages (20 × 20 × 47 cm) equipped with running wheels (8 cm in width, 17 cm in diameter). Running-wheel cages housing single animals were kept in ventilated, light-tight boxes (six cages per box), initially under the same LD cycles in which the animals were raised. Illumination (provided by fluorescent lights) was approximately 10-40 $\mu W\ cm^{-2}$ at 15 cm above the cage bottom. Food and water were available ad libitum. Ambient temperature was approximately 21°C. Cages were changed at least every 28 days, and water bottles every 14 days, without using visible light (infrared viewer, FJW Optical Systems, Palatine, IL, USA) for hamsters held in DD. Each hamster was used only once. All

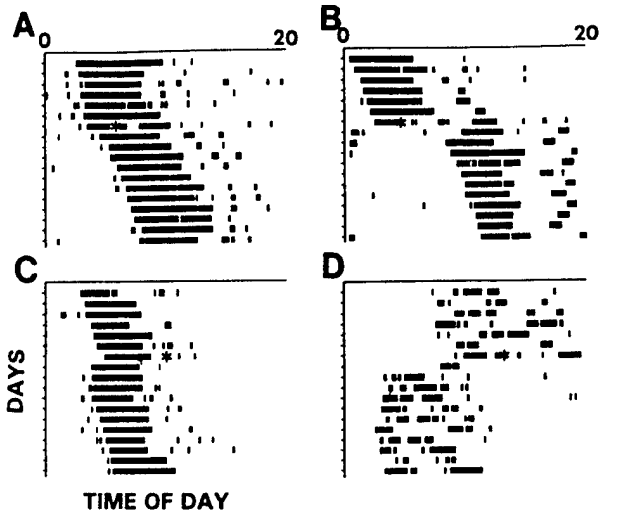

Figure 1. Locomotor activity records from homozygous *tau* mutant hamsters kept for 7 days (A & C) or 49 days (B & D) in DD. The animals whose records are shown in A and B received a light pulse of about 200 μW cm^{-2} at CT 14; those whose records are shown in C and D received the same irradiance light pulse at CT 18. The times of the light pulses are indicated by asterisks; the data are plotted on a 20-h time base, and only the 7 days before and the 14 days after the light pulse are shown.

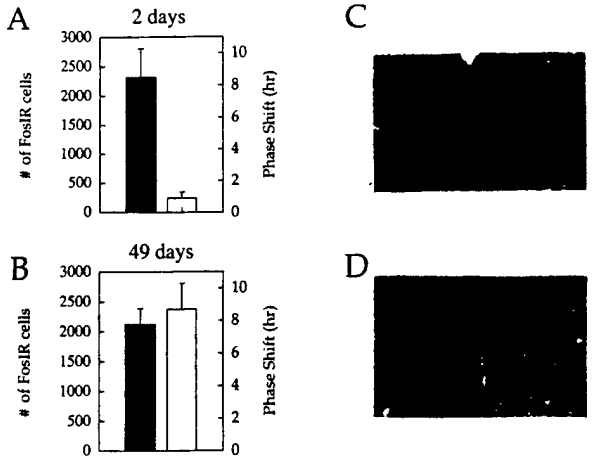

Figure 2. Relationship between magnitudes of phase shifts (open bars) and numbers of Fos immunoreactive (IR) cells in the SCN (shaded bars). Phase shifts were induced by a 60-min bright (2.0×10^2 μW cm^{-2}) light pulse in *tau* mutant hamsters after 2 days (A) or 49 days (B) in DD. Fos immunoreactivity was examined at the end of the 60-min light pulse. Each data point represents the mean ±*SEM* of 5-6 animals for phase shifts and 3-4 animals for Fos IR. Representative Fos immunostaining in the SCN is shown for animals given a light pulse after 2 days (C) or 49 days (D) in DD.

experiments were performed in accordance with the Institute of Laboratory Animal Resources guidelines set forth in the 1985 publication *Guide for the Care and Use of Laboratory Animals*.

Recording of Locomotor Activity

Wheel-running activity was recorded with micro switches activated by the wheel (using Data Quest III, Data Sciences International, St. Paul, MN, USA); activity was counted as the number of wheel revolutions per 6 min.

Photic Stimulation and Circadian Phase

Throughout this manuscript, the word "days" is used to refer to circadian cycles (whether approximately 20 h or 24 h). After at least 10 days of steady state entrainment, hamsters were released into DD. The number of days in DD was varied systematically, and a light pulse of a specific irradiance was then presented at an appropriate phase of the circadian cycle. Light bulbs were wrapped with black plastic when reduced irradiance was required. When it was necessary to give animals light stimuli of different irradiances; animals were put in small plastic cups (10 cm diameter, 20 cm height), which were moved to a light-tight box illuminated by cool white fluorescent light for 60 min; otherwise they were left in their own cages and the cages were moved into the same type of light-tight box. Light irradiance was measured 15 cm above the bottom of the cup or cage. By convention, each day of a free-running circadian rhythm is divided into 24 h of CT. Therefore, the duration of 1 circadian hour is obtained by dividing the period of the circadian rhythm of an individual animal by 24 (e.g., if the free-running period is 20 clock hours, 1 circadian hour is 50 clock minutes). In nocturnal animals, activity onset is defined as CT 12 (thus, CT 18 occurs 6 circadian hours after activity onset). The magnitude and direction (delay or advance) of phase shifts depend upon the circadian phase of stimulation. Maximum phase delays are produced by light stimuli at CT 13-15 and maximum phase advances are produced at CT 18-20 in homozygous *tau* mutant hamsters (Shimomura and Menaker, 1994). In this study, light stimuli beginning at CT 14 were used to produce phase delays and light stimuli beginning at CT 18 to produce phase advances. All light stimuli were 1 h in

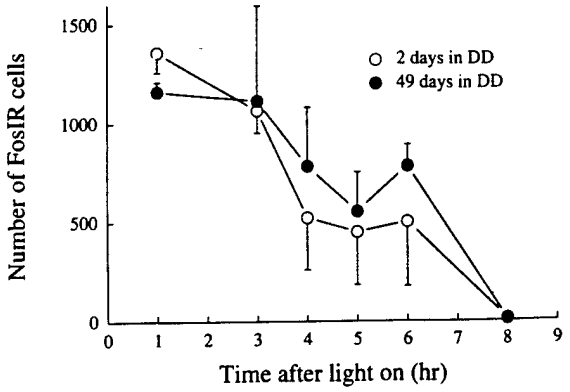

Figure 3. Time course of Fos immunoreactive (IR) in the SCN of *tau* mutant hamsters following a light pulse. Animals received a 60-min light pulse (of 2.0×10^2 μW cm^{-2} irradiance) at CT 14. Open circles represent Fos IR in animals that had been maintained for 2 days in DD, and closed circles represent animals previously kept for 49 days in DD. Each data point represents the mean ±*SEM* of the number of Fos IR cells in the SCN of three animals. The x-axis indicates time after the start of the 60-min light pulse.

duration. After light stimulation, hamsters were returned (using an infrared viewer) to DD for at least 14 days (for measurement of phase shifts) or killed in darkness (for immunocytochemistry or in situ hybridization). During this period, cages were not changed, so as to prevent phase shifts (which can be produced by cage changes) (Reebs and Mrosovsky, 1989).

Data Analysis

The magnitude of phase shifts was determined by measuring the phase difference (using activity onset as a phase reference point) between eye-fitted regression lines through 3-7 consecutive activity onset times immediately prior to the light pulse, and at least 10 consecutive activity onset times after the light pulse (excluding the four cycles immediately after the pulse). The magnitude of all phase shifts is expressed in circadian hours. Differences between two groups were evaluated by Student's *t*-test. Significant difference was defined as $p < .05$.

Immunocytochemistry

Animals were anesthetized with a lethal dose of chloroform by inhalation and then perfused intracardially, first with 20-30 ml physiological saline (0.9%) containing 150 IU heparin/10 ml, followed by 250 ml 2% formaldehyde in 0.01 M phosphate buffer saline (PBS; pH 7.4) with picric acid (15%). After perfusion, brains were removed and post fixed at 4°C. Serial coronal sections were cut at 30 μm or 50 μm using a cryostat and collected in PBS. Free-floating sections were transferred to a solution of normal goat serum (1×30^{-1} in PBS-T) for 30-60 min then directly into primary antiserum. The Fos antiserum used in this study was an anti-Fos (4-17) rabbit polyclonal antiserum purchased from Oncogene Science (Manhasset, NY, USA). The antibodies were used at a dilution of 1:2000 for 48-72 h at 4°C. The sites of antigen-antibody binding were visualized with an avidin-biotin-peroxidase procedure (Elite ABC kit, Vector Labs, Burlingame, CA, USA). Sections were washed in Tris buffer (pH 7.4) before incubation for 3 min in 0.025% diaminobenzidine (DAB) containing 0.003% peroxide. Sections mounted on gelatin-coated slides were dehydrated through graded alcohols into xylene and left overnight before being rehydrated to distilled water and immersed in 0.2% osmium tetroxide solution for 2 min to intensify the DAB reaction. Labeled cell nuclei in the ventrolateral subdivisions of SCN in six consecutive sections were counted without knowledge of the experimental conditions to which the animal had been exposed.

In Situ Hybridization

In situ hybridization was performed essentially as previously described (Kornhauser et al., 1990). Briefly, 30 min after the beginning of the light pulse, animals were killed by decapitation and their eyes were removed in darkness. Brains were quickly removed in dim red light, frozen on dry ice, and stored at –80°C until sectioning. Twenty μm-thick coronal sections were cut and mounted on gelatin/poly-L-lysine coated slides. Sections were air dried, fixed in 5% paraformaldehyde, and hybridized for 18 h at 47°C in a solution of 50% formamide, 300 mM NaCl, 10 mM Tris-HCl (pH 8.0), 1 mM EDTA, 1X Denhardt's solution, 10% dextran sulfate, 10 mM DTT, 0.5 μg ml^{-1} tRNA, 0.5 μg ml^{-1} poly(A), and 2×10^7 cpm ml-1 of ^{35}S-labeled c-*fos* riboprobe (transcribed from a full-length mouse c-*fos* cDNA clone in a pGEM-1 vector, linearized with Bgl II to produce an anti-sense template of approximately 1.8 kb in length, or with Nco I for a sense-strand template of approximately 1.1 kb). Following treatment with 20 μg ml^{-1} RNase A in 2X

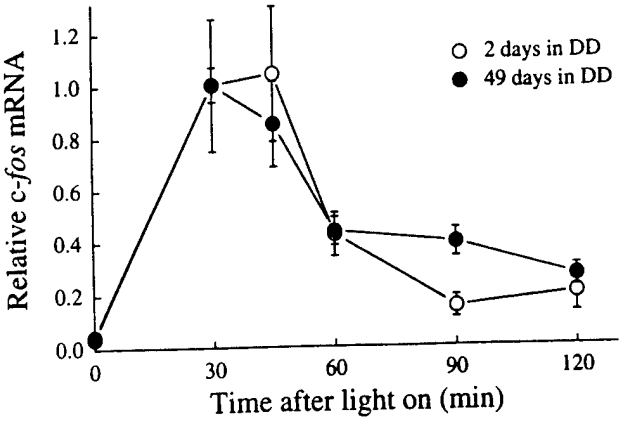

Figure 4. Time course of c-*fos* mRNA in the SCN of *tau* mutant hamsters after a light pulse. Animals received a 60-min light pulse (200 μW cm^{-2} irradiance) at CT 14. Open circles represent relative mRNA levels in animals previously maintained for 2 days in DD, and closed circles represent the levels in animals previously maintained for 49 days in DD. Each point represents the mean ±*SEM* of c-*fos* mRNA levels determined by in situ hybridization (plotted relative to the maximum value). The x-axis indicates time after the start of the 60-min light pulse.

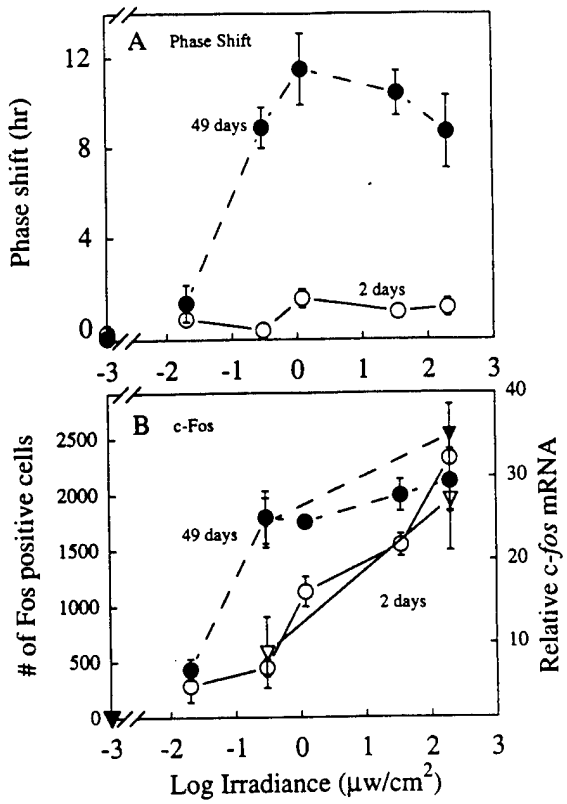

Figure 5. The magnitude of phase shift (A) and Fos induction (B) in the *tau* mutant SCN as a function of light pulse irradiance. Animals that had been previously held for either 2 or 49 days in DD received 60-min light pulses of varying irradiance at CT 14. Animals used for measuring phase shifts were kept in running wheels for 14 days in DD after the light pulse, those for immunocytochemistry were killed at the end of the 60-min light pulse, and those for in situ hybridization were killed 30 min after light onset. In panel A, open circles represent the magnitude of phase shifts after 2 days in DD and closed circles represent the magnitude of phase shifts after 49 days in DD. Each data point represents the mean ±*SEM* of 5-6 animals. In panel B, open circles represent the number of Fos immunoreactive (IR) cells in animals previously kept in DD for 2 days, closed circles represent the number of Fos IR cells in animals previously kept in DD for 49 days, open triangles represent relative c-*fos* mRNA in animals previously kept in DD for 2 days, and closed triangles represent relative c-*fos* mRNA in animals previously kept in DD for 49 days. Each data point represents the mean ±*SEM* of 3-4 animals.

SSC (Standard Saline Citrate) at 37°C for 30 min, slides were washed successively in 2X SSC, 1X SSC, 0.5X SSC, and 0.1X SSC for 30 min each at 47°C and were then dehydrated through an ethanol series. Dried slides were first exposed to X-ray film (Amersham Hyperfilm b-max), and then to autoradiographic emulsion (Kodak NTB-2) for 3 weeks. After developing, sections were stained with cresyl violet.

Quantification of specific hybridization was performed using the Image-1/AT program from Universal Imaging Corporation, as described previously (Kornhauser et al., 1990). From each brain, all intact sections containing portions of the SCN were included in our analysis. Using 100X dark-field magnification, an area of 75 × 75 μm that contained the highest silver grain density in each SCN was analyzed using an "area-brightness" measurement. To normalize each SCN measurement for variations in background, an area of equal size, 225 μm lateral to the first (outside the SCN) was also measured. We defined the difference between the measurement within the SCN and that in the lateral area as the "signal" in each section. Values representing the mean signals, in both SCNs, of all sections from one brain were then normalized by taking their ratio to those obtained from hamsters that received no light.

RESULTS

Magnitude of Phase Shift

To determine whether changes in the magnitude of behaviorally measured phase shifts are paralleled by changes in the expression of c-*fos* in the SCN of *tau*

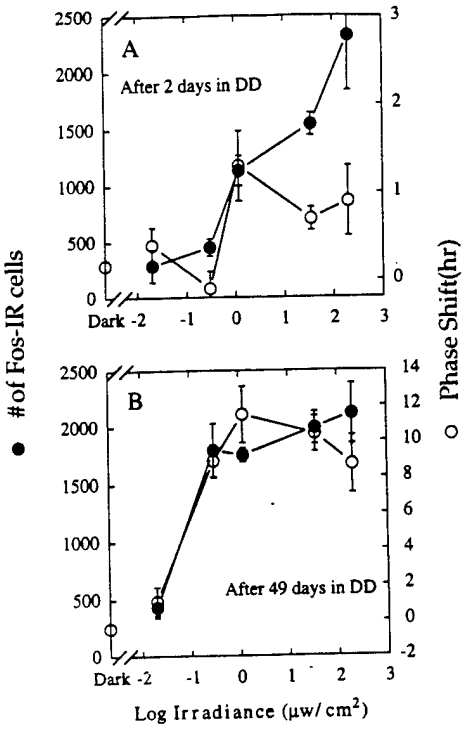

Figure 6. Fos immunoreactive (IR) in the SCN and phase shift responses plotted as a function of stimulus irradiance in animals that had been kept in DD for 2 days (A) or 49 days (B). 60-min light pulses of varying irradiance were given at CT 14, and Fos IR was determined at the end of the 60-min light period. Closed circles represent the mean ±*SEM* of numbers of Fos IR cells from 3-4 animals in each group, and open circles represent the mean (±*SEM*) amplitude of light-induced phase shifts from 5-6 animals in each group.

mutant hamsters, c-*fos* induction was examined in animals previously held for 2 days or 49 days in DD. Fig. 1 shows typical light-induced phase shifts in *tau* mutant hamsters. After 2 days in DD (Fig. 1 A,C), the magnitude of phase shifts was much smaller than after 49 days in DD (Fig. 1 B,D), at both CT 14 and CT 18. Since this difference was larger at CT 14 (Fig. 1 A vs. B), we used light pulses at CT 14 to investigate possible difference in c-*fos* expression. While the magnitude of the maximum phase shifts induced by the brightest light pulses (2.0×10^2 μW cm^{-2}) was dramatically larger after 49 days in DD than after 2 days in DD, the number of Fos IR cells in the SCN detected at 60 min after the onset of light was not significantly different between the two groups (Fig. 2). We next investigated the time course of Fos immunoreactivity to determine if there were differences in rates of synthesis or degradation between the two groups (Fig. 3). After induction by light, the decline in amount of Fos IR appeared to be slightly more gradual after 49 days than after 2 days in DD. Next we investigated the c-*fos* mRNA time course after 2 days or 49 days in DD. The mRNA time courses were essentially similar in the two groups (Fig. 4).

Threshold for Phase Shift

To determine the effect of the animal's light history on the photic thresholds for phase shifting, Fos IR, and c-*fos* mRNA induction, we gave light pulses of varying irradiance at CT 14 to animals previously held in DD for 2 or 49 days (Figs. 5 and 6). The thresholds for phase shifting (Fig. 5A) and for induction of Fos IR and c-*fos* mRNA (Fig. 5B) were both lower after 49 days than after 2 days in DD. As in the first set of experiments, while the maximum phase shift amplitude was obviously greater after 49 days in DD, the maximum number of Fos-positive cells was not significantly different.

The stimulus-response curves for phase shifting and for Fos induction are compared directly in Fig. 6, which are replotted from data in Fig. 5. After 2 days in DD, the effectiveness of light for phase shifting and for Fos induction was closely correlated for light pulses of the lowest three irradiance levels, but this correlation disappeared at the two highest irradiances because the magnitude of the phase shift response saturated at 1.2×10^0 μW cm^{-2} while the number of Fos IR-positive cells continued to increase (Fig. 6A). After 49 days in DD, the thresholds for both phase-shifting and Fos-induction responses were lower. In addition, a significant change in the relationship between the two responses was observed; as in the 2-day DD animals, the thresholds for phase shifting and Fos-IR responses were indistinguishable; however, in the 49-day DD animals (but not in the 2-day DD animals), both responses saturated at the same irradiance (3.0×10^{-1} μW cm^{-2}) and remained closely correlated at higher irradiances (cf. Fig. 6 A,B).

DISCUSSION

In *tau* mutant hamsters, the magnitude of light-induced circadian phase shifts, as well as the irradiance threshold for phase shifting, are dramatically affected by the prior light history, especially by the

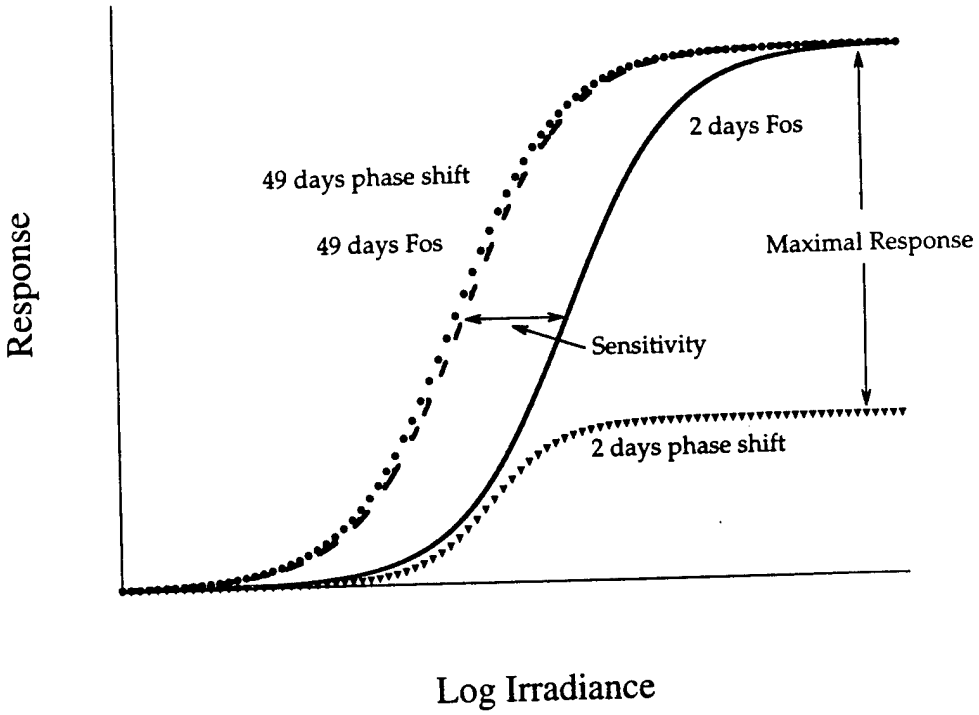

Figure 7. Diagrammatic illustration of the changes in the relationship between Fos induction and phase shift responses in hamsters held for 2 or 49 days in DD (see text for discussion).

time spent in DD (Shimomura and Menaker, 1994). In this further study of the *tau* mutant hamster light response, we found that the maximum level of Fos induction in the SCN in response to a bright light pulse was not affected by the duration of prior exposure to DD. However, the sensitivity of the light-induced expression of c-*fos* in the SCN was dependent upon the duration of prior exposure to DD. The irradiance threshold for c-*fos* induction was much lower after 49 days than after 2 days in DD. This decrease in threshold (i.e., increase in light sensitivity) for the induction of c-*fos* mRNA and Fos IR paralleled the change in threshold observed for behavioral phase shifting.

These changes in the relationship between Fos induction and phase shift responses are illustrated diagrammatically in Fig. 7. After 2 days in DD, the thresholds for phase shifts and for Fos induction are correlated, but the phase shift response reaches saturation with increasing irradiance, whereas Fos induction continues to increase up to the highest irradiance that can be produced by our experimental apparatus. After 49 days in DD, the thresholds for both responses are lower and the responses increase in parallel. However, while the maximum Fos induction is approximately the same as after 2 days in DD, the amplitudes of phase shifts are dramatically larger. Thus, with prolonged time in DD, Fos induction shows an increase in sensitivity but the same maximum response, while the phase shift response increases both in sensitivity and in maximum response.

It is not clear whether such differences in both phase shift and c-*fos* expression will be found to be general characteristics when comparing *type 1* (low amplitude) and *type 0* (high amplitude) phase resetting. There are several ways other than prolonged exposure to DD to produce *type 0* resetting in *tau* mutant hamsters. For example, *type 0* resetting can be produced by pre-entrainment to some but not other T-cycles. When animals are entrained to LD = 1:19, phase shifts of up to 10 h can be induced by light pulses at CT 14, whereas animals pre-entrained to LD = 1:18 and given identical light pulses show shifts of less than 1 h (Shimomura and Menaker, 1994). Comparison of c-*fos* induction in these two groups could be used to distinguish between direct effects of prolonged darkness and the effects of prolonged darkness on cir-

cadian organization. Because *type 0* resetting is rarely observed in wild type hamsters, it would also be informative to determine whether any circumstances exist in which the phenomena observed in this study occur in wild type hamsters (see Elliott, 1994).

The induction by light of the immediate early genes c-*fos* and *jun*-B in the SCN is closely correlated in several respects with light-induced phase shifting of behavioral circadian rhythms (for review, see Kornhauser et al., 1996). Because of this relationship, it has been proposed that transcription factors such as AP-1 (composed of Fos/JunB dimers) could play a role in transducing the light signal into changes in the expression of genes involved in the circadian timing mechanism (Kornhauser et al., 1992; Takeuchi et al., 1993). Such hypotheses should give rise to specific predictions about the relationship between Fos expression and phase shifting, testable in a variety of circumstances where the circadian system shows distinctive or atypical responses to light. In the current study, dramatic plasticity is observed in two features of the phase-shifting response—the magnitude of phase shifts and light sensitivity. Therefore, correlated changes in the magnitude and sensitivity of Fos induction can be proposed as criteria for testing the simplest possible type of causal relationship: the hypothesis that Fos induction (acting in concert with other transcription factors) results in phase shifts and also determines the magnitude of those shifts.

Our results indicate that the dramatic increase in the amplitude of phase shifts observed after prolonged exposure to DD is not paralleled by a similar increase in Fos induction. The number of Fos-positive cells does not directly correlate with the magnitude of light-induced phase shifts. This result is consistent with previous work that compared the number of Fos IR cells between wild and *tau* mutant hamsters (Grosse et al., 1995).

On the other hand, we found that even though the thresholds for induction of behavioral phase shifts and c-*fos* (both mRNA and protein) expression were lower after 49 days than after 2 days in DD, the thresholds for both responses were closely correlated under all conditions. Kornhauser et al. (1990) have reported that the thresholds for inducing behavioral phase shifting and c-*fos* mRNA are quantitatively correlated in wild type hamsters. The present study demonstrates that in *tau* mutant hamsters, the irradiance threshold for induction of both c-*fos* mRNA and Fos IR in the SCN is correlated with that for induction of phase shifts, and furthermore that this correlation is maintained when the phase-shifting threshold is changed by prior history. The thresholds for inducing behavioral phase shifts and Fos by light also change during aging in golden hamsters (Zhang et al., 1996). Young animals (~8 weeks of age) are more sensitive to light than old animals (18 months old) in both behavioral phase shifting and Fos induction by light. In that study as in the present one, even when the threshold for behavioral phase shifts is altered by the animal's history, the threshold for c-*fos* induction is changed in the same direction and by the same amount.

These two sets of results are consistent with the idea that Fos expression may be involved in the signaling mechanism by which light produces phase shifts. However, they indicate that if Fos does participate in the phase-shifting mechanism, it may act either as a trigger or as a permissive signal, but that the level of Fos produced does not by itself determine the magnitude of the phase shift. Stated differently, although Fos/JunB dimers may act to regulate gene expression, which ultimately leads to phase shifts, the amplitude of the response to this input pathway is likely to be regulated by some other (downstream) component.

The idea that a signaling component other than Fos normally limits (or perhaps even regulates) the amplitude of phase shifts is consistent with analysis of the irradiance response curves obtained in the present study from animals that had been exposed to different light regimes (Fig. 7). In animals that had been in DD for only 2 days, the amount of Fos induction increases continuously with increasing irradiance, far beyond the irradiance at which the phase-shifting response reaches saturation. Therefore, the amplitude of the phase shift must be limited by something other than Fos. In contrast, in animals that had been in DD for 49 days, Fos induction attains similar levels to those observed in 2-day DD animals, but phase shift magnitude now rises in concert with Fos to much higher levels. One interpretation of this difference is that after prolonged periods in DD, some change occurs such that the hypothetical other signaling component is no longer limiting, and higher Fos levels can produce the observed larger phase shifts. This other component could be an integral part of the circadian timing mechanism itself or part of the light input pathway to the clock. Mutations such as *tau* that affect circadian period are likely to produce alterations in the function of one or more molecular components of the mechanism that generates circadian oscillations. This muta-

tion also changes the amplitude of the PRC to nonphotic stimuli (Mrosovsky et al., 1992). Period mutations that are known to affect molecular components of the clock mechanism in both *Drosophila* and *Neurospora* have been shown to affect PRC amplitude (Konopka et al., 1989; Dharmananda, 1980). The fact that large changes in the amplitude of behavioral phase shifts, dependent upon light history, are observed more generally in *tau* mutant than in wild type hamsters (but see Elliott, 1994) is consistent with the suggestion that these changes are a consequence of pacemaker characteristics that have been altered by the mutation.

Recently, putative mammalian orthologs to the *Drosophila period* gene have been reported (called *mPer1* and *mPer2*) (Sun et al., 1997; Tei et al., 1997; Albrecht et al., 1997; Shearman et al., 1997). *mPer1* and *mPer2* mRNA show circadian oscillations in mouse SCN, and *mPer1* was rapidly induced by a brief light pulse in the subjective night (Albrecht et al., 1997; Shigeyoshi et al., 1997; Shearman et al., 1997). The photic threshold for behavioral phase shifting and *mPer1* expression in the SCN were quantitatively correlated (Shigeyoshi et al., 1997), and the time course of *mPer1* expression was slightly slower than that of c-*fos* expression (Albrecht et al., 1997). Therefore, it will be of great interest to compare *mPer1* induction by light in the SCN of *tau* mutant hamsters that have been held in DD for 2 or 49 days as a test of the possibility that *mPer1* expression is being influenced by immediate early genes.

Although the model described above accounts for the observed correlations between Fos expression and phase shifting, it is important to emphasize that other possible interpretations of these data are equally reasonable and that thus far there is only limited direct evidence for a causal relationship between Fos and phase shifting (Wollnik et al., 1995; Honrado et al., 1996). It remains to be discovered which genes in which SCN cells are the targets of transcriptional regulation by c-*fos* and *jun*-B, and what role these genes may play in the cellular events leading to resetting the clock.

ACKNOWLEDGMENTS

We thank Vinessa Alones and Denise Holmes for technical assistance. This research was supported by AFOSR Grant No. F49620-93-1-0453 to MM, F31 MH10241 to JMK, R01 MH 49241 and P01 AG11412 to JST, and P30 HD28048 to Fred W. Turek.

REFERENCES

Albrecht U, Sun ZS, Eichele G, and Lee CC (1997) A differential response of two putative mammalian circadian regulators *mper1* and *mper2*. Cell 91:1055-1064.

Aronin N, Sagar SM, Sharp FR, and Schwartz WJ (1990) Light regulates expression of a Fos related protein in rat suprachiasmatic nuclei. Proc Natl Acad Sci U S A 87:5959-5962.

Bohmann D, Bos TJ, Admon A, Nishimura T, Vogt PK, and Tjian R (1987) Human proto-oncogene c-*jun* encodes a DNA binding protein with structural and functional properties of transcription factor AP-1. Science 238:1386-1392.

Castel M, Belenky M, Cohen S, Wagner S, and Schwartz WJ (1997) Light-induced c-*fos* expression in the mouse suprachiasmatic nucleus: Immunoelectron microscopy reveals co-localization in multiple cell types. Eur J Neurosci 9:1950-1960.

Curran T and Franza BR (1988) Fos and Jun: The AP-1 connection. Cell 55:395-397.

Curran T, Rauscher FJ, Cohen DR, and Franza BR (1988) Beyond the second messenger: Oncogenes and transcription factors. Cold Spring Harb Symp Quant Biol 53:769-777.

Dharmananda S (1980) Studies of the circadian clock of Neurospora crassa: Light-induced phase shifting. Ph.D. thesis at University of California Santa Cruz.

Earnest DJ, Iadarola M, Yeh HH, and Olschowak JA (1990) Photic regulation of c-*fos* expression in neural components governing the entrainment of circadian rhythms. Exp Neurol 109:353-361.

Elliott JA (1994) Type 0 PRC in hamsters: Influence of photoperiod and dim nocturnal illumination. Society for Research on Biological Rhythms Abstract 189.

Greenberg ME and Ziff EB (1984) Simulation of 3T3 cells induces transcription of the c-*fos* proto-oncogene. Nature 311:433-437.

Grosse J, Loudon ASI, and Hastings MH (1995) Behavioral and cellular response to light of the circadian system of *tau* mutant and wild type Syrian hamsters. Neurosci 65:587-597.

Honrado GI, Johnson RS, Golombek DA, Spiegelman BM, Papaioannou VE, and Ralph MR (1996) The circadian system of c-*fos* deficient mice. J Comp Physiol A 178:563-570.

Konopka RJ, Pittendrigh CS, and Orr O (1989) Reciprocal behavior associated with altered homeostasis and photosensitivity of *Drosophila* clock mutants. J Neurogenet 6:1-10.

Kornhauser JM, Mayo KE, and Takahashi JS (1996) Light immediate-early genes and circadian rhythms. Behav Genet 26:221-240.

Kornhauser JM, Nelson DE, Mayo KE, and Takahashi JS (1990) Photic and circadian regulation of c-*fos* gene ex-

pression in the hamster suprachiasmatic nucleus. Neuron 5:127-134.

Kornhauser JM, Nelson DE, Mayo KE, and Takahashi JS (1992) Regulation of *jun*-B messenger RNA and AP-1 activity by light and a circadian clock. Science 255:1581-1584.

Lau LF and Nathans D (1987) Expression of set of growth-related immediate early genes in BALB/c 3T3 cells: Coordinate regulation with c-*fos* or c-*myc*. Proc Natl Acad Sci U S A 84:1182-1186.

Lee W, Haslinger A, Karin M, and Tjian R (1987) Activation of transcription by two factors that bind promotor and enhancer sequences of human metallothionein gene and SV40. Nature 325:368-372.

Moore RY (1995) Organization of the mammalian circadian system. In *Ciba Symposium on Circadian Clocks and Their Adjustment*, DJ Chadwick and K Ackrill, eds, pp 88-106, Wiley, West Sussex UK.

Mrosovsky N, Salmon PA, Menaker M and Ralph MR (1992) Nonphotic phase shifting in hamster clock mutants. J Biol Rhythms 7:41-49.

Muller RG, Bravo R, Burckhardt J, and Curran T (1984) Induction of c-*fos* gene and protein by growth factors precedes activation of c-*myc*. Nature 312:716-720.

Ralph MR and Menaker M (1988) A mutation of the circadian system in golden hamsters. Science 241:1225-1227.

Rauscher FJ III, Sambucetti LC, Curran T, Distel RJ, and Spiegelman BM (1988) A common DNA binding site for Fos protein complexes and transcription factor AP-1. Cell 52:471-480.

Rea MA (1989) Light regulates fos-related protein immunoreactivity in the rat suprachiasmatic nuclei. Brain Res Bull 23:577-581.

Reebs SG and Mrosovsky N (1989) Effects of induced wheel running on the circadian activity rhythms of syrian hamsters: Entrainment and phase response curve. J Biol Rhythms 4:39-48.

Rusak B, McNaughton L, Robertson HA, and Hunt SP (1992) Circadian variation in photic regulation of immediate-early gene mRNA in rat suprachiasmatic nucleus cells. Mol Brain Res 14:124-130.

Rusak B, Robertson HA, Wisden W, and Hunt SP (1990) Light pulses that shift rhythms induce gene expression in the suprachiasmatic nucleus. Science 248:1237-1240.

Sassone-Corsi P, Lamph WW, and Verma IM (1988) Regulation of proto-oncogene fos: A paradigm for early response genes. Cold Spring Harb Symp Quant Biol 53:749-760.

Shearman L, Zylka MJ, Weaver DR, Kolakowski LF Jr, and Reppert SM (1997) Two period homologs: Circadian expression and photic regulation in the suprachiasmatic nuclei. Neuron 19:1261-1269.

Shigeyoshi Y, Taguchi K, Yamamoto S, Takeida S, Yan L, Tei H, Moriya T, Shibata S, Loros JJ, Dunlop JC, and Okamura H (1997) Light-induced resetting of mammalian circadian clock is associated with rapid induction of the *mPer1* transcript. Cell 91:1043-1053.

Shimomura K and Menaker M (1994) Light-induced phase shifts in *tau* mutant hamsters. J Biol Rhythms 9:97-110.

Sun ZS, Albrecht OZ, Bailey J, Eichele G and Lee CC (1997) RIGUI a mammalian ortholog of the *Drosophila* period gene. Cell 90:1003-1011.

Takeuchi J, Shannon W, Aronin N, and Schwartz WJ (1993) Compositional changes of AP-1 DNA binding proteins are regulated by light in a mammalian circadian clock. Neuron 11:825-836.

Tei H, Okamura H, Shigeyoshi Y, Fukuhara C, Ozawa T, Hirose M, and Sakaki Y (1997) Circadian oscillation of a mammalian homologue of the *Drosophila period* gene. Nature 389:512-516.

Winfree AT (1980) *The Geometry of Biological Time*, Springer-Verlag, New York.

Wollnik F, Brysch W, Uhlmann E, Gillardon F, Bravo R, Zimmermann M, Schlingensiepen KH, and Herdegen T (1995) Block of c-*fos* and JunB expression by antisense oligonucleotides inhibits light-induced phase shifts of the mammalian circadian clock. Eur J Neurosci 7:388-393.

Zhang Y, Kornhauser JM, Zee PC, Mayo KE, Takahashi JS, and Turek FW (1996) Effects of aging on light-induced phase-shifting of circadian behavioral rhythms: Fos expression and CREB phosphorylation in the hamster suprachiasmatic nucleus. Neurosci 70:951-961.

The Journal of Neuroscience, December 15, 1998, 18(24):10709–10723

Rhythmic Properties of the Hamster Suprachiasmatic Nucleus *In Vivo*

Shin Yamazaki, Marie C. Kerbeshian, Craig G. Hocker, Gene D. Block, and Michael Menaker

National Science Foundation Center for Biological Timing, Department of Biology, University of Virginia, Charlottesville, Virginia 22903

We recorded multiple unit neural activity [multiunit activity (MUA)] from inside and outside of the suprachiasmatic nucleus (SCN) in freely moving male golden hamsters housed in running-wheel cages under both light/dark cycles and constant darkness. The circadian period of MUA in the SCN matched the period of locomotor activity; it was ~24 hr in wild-type and 20 hr in homozygous *tau* mutant hamsters. The peak of MUA in the SCN always occurred in the middle of the day or, in constant darkness, the subjective day. There were circadian rhythms of MUA outside of the SCN in the ventrolateral thalamic nucleus, the caudate putamen, the accumbens nucleus, the medial septum, the lateral septum, the ventromedial hypothalamic nucleus, the medial preoptic region, and the stria medullaris. These rhythms were out-of-phase with the electrical rhythm in the SCN but in-phase with the rhythm of locomotor activity, peaking during the night or subjective night. In addition to circadian rhythms, there were significant ultradian rhythms present; one, with a period of ~80 min, was in antiphase between the SCN and other brain areas, and another, with a period of ~14 min, was in-phase between the SCN and other brain areas. The periods of these ultradian rhythms were not significantly different in wild-type and *tau* mutant hamsters. Of particular interest was the unique phase relationship between the MUA of the bed nucleus of the stria terminalis (BNST) and the SCN; in these two areas both circadian and ultradian components were always in-phase. This suggests that the BNST is strongly coupled to the SCN and may be one of its major output pathways. In addition to circadian and ultradian rhythms of MUA, neural activity both within and outside the SCN was acutely affected by locomotor activity. Whenever a hamster ran on its wheel, MUA in the SCN and the BNST was suppressed, and MUA in other areas was enhanced.

Key words: circadian; ultradian; suprachiasmatic nucleus; in vivo *recording; hamster;* tau *mutant; locomotor activity; bed nucleus of the stria terminalis; MUA*

Circadian locomotor activity rhythms in mammals are generated by an endogenous pacemaker located in the suprachiasmatic nucleus (SCN) of the hypothalamus (for review, see Turek, 1985; Meijer and Rietveld, 1989; Klein et al., 1991). Lesions of the SCN cause arrhythmicity of locomotor activity (Moore and Eichler, 1972; Stephan and Zucker, 1972; Rusak and Zucker, 1979), and transplants of fetal SCN tissue restore circadian periodicities (Sawaki et al., 1984; Lehman et al., 1987; Ralph et al., 1990). The SCN exhibits circadian rhythms in several *in vitro* preparations: the acute slice (Green and Gillette, 1982; Groos and Hendricks, 1982; Shibata and Moore, 1988), slice culture (Bos and Mirmiran, 1990; Herzog et al., 1997), and dispersed cell culture (Welsh et al., 1995; Liu et al., 1997). Both slice and dispersed cell cultures of SCN also display circadian rhythms of peptide release (Murakami et al., 1991; Watanabe et al., 1993; Shinohara et al., 1995). In contrast the physiology of the SCN *in vivo* and its relationship to circadian behavior in the intact animal have received little experimental attention.

To understand how the circadian clock controls locomotor behavior, we need to understand its connections to the motor control system. Although output pathways from the SCN circadian pacemaker are not completely described, the motor control system in mammals is relatively well characterized (Wichmann et al., 1995; Bergman et al., 1998). Because there are no known direct neural connections between the SCN and motor control areas of the brain, it is likely that either humoral factors and/or "relay nuclei" serve to connect the SCN with the motor centers.

Not only does the SCN regulate locomotor activity but there is reason to believe that locomotor activity feeds back on the SCN. The period of the free-running rhythm of rats housed in cages with a running wheel is different from that of rats housed in cages without a wheel (Yamada et al., 1988, 1990; Shioiri et al., 1990). Locking of the running wheel changes the free-running period in mice (Edgar et al., 1991). Access to running wheels induces phase shifts of locomotor activity in hamsters (Mrosovsky, 1988; Reebs and Mrosovsky, 1989) as does injection of triazolam, which increases locomotor activity (van Reeth et al., 1987). In mice, forced treadmill running induces phase shifts of circadian rhythms and is able to entrain them (Marchant and Mistlberger, 1996).

The apparent complexity of the relationship between the SCN and locomotor centers, almost certainly involving reciprocal in-

Received July 29, 1998; revised Sept. 28, 1998; accepted Oct. 1, 1998.

This research was supported by the National Science Foundation (NSF) Science and Technology Center for Biological Timing along with Air Force Grants F49620-98-1-0174 to M.M. and F49620-97-1-0012 to G.D.B and M.M., by the National Institutes of Health postdoctoral National Research Service Award NS09329 to C.G.H., and by an NSF postdoctoral fellowship in Biosciences Related to the Environment to M.C.K. We thank Dr. M. E. Geusz for computer programming for recording neural activity (for spike discrimination) and Dr. M. Kawasaki for discussing amplifier circuit design. Also our special thanks to Drs. M. Takahashi and M. Nishihara for general information on multiunit activity recording and to Dr. S.-I. T. Inouye for information on electrode design.

We dedicate this work to Professor Hiroshi Kawamura on the occasion of his 70th birthday (January 26, 1997).

Correspondence should be addressed to Dr. Shin Yamazaki, National Science Foundation Center for Biological Timing, Department of Biology, Gilmer Hall, University of Virginia, Charlottesville, VA 22903.

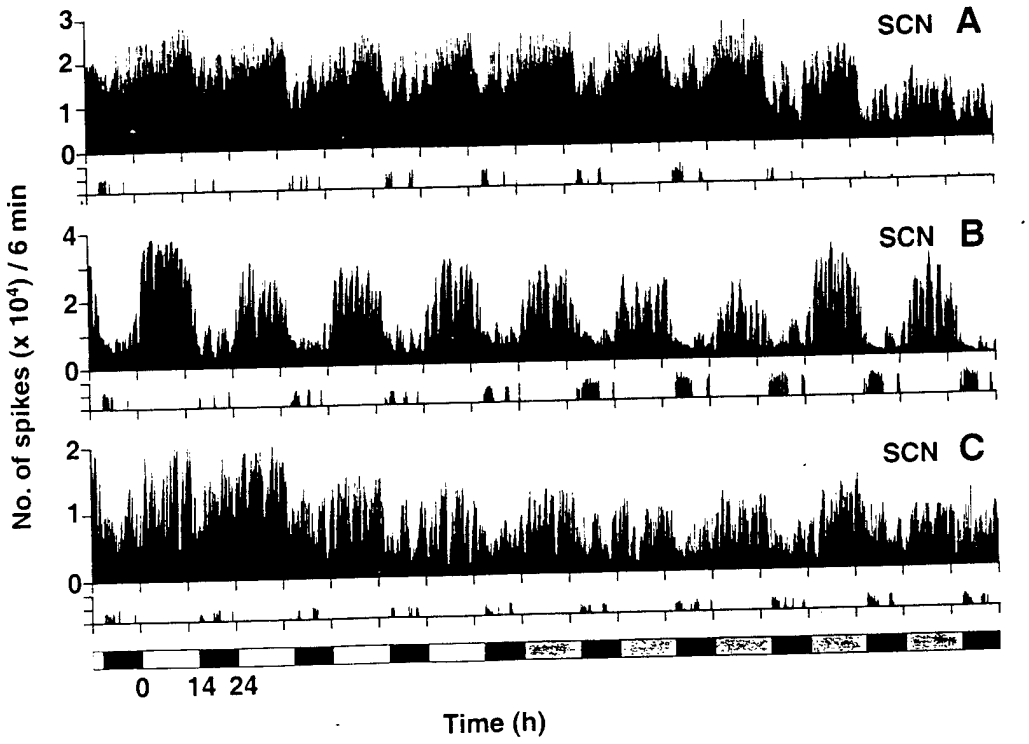

Figure 1. Examples of MUA recorded for 10 d from the SCN of three wild-type hamsters. Animals were kept in light/dark cycles (14:10 hr LD) for 4 d and then released into constant darkness (lighting condition indicated at the *bottom* of the figure). Neuronal spikes are plotted in 6 min bins. Wheel-running activity is plotted at the *bottom* of *A–C* as the number of revolutions per 6 min; the *y*-axis for this portion of the figure shows 0–200 revolutions per 6 min. *A*, Recorded from the ventrolateral portion of the central region of the left SCN. *B*, Recorded from the ventromedial portion of the right SCN at the center of the rostrocaudal axis. *C*, Recorded from the ventromedial portion of the right SCN near the caudal end of the nucleus.

teractions, and the fact that direct neuronal interconnections appear to be absent provide a strong rationale for exploring the functional relationships *in vivo*. We have perfected a technique that allows us to record neuronal activity of several brain regions in freely moving hamsters, enabling us to correlate electrical activity within the SCN with activity in other brain regions and with locomotor activity. We have used this technique to describe the electrical characteristics of the SCN *in vivo*, the differences between the *tau* mutant and wild-type hamsters, the relationship between the SCN and other regions of the brain, and the effect of the animal's locomotor behavior on SCN activity. The results provide a new framework for understanding the regulation of locomotor behavior by the circadian timing system.

MATERIALS AND METHODS

Animals. Three- to five-month-old golden hamsters (LVG wild type from Charles River Laboratories, Wilmington, MA; LVG background *tau* mutant animals from our colony) were used in this study. Animals were entrained for at least 2 weeks to light/dark cycles (LDs) (14:10 hr LD for wild types; 11.7:8.3 hr LD for *tau* mutants; light intensity of ~300 lux at cage level). We monitored wheel-running activity throughout the experiments and used only animals that showed clear locomotor rhythmicity.

Electrode implantation. We implanted one or two bipolar electrodes constructed from pairs of Teflon-coated stainless steel wires (bare diameter, 130 μm; A-M Systems, Everett, WA; tip distance, ~150 μm for recording from the SCN and 200–300 μm for other brain regions) and an uncoated platinum–iridium wire (diameter, 130 μm; A-M Systems) used as a signal ground in the cortex. Wires were connected to an eight pin IC socket wrapped in insulated copper tape. Distances between any two bipolar electrodes were determined according to the recording sites chosen.

Electrode implantation was performed under pentobarbital anesthesia (90 mg/kg, i.p.). Animals were placed in a stereotaxic instrument with the nose bar set at −2 mm (David Kopf Instruments, Tujunga, CA). Four self-tapping screws (#0 × 1/8 inch; Small Parts, Miami Lakes, FL) were implanted into 1 mm holes in the skull made with a dental drill. We used different stereotaxic coordinates for wild-type and *tau* mutant hamsters because the shape of bregma in *tau* mutants is different and more variable than is that in wild types. Wild-type SCN coordinates were 0.7 mm anterior to bregma, 0.2 mm lateral to the midsagittal, and 8.0–8.2 mm below the dural surface. *Tau* mutant coordinates were 1.0–1.2 mm anterior to bregma, 0.2 mm lateral to the midsagittal, and 7.9–8.1 mm below the dural surface. The electrode was secured to the screws and the skull with dental cement.

Recording procedure. One week after surgery, each hamster was transferred to a 24 cm (width) × 21 cm (length) × 30 cm (height) cage with a running wheel 21 cm in diameter mounted on one side to allow the hamster equipped with wires access to the wheel. The electrodes were connected to head stage buffer amplifiers (J-FET input OP Amp; TL084) located on the hamster's head. Buffer amplifiers were connected to a 12 channel slip ring (Airflyte Electronics Company, Bayonne, NJ) that allowed free movement for the animal. The wires between the head stage amplifiers and the slip ring were protected by a stainless steel spring. Output signals were processed by differential input integration amplifiers (INA 101 AM; Burr-Brown, Tucson, AZ; gain, ×10) and then fed into AC amplifiers (OP Amp, 4558; bandpass, 500 Hz to 5 kHz; gain, 10,000). Spikes were discriminated by amplitude and counted in 1 min bins using a computer-based window discrimination system (DAS-1801ST AD board; Keithley Metrabyte, Taunton, MA). Wheel revolutions were recorded using the Data Quest system (Data Science International, St. Paul, MN).

Reduction of recording noise. In recording neural activity from freely moving animals, the biggest problem is noise. We reduced microphonic noise, which is caused by mechanical disturbances such as wire movements, by mounting the buffer amplifiers on the head (effectively decreasing the impedance). We directly coupled the output signals to the integration amplifier (without any capacitors or resistors) to provide a high common mode rejection ratio that can reduce non-neuronal signals such as muscle potentials. We also used shielding material around the electrode and its vicinity to reduce noise from the animal's scratching. Because we could not entirely remove this source of noise, we used a

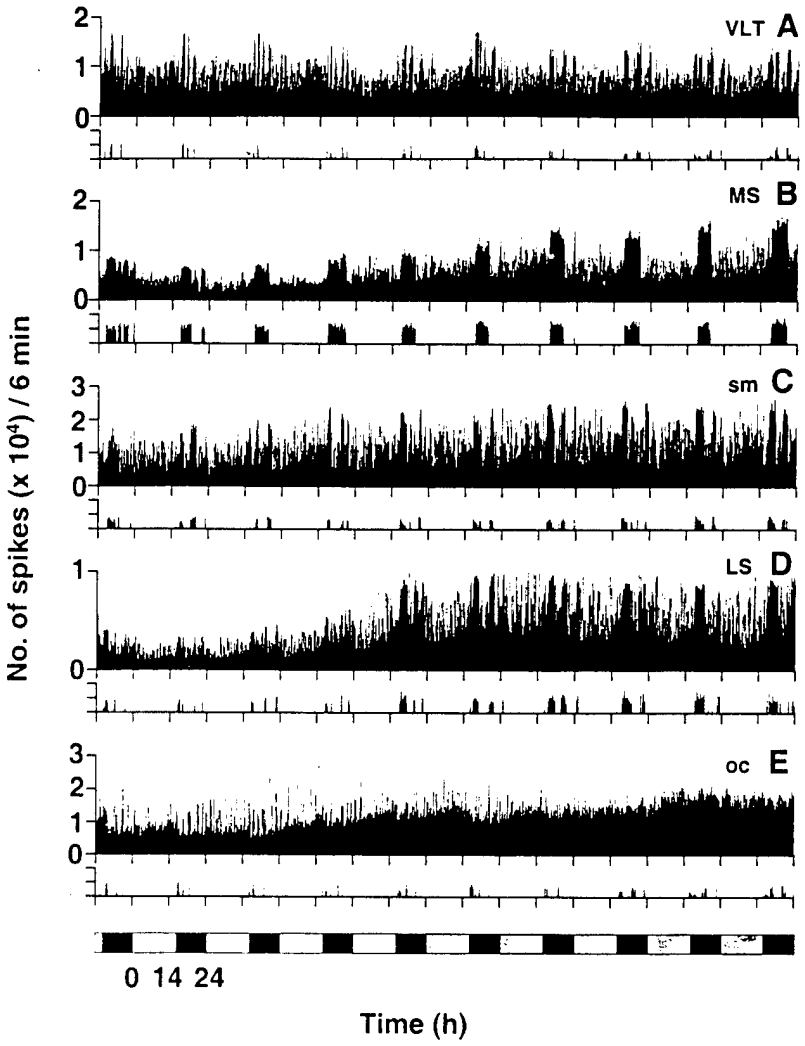

Figure 2. Daily and circadian rhythms of neural activity in several regions of the brain. MUA and locomotor activity are plotted in 6 min bins as in Figure 1. Recordings were made from the following: *A*, right side of the ventrolateral thalamic nucleus (*VLT*); *B*, right side of the medial septum (*MS*); *C*, right side of the stria medullaris (*sm*); *D*, right side of the LS; *E*, the optic chiasm (*oc*). Each plot represents a different wild-type hamster except for *A* (same animal as in *E*) and *C* (same animal as in Fig. 1*C*). Note (most clearly in *B*) that the peak of neural activity coincides with wheel-running activity.

highly effective low-cut filter (500 Hz). Using these techniques, we reduced electrical noise generated by chewing or moving to undetectable levels. Although scratching did generate detectable electrical noise, this activity was rare and did not create a problem in the analysis.

Identification of recording sites. After the electrical recordings, each hamster was anesthetized with halothane, the head amplifier was disconnected, and a small positive current (50 μA; 10 sec) was passed through the recording electrodes. The brain was removed and fixed in Zamboni's fixative solution for a few days. Frozen sections (40 μm thick) were stained with potassium ferrocyanide (5% potassium ferrocyanide in 10% HCl). Blue spots of deposited iron were used for identification of recording sites.

Data analysis. The first report of SCN neuronal recordings from freely moving rodents appeared 19 years ago and played a pivotal role in identifying the SCN as the central mammalian circadian pacemaker (Inouye and Kawamura, 1979). Since then little use has been made of this technique. A primary reason for hesitation in the use of *in vivo* recording techniques is that changes in neuronal oscillations are oftentimes difficult to identify in the raw data, and thus robust time series statistical analysis is required. No single time series analysis tool can be applied in all cases. We applied a new method, singular-spectrum analysis (SSA), in combination with older methods. Periodicities in multiunit activity (MUA) recorded *in vivo* were determined using SSA in combination with the multitaper method (MTM) approach to the fast Fourier transform (Thomson, 1982; Vautard et al., 1992).

Singular-spectrum analysis or SSA is a linear, nonparametric method based on a principal component analysis in the vector space of the delay coordinates for a times series (Elsner and Tsonis, 1996). In SSA, a single time series is expanded into a set of multivariate time series of length M, known as the "window length." M determines what range of frequencies can be resolved as a stationary signal in the calculated principal components. The principal component analysis orders the expanded time series as a new coordinate system with most information along the first coordinates. The principal components are processes of length $N - M + 1$ that can be thought of as weighted moving averages of the time series in which each accounts for a certain percentage of the total variance. SSA allows optimal detrending, identification of the noise floor in spectral estimates, and identification of intermittent oscillatory components in the data. In practice, we found that we could with reasonable success divide the data into four parts (trend variance, circadian variance, ultradian components variance, and noise variance) by use of two window lengths on the MUA data. M was set at 36 hr (M = 360 for 6 min bins) for the circadian time scale and 5 hr for the ultradian time scale. SSA cannot resolve periods longer than M and treats them as trends. If M is much greater than the average lifetime of an episode of oscillation, SSA cannot resolve the intermittent oscillation.

We used SSA for signal reconstruction from the noisy MUA data. Simple noise reduction by applying a fixed low-pass filter to the data is not appropriate when the spectrum is not monotonic. Because steps were taken to minimize instrument noise and a low-cut filter was used (500 Hz) before binning the impulses in the MUA data, noise is represented here mostly by random impulses from populations of neurons near the electrode. Optimal filtering of signals that are not completely stable requires methods such as Wiener filtering or SSA. Both provide optimal filters in a least squares sense. However Weiner filters arbitrarily require harmonic functions as a basis. SSA, in contrast, uses data-determined general functions that do not require any previous hypotheses about the noise variance. Unlike SSA, the Wiener method requires smooth and very reliable estimates of the power spectrum that are impossible to obtain with very short data sets. "Noise-free" circadian or ultradian time

osci., December 15, 1998, 18(24):10709–10723

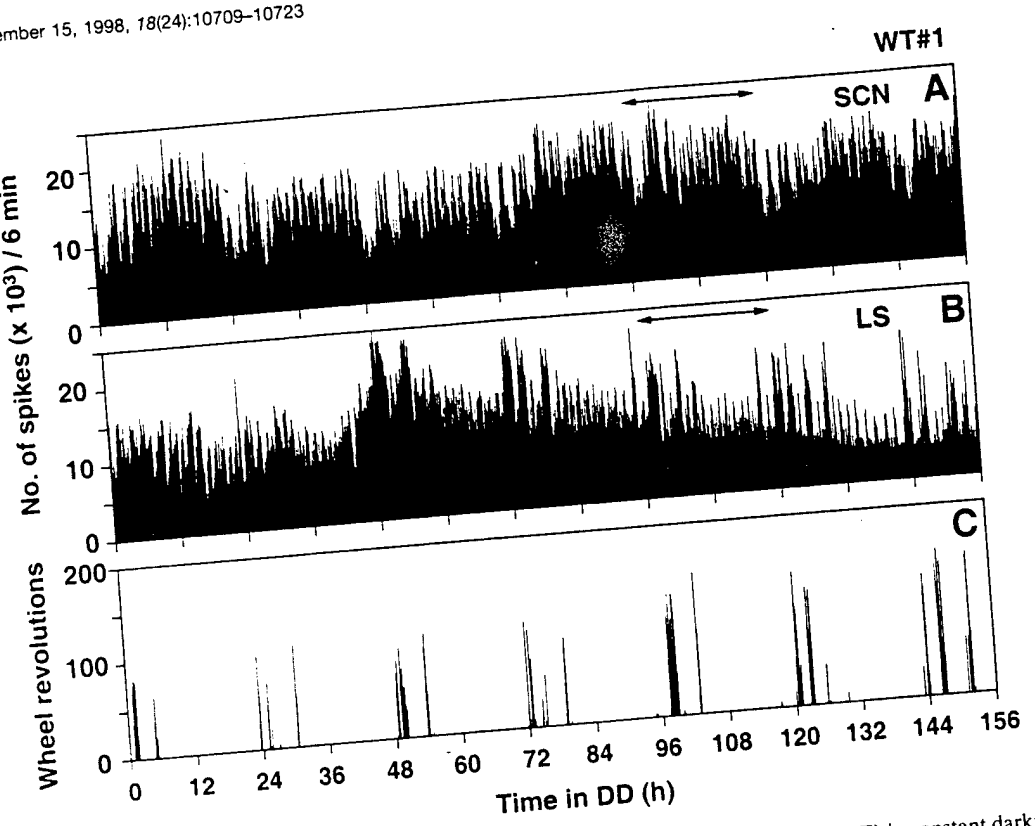

3. Wheel-running behavior and neural activity records from the SCN and LS of a wild-type hamster (*WT*) in constant darkness. Electrodes were in the left ventromedial region of the central SCN and in the right LS. The time scale shows hours after the hamster was released into constant ss. *A*, MUA in the SCN in 6 min bins. *B*, MUA in the LS in 6 min bins. *C*, Wheel revolutions per 6 min. The data marked by the *double-headed* are presented below (see Fig. 8).

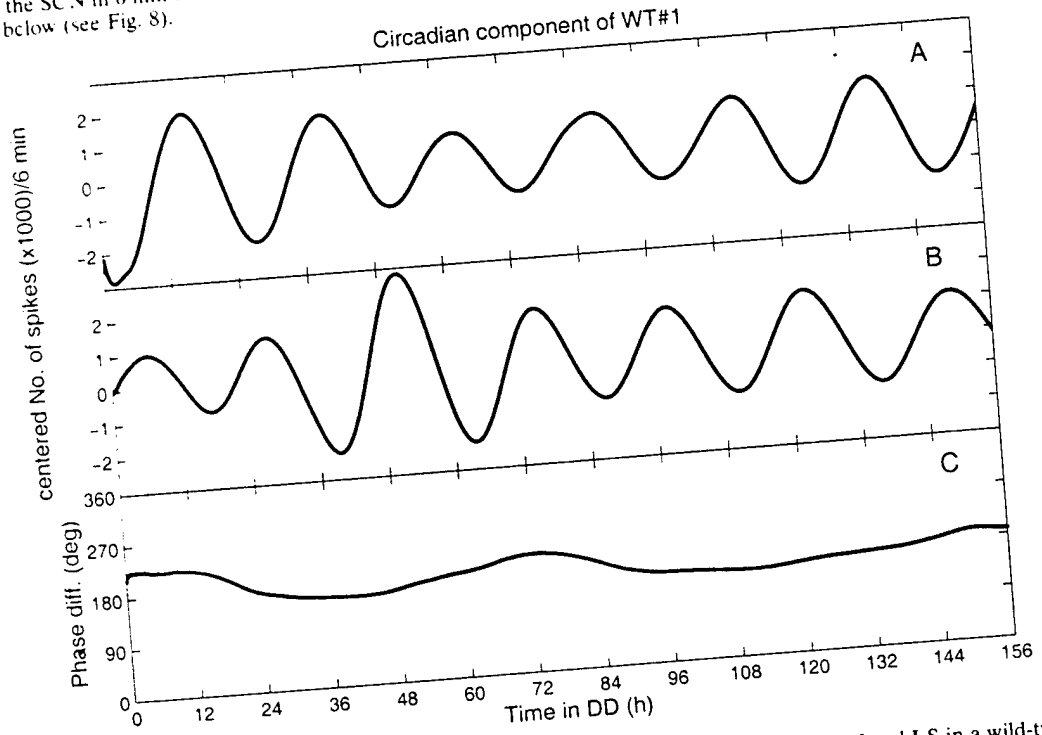

igure 4. Mathematical analysis of the phase angle difference of the circadian rhythms recorded in the SCN and LS in a wild-type hamster. Original ata are shown in Figure 3*A*,*B*. Data reconstructed by SSA for the SCN (*A*) and for the LS (*B*). *C*, Instantaneous phase angle difference between the ircadian rhythms shown in *A* and *B*. The time series *A* and *B* were individually converted to their Hilbert transforms (the time series with a 90° phase hift). The resultant time series are series of complex numbers representing the original data (real part) and the Hilbert transform (imaginary part). The nagnitude of each of these complex numbers is an estimate at that time of the circadian rhythm amplitude (data not shown). The angle of each of these complex numbers is an estimate at that time of the phase of the circadian rhythm relative to the beginning. The difference between the angles of *A* and *B* at each point is the instantaneous phase difference between the two circadian rhythms.

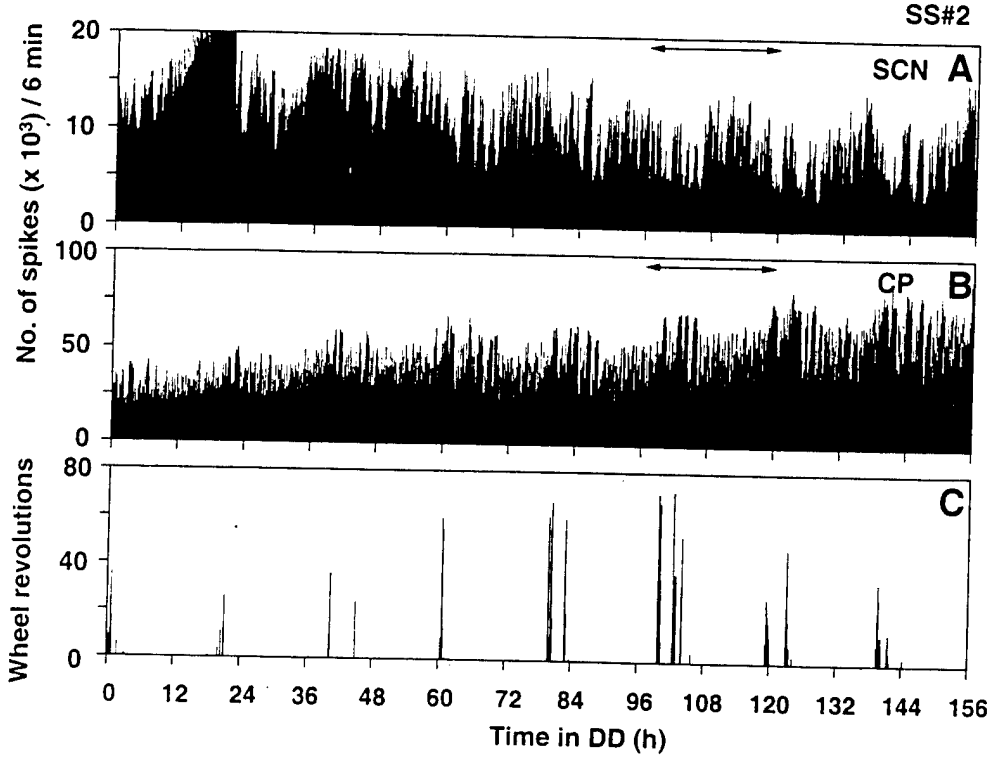

Figure 5. Wheel-running behavior and neural activity records from the SCN and CP of a *tau* mutant hamster in constant darkness. Electrodes were located in the right ventromedial part of the central region of the SCN and in the right CP. *A*, MUA in the SCN in 6 min bins. *B*, MUA in the CP in 6 min bins. *C*, Wheel revolutions per 6 min. The data marked by the *double-headed arrows* are presented below (see Fig. 10). *SS*, Homozygous *tau* mutant.

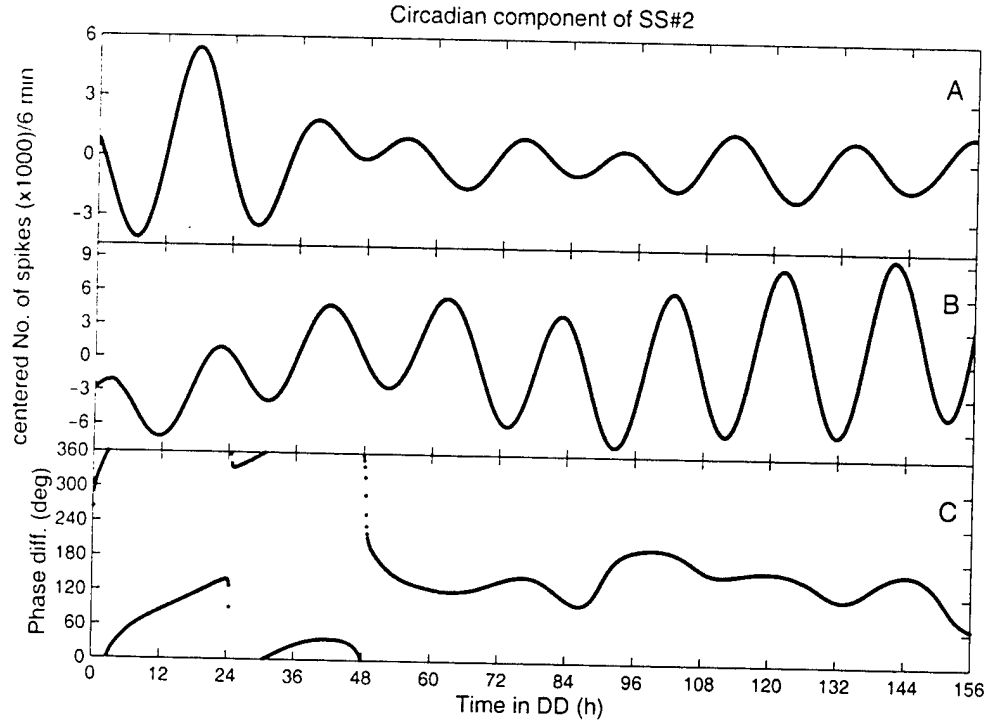

Figure 6. Mathematical analysis of the phase angle difference of the circadian rhythms recorded in the SCN and CP in a *tau* mutant hamster. Original data are shown in Figure 5. *A*, *B*, Data reconstructed by SSA for the SCN (*A*) and for the CP (*B*). *C*, Instantaneous phase angle difference between the circadian rhythms shown in *A* and *B*.

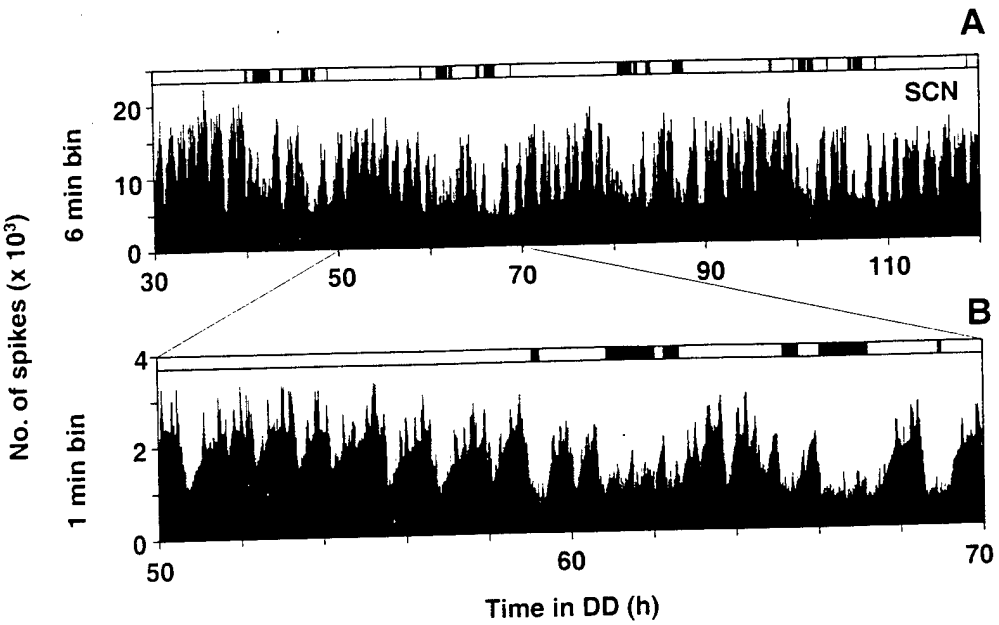

Figure 7. Circadian and ultradian rhythms of MUA in the SCN of a *tau* mutant hamster in constant darkness. In this case, the bipolar electrode became separated in the brain, with one electrode positioned on the left side and the other positioned on the right side of the ventromedial region of the caudal SCN. *Top bars* of *A* and *B* show wheel-running activity, plotted as a *black bar* when the wheel revolved more than once in 6 min. The time scale shows hours after the animal was released into constant darkness. *A*, Plot of MUA in 6 min bins. *B*, Expanded plot of 20 hr (one circadian cycle for the *tau* mutant hamster) of data from *A* with neuronal activity in 1 min bins showing ultradian rhythms of both periods as well as the negative correlation between wheel-running activity and neural activity.

series were therefore reconstructed from the SSA filters. By this method, oscillatory signals that accounted for as little as 3% of the total variance could be detected. Monte Carlo simulations assuming either white noise or correlated noise were used to evaluate the background noise level in the SSA spectra. By selecting only those principal components associated with the circadian variance of the data, we could derive an optimal (in the least squares sense) "noiseless" reconstruction of the circadian waveform in the data. Each waveform in the reconstructed time series is essentially a local fit allowing us to calculate a mean period from each animal's data set. This local noise-free fit also allowed us to determine the phase relationship as a function of time between two different locations in the brain. Periods of the ultradian rhythms were determined with one or more of the following: SSA-MTM, power spectrum estimates [e.g., maximum entropy method (MEM)], or visual inspection of the raw

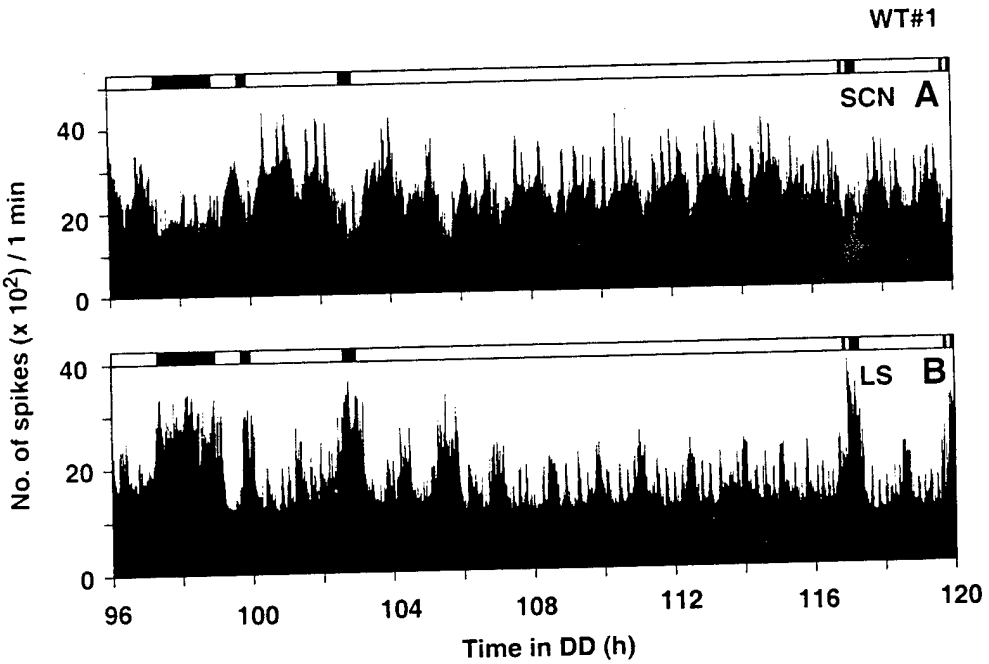

Figure 8. Ultradian rhythms in neural activity records from the SCN and LS of a wild-type hamster. *A*, Expanded plot of the 24 hr neural activity record in 1 min bins from the SCN (from Fig. 3*A*, *double-headed arrow*). The *top bar* shows wheel-running activity, plotted as a *black bar* whenever the wheel revolved more than once in 6 min. *B*, Expanded plot of the concurrent record from the LS (from Fig. 3*B*, *double-headed arrow*). Note the negative correlation of neural activity with wheel-running activity in the SCN and the positive correlation in the LS.

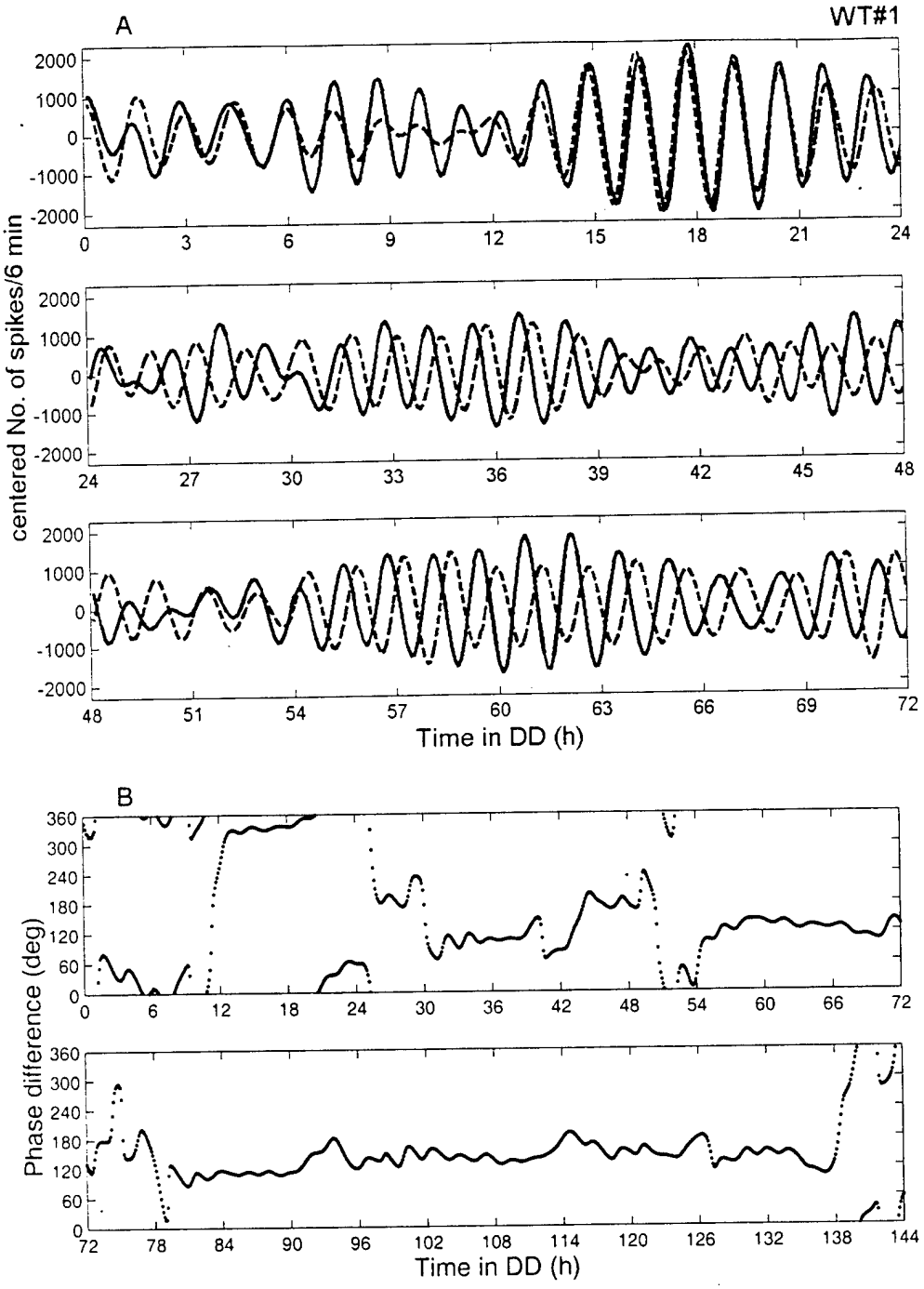

Figure 9. Mathematical analysis of ultradian rhythms recorded from the SCN and LS (from Fig. 3*A*,*B*). *A*, Data reconstructed by SSA of the 80 min ultradian rhythms in the SCN (*solid line*) and the LS (*dotted line*) for the first 72 hr of the record. *B*, Phase angle difference of the 80 min ultradian rhythms between the SCN and the LS plotted for 144 hr (see text and Fig. 4 for details).

data. MEM was performed on the data after the trend and circadian variances were removed (determined by SSA). The order of the MEM (M, number of poles in the autoregressive model) was kept much lower than the number of data points and varied over the range to monitor stability of peaks of interest in the spectrum (M, 20–60; $N > 1600$). MEM is fully consistent with SSA so that the additive property of the spectra is conserved exactly (Vautard et al., 1992). Periods of very short ultradian rhythms were determined by visual inspection; areas of high-frequency ultradian activity were measured for the average period, and measurements from six areas per animal were averaged to obtain the period. The periods of the wheel-running activity were obtained by using a standard chi-square periodogram for comparison with the other methods (see Table 1).

Phase analysis. We used the discrete Hilbert transform of the SSA-reconstructed waveforms to estimate the instantaneous phase difference between the oscillations inside and outside the SCN. The Hilbert transform is the imaginary part of the analytical signal of a real time series (Bendat and Piersol, 1986). An estimate of the imaginary part from the real part of the time series can be calculated by assuming the signal is causal (a sequential time series) and by using the inverse of a one-sided Fourier transform (fast Fourier transform coefficients that correspond to negative frequencies are set to zero before doing the inverse transform). The

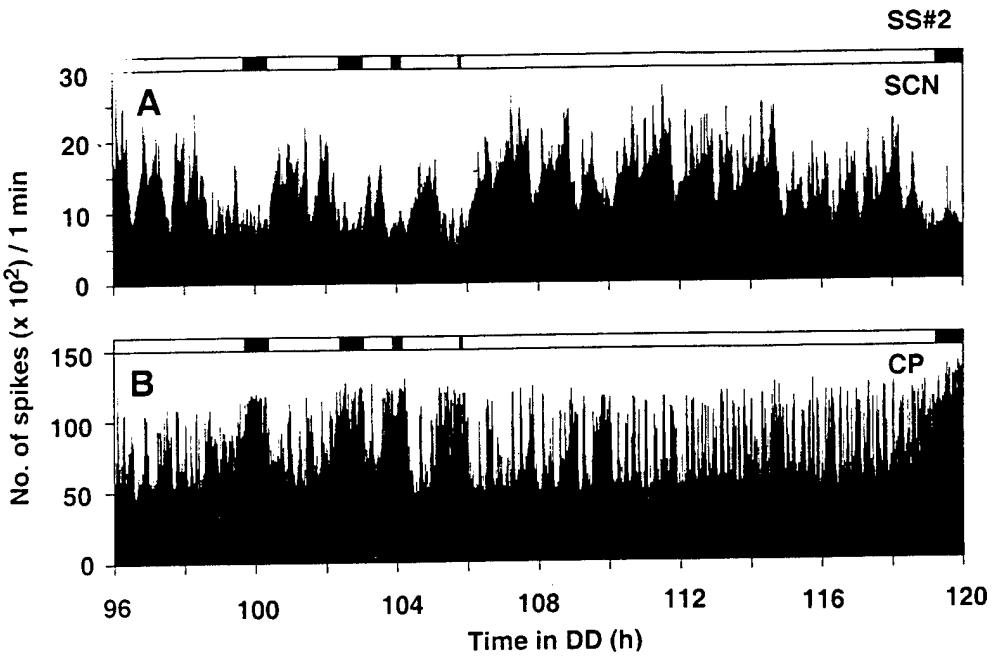

Figure 10. Ultradian rhythms in neural activity records from the SCN and CP in a *tau* mutant hamster. *A*, Expanded plot of 24 hr neural activity in 1 min bins from the SCN (from Fig. 5*A*, *double-headed arrow*). The *top bar* shows wheel-running activity, plotted as a *black bar* whenever the wheel revolved more than once in 6 min. *B*, Expanded plot of the concurrent record from the CP (from Fig. 5*B*, *double-headed arrow*). Note the positive (*CP*) and negative (*SCN*) correlations with wheel-running behavior.

resultant time series is phase shifted 90° from the original time series. This process is sensitive to noise and requires a filtered input such as that provided by SSA. The temporal change in the relative phase between the oscillations recorded in different brain regions was examined using this method. Circular statistics were used to compute the mean phase difference for the circadian rhythms in different brain regions (Fisher, 1995).

Experimental protocols. To observe daily and circadian changes of neural activity in and outside of the SCN, we recorded MUA from 20 wild-type hamsters implanted with two electrodes. One electrode was directed into the SCN, and the other was aimed at one of several regions outside of the SCN. Animals were recorded for 4 d in a light:dark cycle (14:10 hr LD; light intensity of ~300 lux at cage level), followed by 6 d in constant darkness (DD). To evaluate the effects of the *tau* mutation on the rhythmic properties, we recorded MUA from 10 wild-type and 14 *tau* mutant hamsters implanted with two electrodes, one aimed at the SCN and the other at one of the following sites: the lateral septum (LS), the caudate putamen (CP), the ventrolateral region of the thalamus, and the bed nucleus of the stria terminalis (BNST). These hamsters were placed into DD at the time of their normal lights off, and MUA was recorded for 7 d. We only used data from implantations in which both wires of each electrode were located in the same nucleus. We sometimes observed one wire located in the SCN, while the other was in the surrounding area; in those cases the data were discarded.

RESULTS

Circadian rhythms both within and outside the SCN

MUA recorded in the SCN showed clear daily (LD) and circadian (DD) rhythms (Fig. 1). Peak impulse frequency of these rhythms always occurred at the middle of the day (LD) or subjective day (DD), in antiphase with the hamster's nocturnal wheel-running activity. The amplitude of the neuronal activity rhythms varied from experiment to experiment and was not strongly correlated

Table 1. Summary of circadian and ultradian periods

		Neural activity in the SCN		
	Wheel-running activity (hr)	Circadian (hr)	Ultradian 1 (min)	Ultradian 2 (min)
WT#1	24.3	24.5	84	14
WT#2	24.2	24.1	75	14
WT#3	23.9	23.8	87	14
WT#5	24.2	24.1	76	15
Mean ± SE	24.15 ± 0.09	24.13 ± 0.14	80.5 ± 3.0	14.3 ± 0.3
SS#2	19.8	19.7	75	15
SS#4	20.1	20.3	78	15
SS#5	20.0	20.1	99	12
SS#7	19.8	19.7	71	15
Mean ± SE	19.93 ± 0.08	19.95 ± 0.15	80.8 ± 6.3	14.3 ± 0.8
Two-tailed *t* test	$p < 0.0005$	$p < 0.0005$	$p = 0.97$	$p = 1.00$

Seven days of MUA and wheel-running activity were collected simultaneously in constant darkness (WT, wild type; SS, homozygous *tau* mutants). Periods of wheel-running rhythms were obtained by chi-square periodogram. Periods of circadian and ultradian 1 rhythms of MUA were determined by SSA. Periods of ultradian 2 rhythms were determined by visual inspection. (See text for details of analysis methods.)

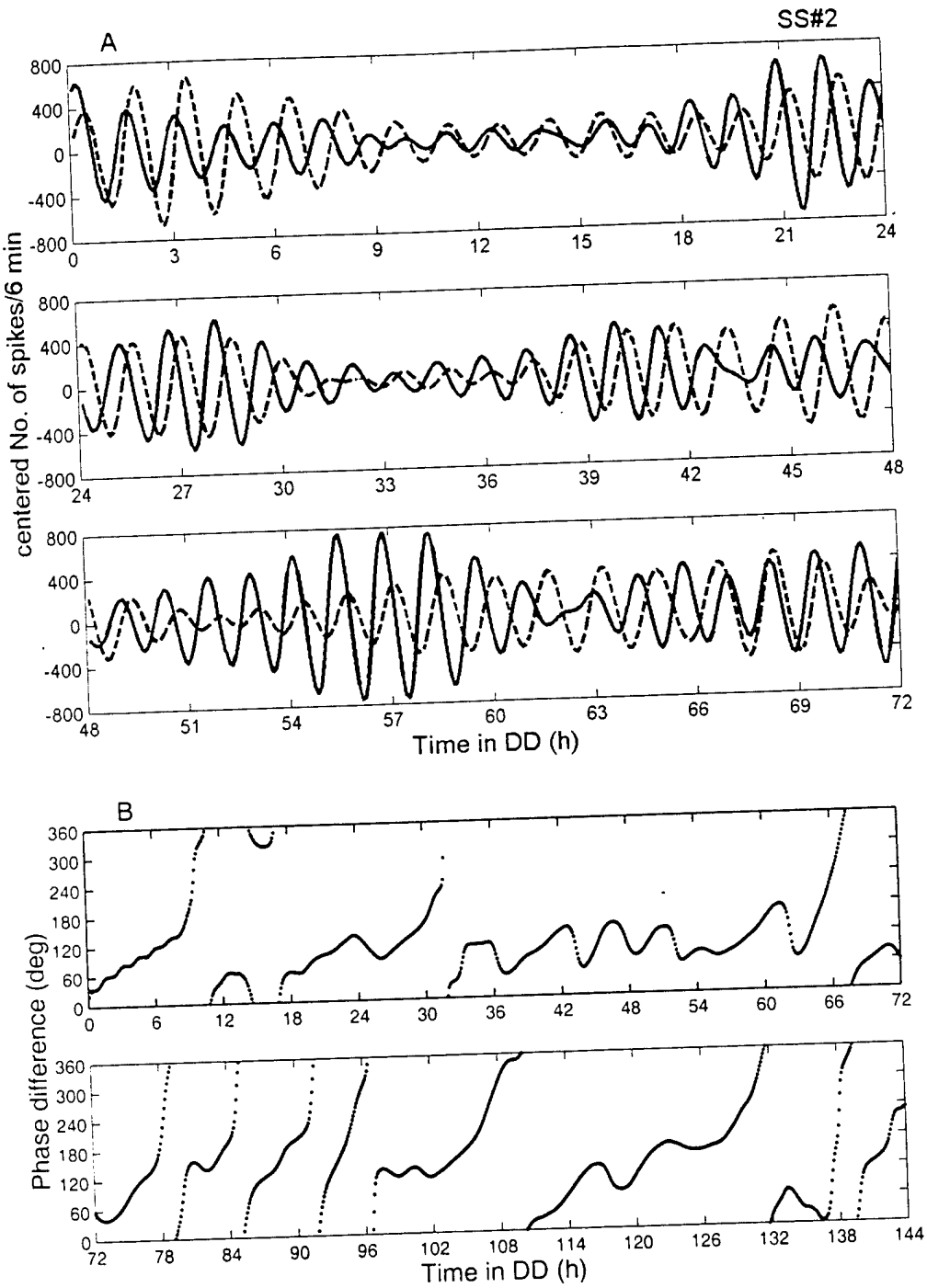

Figure 11. Mathematical analysis of the ultradian rhythms recorded from the SCN and CP in a *tau* mutant hamster. *A*, Data reconstructed by SSA of the 80 min ultradian rhythms in the SCN (*solid line*) and the CP (*dotted line*) for the first 72 hr of the record. *B*, Phase angle difference of the 80 min ultradian rhythms between the SCN and the CP plotted for 144 hr (see text and Fig. 4 for details).

with the recording site, although recordings obtained in the ventral portion of the SCN tended to have a higher amplitude than did those from the dorsal portion. Although the recording sites were nearly identical for the animals whose records are shown in Figure 1, *B* and *C*, the MUA displayed in Figure 1*B* has higher average amplitude oscillations than does that in Figure 1*C*. SSA detected a significant circadian (or daily) oscillation with a centered amplitude of ~10,000 spikes per 6 min interval from the data plotted in Figure 1*B*. The centered amplitude from data shown in Figure 1*C* was approximately one-fourth as large.

There was no consistent relationship between overall levels of locomotor activity and MUA activity. For example, the wheel-running activity of animals shown in Figure 1, *A* and *B*, was quite variable (on some nights the hamsters ran much more than on others), yet the amplitude of the MUA rhythms remained relatively constant. Furthermore, in all three examples in Figure 1, the amplitude of MUA oscillation in the SCN did not change when the animals were released from LD into DD. Even in the case of the animal whose data are shown in Figure 1*A*, in which the electrode was located in the lateral portion of the SCN (which

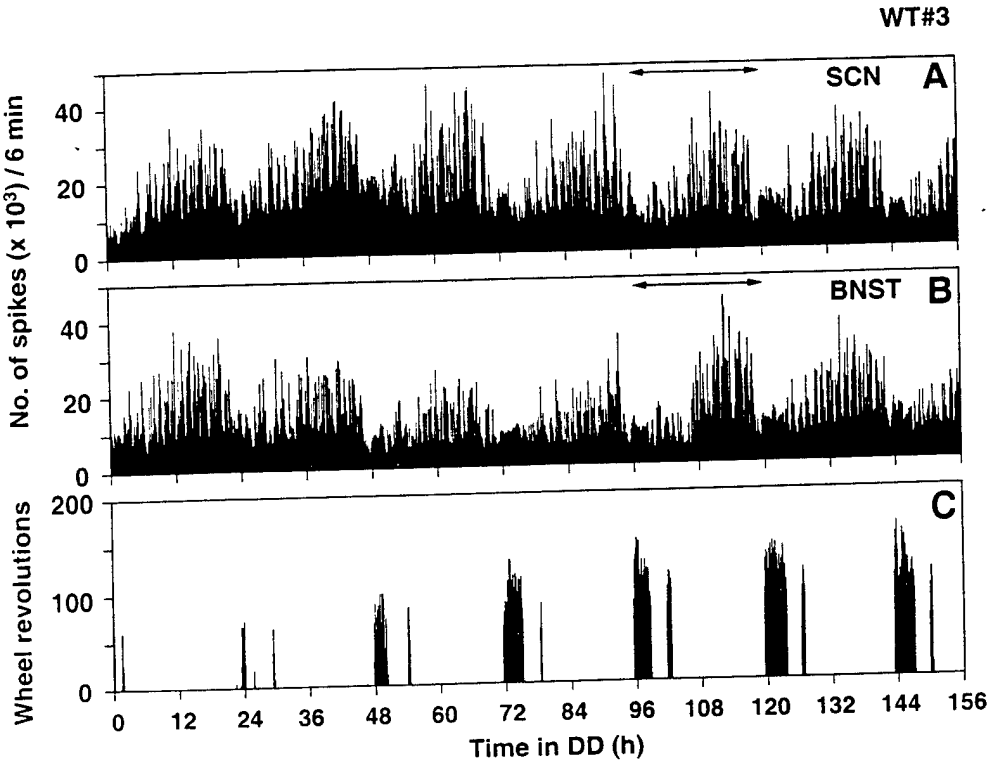

Figure 12. Neural activity records obtained simultaneously from the SCN and the BNST in a wild-type hamster in constant darkness. Electrodes were located in the right ventromedial portion of the central SCN and in the right anteromedial portion of the BNST. *A*, MUA in the SCN in 6 min bins. *B*, MUA in the BNST in 6 min bins. *C*, Wheel revolutions per 6 min. The data marked by the *double-headed arrows* are presented below (see Fig. 14). Note the almost perfect phase lock between these two regions and that both are in antiphase with wheel running.

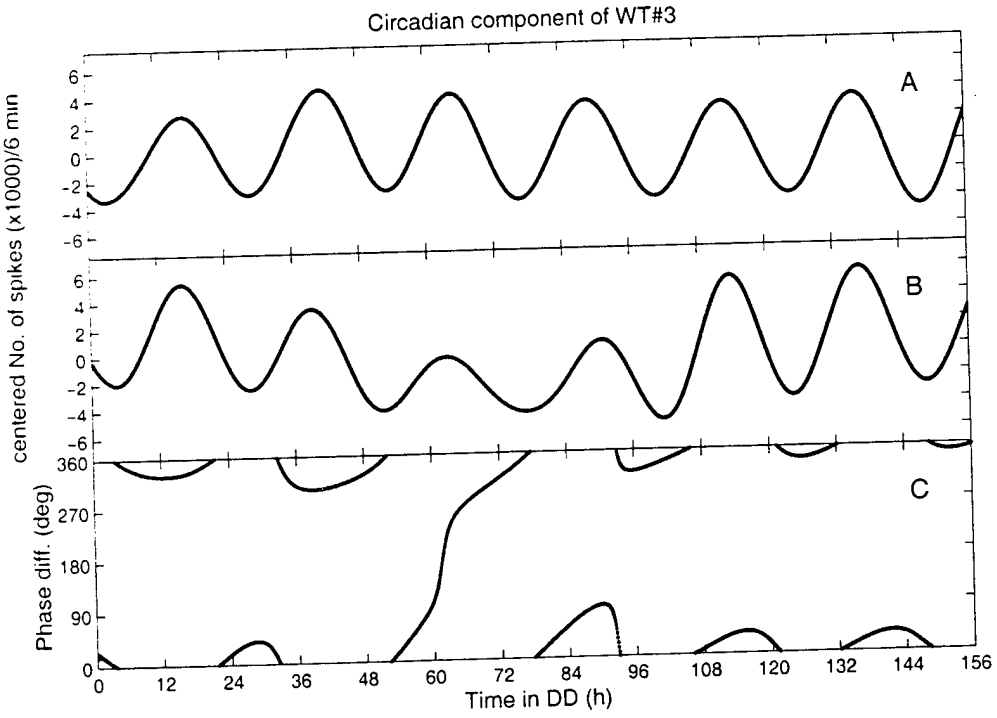

Figure 13. Mathematical analysis of the phase angle difference of the circadian rhythms recorded in the SCN and the BNST in a wild-type hamster (original data in Fig. 12). *A*, *B*, Data reconstructed by SSA for the SCN (*A*) and for the BNST (*B*). *C*, Instantaneous phase angle difference between the circadian rhythms shown in *A* and *B* (see text and Fig. 4 for details).

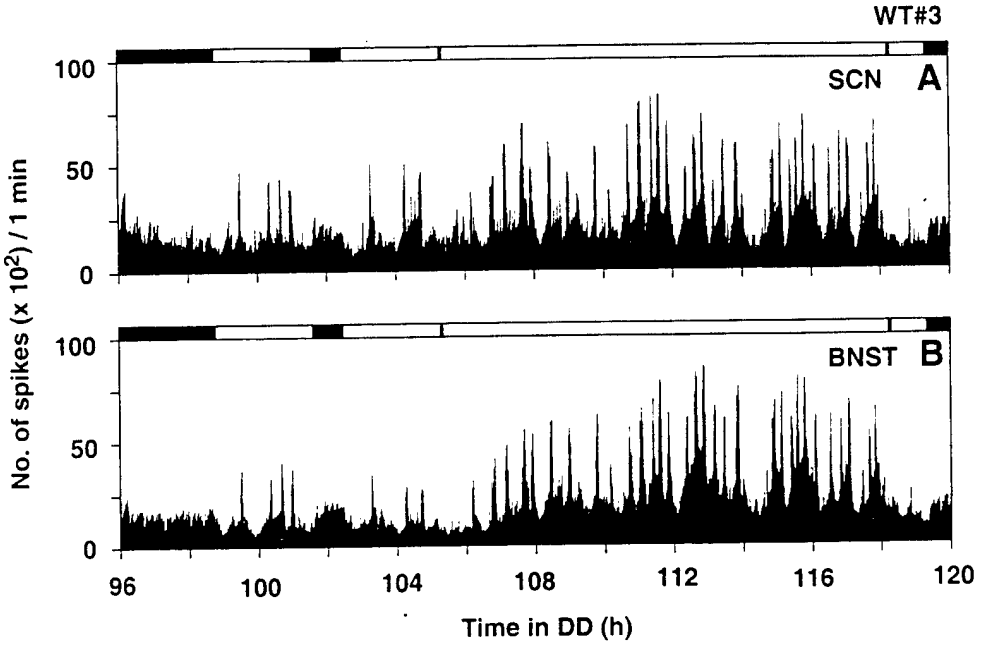

Figure 14. Ultradian rhythms of neural activity recorded from the SCN and the BNST in a wild-type hamster. *A*, Expanded plot of 24 hr neural activity record in 1 min bins from the SCN (from Fig. 12*A*, *double-headed arrow*). The *top bar* shows wheel-running activity, plotted as a *black bar* whenever the wheel revolved more than once in 6 min. *B*, Expanded plot of 24 hr neural activity record in 1 min bins from the BNST (from Fig. 12*B*, *double-headed arrow*). Note that both the 80 and 14 min ultradian rhythms are usually in-phase.

receives the retinal projection), light did not have an acute effect on the MUA.

Most regions outside of the SCN also showed clear daily or circadian rhythms (Fig. 2). The ventrolateral thalamic nucleus (n = 3), the CP (n = 3), the accumbens nucleus (n = 1), the medial septum (n = 1), the LS (n = 6), the ventromedial hypothalamic nucleus (n = 2), the medial preoptic region (n = 1), and the stria medullaris (n = 3) all exhibited circadian rhythms with peak impulse activity occurring at night or subjective night that, unlike the electrical activity rhythm in the SCN, was in-phase with locomotor activity. SSA of activity in the optic chiasm (n = 2) revealed no circadian components, but ultradian rhythms were present and were stronger in LD than in DD.

There were clear correlations between electrical activity in the SCN and in other brain regions. The data in Figure 3 were recorded from a wild-type hamster in DD. MUA from the SCN (Fig. 3*A*) and the LS (Fig. 3*B*) and wheel-running activity (Fig. 3*C*) were collected simultaneously; all three data sets contain significant circadian components. Figure 4 presents reconstructed waveforms of the circadian components using the SSA method. Circadian rhythms in the SCN (Fig. 4*A*) and LS (Fig. 4*B*) were tightly locked in an antiphase relationship (Fig. 4*C*). Their periods were matched to that of the wheel-running activity rhythm that was in antiphase to the SCN. The data in Figure 5 were recorded from a *tau* mutant hamster. MUA was recorded from the SCN (Fig. 5*A*) and CP (Fig. 5*B*). Both regions showed significant circadian rhythms that matched the 20 hr period of the wheel-running rhythm (Fig. 5*C*). The phase angle difference between these two brain regions was also stable in antiphase (Fig. 6; sometimes, as in this example, stable phase relationships did not develop the first cycle or two of constant darkness). Other examples (SCN and LS in a wild type, n = 1; SCN and ventrolateral thalamus in a wild type, n = 1; and SCN and ventrolateral thalamus in a *tau* mutant, n = 1) showed similar phase relationships.

Ultradian rhythms

MUA in the SCN and in other brain regions displayed ultradian components in addition to circadian ones. We succeeded in identifying a significant circadian component and two ultradian components from the time series data in all brain regions analyzed. Figure 7 shows an example of MUA recorded from the SCN in a *tau* mutant hamster in DD. As expected, an ~20 hr circadian component in antiphase to the wheel-running activity rhythm was present. The record also shows a clear ultradian component with a period of ~80 min. Furthermore, in expanded plots we could detect a higher frequency rhythm of ~14 min that was most clearly expressed around the peak of the 80 min oscillation.

Expanded plots of 24 hr segments recorded from the SCN (Fig. 3*A*) and the LS (Fig. 3*B*) of a wild-type hamster are shown in Figure 8, *A* and *B*, respectively. These data contain two ultradian components, ~80 and ~14 min. The two components were identified by spectral analysis and visual inspection, respectively. The time domain SSA reconstructions of the ~80 min ultradian oscillations in the SCN and the LS were in-phase with each other on the first day after transfer from LD to DD; however by the second day in DD they had shifted to an antiphase relationship (Fig. 9*A*,*B*). The ~14 min ultradian rhythms appeared to be in-phase between the SCN and the LS (Fig. 8). We obtained similar results from two other wild-type hamsters (recorded from the SCN and the ventrolateral thalamus or LS).

The ultradian components recorded from *tau* mutant hamsters also had periods of ~80 and ~14 min. Time series analysis and visual inspection of simultaneous recordings from the SCN and the CP in a *tau* mutant hamster revealed these two ultradian components (Fig. 10). In this data set the phase relationships of

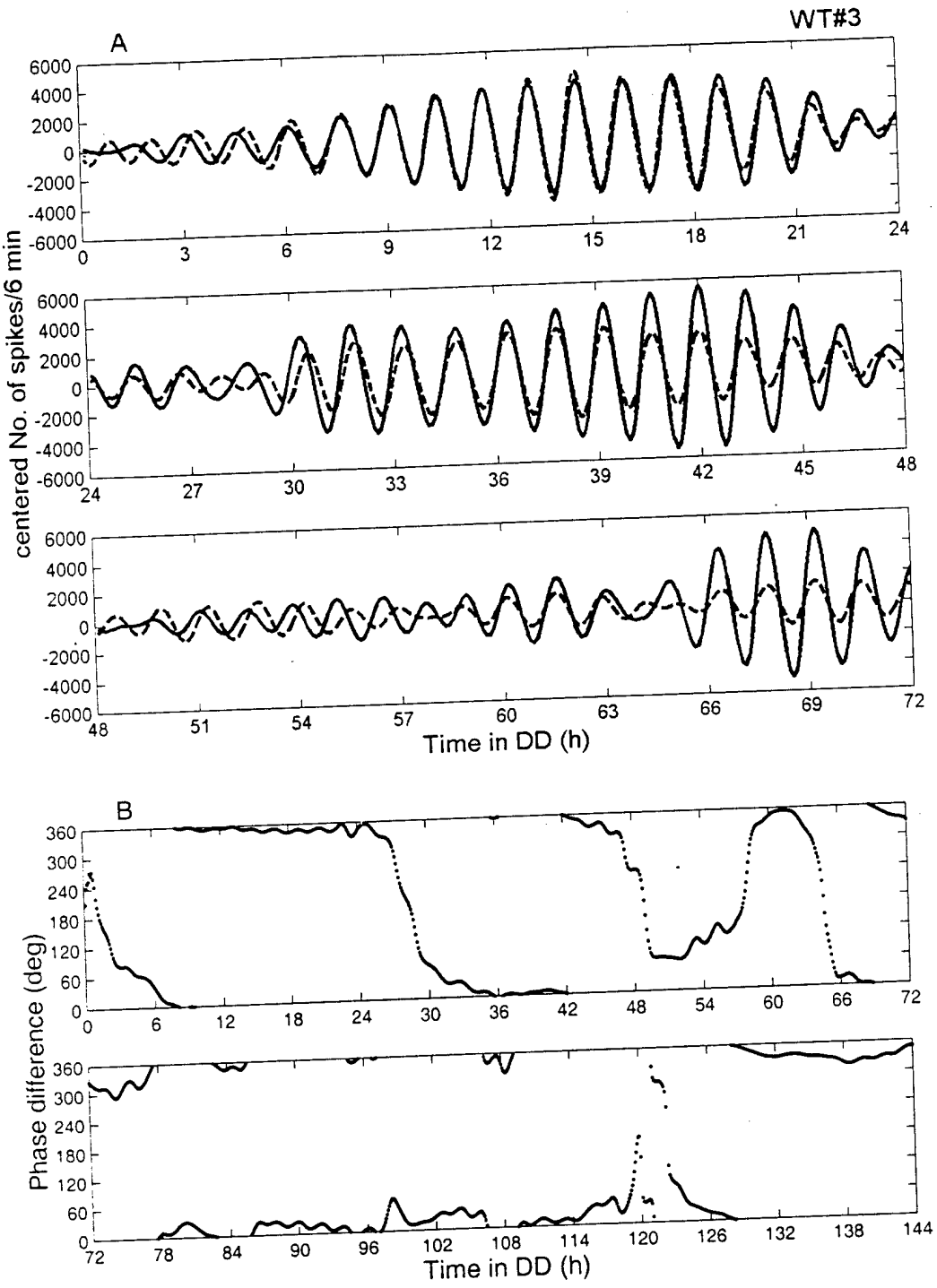

Figure 15. Mathematical analysis of the ultradian rhythms recorded from the SCN and the BNST in a wild-type hamster. *A*, Data reconstructed by SSA of the 80 min ultradian rhythms in the SCN (*solid line*) and the BNST (*dotted line*) for the first 72 hr of the record. *B*, Phase angle difference of the 80 min ultradian rhythms between the SCN and the BNST plotted for 144 hr (see text and Fig. 4 for details).

the 80 min oscillations in the two areas were often in antiphase, but their phase relationship was much less stable than in similar recordings from wild types (Fig. 11). As in wild types, the ~14 min rhythms always appeared to be in-phase (Fig. 10). A second *tau* mutant hamster in which electrical recordings were obtained from the SCN and the ventrolateral thalamus exhibited similar properties.

Effects of the *tau* mutation on the circadian and ultradian periods of MUA

The period of the rhythm of wheel-running activity in wild-type hamsters was ~24 hr and closely matched the circadian component of the electrical activity in the SCN. To assess the effect of the *tau* mutation on the rhythmic properties in the SCN, we obtained four 1-week-long recordings for analysis of the period of

the rhythm in DD. The ~20 hr period of wheel-running rhythms in *tau* mutants closely matched the circadian MUA rhythms in the SCN. There were no significant differences between wild type and *tau* mutants in the periods of the ultradian components (80 and 14 min). The variation in frequency among animals within each genotype was as great as that between genotypes (Table 1).

Effect of wheel running on MUA

Locomotor activity affects the expression of MUA in the SCN and elsewhere in the brain. MUA in the SCN was decreased during wheel running, whereas MUA in other areas was enhanced (Figs. 1–3, 5, 7, 8, 10). These changes in the levels of MUA were precisely correlated with locomotor activity and were more pronounced the more vigorously the animals ran in their wheels.

Phase of MUA in the BNST

In contrast to MUA from all other recording sites outside of the SCN, MUA recorded from the anteromedial part of the BNST exhibited oscillations (circadian and ultradian) in-phase with the SCN (Figs. 12, 13, 14, 15). As seen in the SCN and again in contrast to that seen at other sites, neural activity in the BNST was suppressed during wheel running (Figs. 12, 14). We also observed similar phase relationships in one recording from the posteromedial part of the BNST of a wild-type animal and from the anteromedial part of the BNST in one *tau* mutant.

DISCUSSION

Circadian rhythms in electrical activity

Inouye and Kawamura (1979) reported that the MUA in the SCN recorded from freely moving rats displayed a circadian rhythm with peak impulse frequency occurring during the day. They also recorded MUA circadian rhythms from regions outside the SCN that exhibited peak activity at night, out-of-phase with the SCN rhythm and in-phase with the animal's locomotor activity. Because MUA in the SCN remained rhythmic after the nucleus was isolated (within a hypothalamic island), while the rhythms outside of the SCN disappeared, they concluded that the circadian pacemaker was in the SCN and that rhythms outside the SCN were being driven (in antiphase) by the SCN (Inouye and Kawamura, 1982). Later, Yamazaki et al. (1994) showed that the circadian rhythm of ATP content in the SCN of rats is also in antiphase with this rhythm in the anterior hypothalamus and CP. Our results with hamsters are in good general agreement with the results in rats. We find that the circadian rhythms of MUA within the SCN are out-of-phase with those recorded from brain areas outside the SCN, with the important exception of the BNST, an area from which Inouye and Kawamura did not record.

We found that the period of the circadian rhythm in MUA both within and outside of the SCN was affected as expected by the *tau* mutation and matched the period of wheel-running behavior both in wild-type hamsters (~24 hr) and in *tau* mutants (~20 hr). Davies and Mason (1994) reported a circadian electrical activity rhythm with a period of ~20 hr from *tau* mutant SCN in acute slice preparation that was monitored for 36 hr. Liu et al. (1997) reported that circadian periodicities of electrical activity in SCN cells dispersed in cell culture from homozygous, heterozygous, and wild-type hamsters exhibit free-running periods that correlate with their genotype. Our results obtained *in vivo* confirm that the altered period of neuronal activity is expressed within the SCN of intact *tau* mutant hamsters. The correspondence of the *in vivo* with the *in vitro* results provides important confirmation of the usefulness of the *in vitro* model. We know that at least the normal period of the intact SCN is conserved in the dish.

The genetically determined period of the SCN is also conserved in transplantation experiments in which the locomotor rhythms restored by transplanted SCN tissue have the periods determined by the genotype of the donor not the host (Ralph et al., 1990; Vogelbaum and Menaker, 1992; Silver et al., 1996). However, the data of Silver et al. (1996) suggest strongly that in the transplant experiments the link between the transplanted tissue and the host's locomotor system is hormonal not neural. Therefore, although the several studies of SCN rhythmicity using *in vitro*, transplant, and *in vivo* methods are consistent, they leave open questions about the functional connections of the SCN with the motor control system. In particular, it will be important to determine the roles of both neural and humoral SCN outputs in controlling locomotor behavior in intact animals.

Ultradian rhythms

MUA from the SCN exhibited two different, clearly discernable ultradian components after several days in constant darkness. The 80 min ultradian rhythm was out-of-phase with other brain regions (except the BNST in which all rhythms were always in-phase with those in the SCN). However, immediately after transfer from LD to DD, the 80 min rhythms within and outside the SCN were temporarily in-phase. In the *tau* mutant, these rhythms sometimes ran independently. This suggests that 80 min ultradian pacemakers may be located both in and outside of the SCN and that the light/dark cycle may influence their phase relationships. A similar ultradian rhythm can be observed in figures published by Kawamura and Inouye (1979; their Fig. 5) and Inouye and Kawamura (1982; their Fig. 7), which show data from MUA recorded in rat within a hypothalamic island containing the SCN as well as outside of the island. That observation supports the idea that ultradian periodicities are generated from sites both within and outside the SCN. Recently, Meijer et al. (1997) found significant ultradian periods of 4 hr and 170, 130, and 100 min in rat SCN *in vivo* and a significant period of 3.5 hr in rat SCN *in vitro*. MUA from optic chiasm in hamster and rat (Inouye and Kawamura, 1979; Omata and Kawamura, 1988) has been reported to contain circadian components. However, in our recordings we observed only ultradian rhythms from this site.

The source and mechanism for the generation of ultradian periodicities within the brain are obscure, and there are many possible candidates [e.g., in the posterior hypothalamic area of the conscious rat, the release rates of the catecholamines and histamine fluctuate with the following periods: histamine, 83 min; dopamine and noradrenaline, 92 min; and adrenaline, 99 min (Dietl et al., 1992; Prast et al., 1992; Grass et al., 1996)].

Very short (~14 min) ultradian rhythms were present in all brain regions from which we recorded. Although not observable by our spectral analysis methods because of limitations in sampling frequency resolution and signal frequency variability, this periodicity was easily detectable visually in displays of the recordings. The rhythm was in-phase among all brain regions. The ~14 min period is significantly longer than an ultradian periodicity reported previously by Miller and Fuller (1992), who observed rhythms with periods of ~120 sec that were lengthened by retinal illumination in urethane-anesthetized rats.

We failed to find any differences in the periods of ultradian rhythms of *tau* mutant and wild-type hamsters, even though the circadian periodicity of the *tau* mutant is shortened by >15 percent. This suggests that the *tau* mutation may affect circadian

but not ultradian rhythms of MUA. This is in contrast to its effect on luteinizing hormone pulsatility (Loudon et al., 1994) and to the effect of mutations in the *per* gene in *Drosophila* that alter the periods of both circadian rhythms and high-frequency neural rhythms involved in the control of the courtship song (Kyriacou, 1990). However, our data do suggest that ultradian rhythms of MUA in *tau* mutants may have more variable periods and phase relationships than do those in wild types, although we are presently unable to quantify this difference.

Bed nucleus rhythmicity

Unexpectedly, and uniquely among all sites in which recordings have been made, the circadian rhythm of electrical activity in the BNST is in-phase with the SCN electrical activity rhythm. In a previous study Inouye (1983) recorded MUA from seven regions of the rat brain (not including the BNST), but only the SCN showed a circadian rhythm that peaked during the day; rhythms from all the other sites peaked at night. In our recordings, ultradian rhythms in the BNST were also in-phase with those in the SCN. Cross-spectral estimates suggest that the BNST and SCN are tightly coupled to each other (data not shown).

There is anatomical evidence that SCN efferent pathways reach the BNST (Kalsbeek et al., 1993; Morin et al., 1994). However, it does not appear that the BNST projects to the SCN (Numan and Numan, 1996). The BNST may therefore be part of an output pathway from the SCN to locomotor centers. This would be completely consistent with our data. The BNST is a complex nucleus with several subdivisions; it has been reported to be involved in the control of photoperiod measurement (Raitiere et al., 1995), maternal behavior (Numan and Numan, 1996), and mating behavior (Wood and Newman, 1993), all of which may be influenced by the circadian system. Our preliminary data from lesion studies suggest that the BNST may be involved in controlling the level and pattern of locomotor activity (Yamazaki et al., 1997).

Effects of locomotor activity on SCN electrical activity

Our data demonstrate that an animal's movements affect electrical activity in several brain areas. Wheel-running activity acutely decreased SCN (and BNST) neural activity and enhanced neural activity outside the SCN (see also Meijer et al., 1997). Although we were not able to determine the causal relationship involved (i.e., does increased activity in extra-SCN regions lead to inhibition of SCN activity or vice versa?), we believe that this finding has great potential significance. It is intriguing to speculate that reductions in SCN neural activity associated with locomotor activity may underlie the "nonphotic" phase shifts of circadian rhythms that are produced by vigorous wheel running (Reebs and Mrosovsky, 1989).

The work reported here represents a level of analysis of mammalian circadian organization that has been almost completely neglected since it was pioneered by Inouye and Kawamura 20 years ago. Technical and conceptual advances over the past two decades have made it more tractable, although it is still labor intensive. In spite of the inherent difficulty of obtaining it, knowledge of the dynamics of electrical activity in the several brain regions controlling circadian behavior in intact, unanesthetized animals is likely to be essential for an understanding of this important regulatory system.

REFERENCES

Bendat JS, Piersol AG (1986) The Hilbert transform. In: Random data: analysis and measurement procedures, 2nd Edition, pp 484–516. New York: Wiley.

Bergman H, Feingold A, Nini A, Raz A, Slovin H, Abeles M, Vaadia E (1998) Physiological aspects of information processing in the basal ganglia of normal and Parkinsonian primates. Trend Neurosci 21:32–38.

Bos NPA, Mirmiran M (1990) Circadian rhythms in spontaneous neuronal discharges of the cultured suprachiasmatic nucleus. Brain Res 511:158–162.

Davies IR, Mason R (1994) *Tau*-mutant hamster SCN clock neurons express a 20 h firing rate rhythm *in vitro*. NeuroReport 5:2165–2168.

Dietl H, Prast H, Philippu A (1992) Pulsatile release of catecholamines in the hypothalamus of conscious rats. Naunyn Schmiedebergs Arch Pharmacol 347:28–33.

Edgar DM, Martin CE, Dement WC (1991) Activity feedback to the mammalian circadian pacemaker: influence on observed measures of rhythm period length. J Biol Rhythms 6:185–199.

Elsner JB, Tsonis AA (1996) Singular spectrum analysis: a new tool in time series analysis. New York: Plenum.

Fisher NI (1995) Statistical analysis of circular data. Cambridge, UK: Cambridge UP.

Grass K, Prast H, Philippu A (1996) Influence of mediobasal hypothalamic lesion and catecholamine receptor antagonists on ultradian rhythm of EEG in the posterior hypothalamus of the rat. Neurosci Lett 207:93–96.

Green DJ, Gillette R (1982) Circadian rhythm of firing rate recorded from single cells in the rat suprachiasmatic brain slice. Brain Res 245:198–200.

Groos G, Hendricks I (1982) Circadian rhythms in electrical discharge of rat suprachiasmatic neurons recorded *in vitro*. Neurosci Lett 34:283–288.

Herzog ED, Geusz ME, Khalsa SBS, Straume M, Block GD (1997) Circadian rhythms in mouse suprachiasmatic nucleus explants on multimicroelectrode plates. Brain Res 757:285–290.

Inouye S-IT (1983) Does the ventromedial hypothalamic nucleus contain a self-sustained circadian oscillator associated with periodic feedings? Brain Res 279:53–63.

Inouye S-IT, Kawamura H (1979) Persistence of circadian rhythmicity in a mammalian hypothalamic "island" containing the suprachiasmatic nucleus. Proc Natl Acad Sci USA 76:5962–5966.

Inouye S-IT, Kawamura H (1982) Characteristics of a circadian pacemaker in the suprachiasmatic nucleus. J Comp Physiol [A] 146:153–160.

Kalsbeek A, Teclemariam-Mesbah R, Pevet P (1993) Efferent projections of the suprachiasmatic nucleus in the golden hamster (*Mesocricetus auratus*). J Comp Neurol 332:293–314.

Kawamura H, Inouye S-IT (1979) Circadian rhythm in a hypothalamic island containing the suprachiasmatic nucleus. In: Biological rhythms and their central mechanism (Suda M, Hayaishi O, Nakagawa H, eds), pp 335–341. Amsterdam: Elsevier Science.

Klein DC, Moore RY, Reppert SM (1991) Suprachiasmatic nucleus: the mind's clock. New York: Oxford UP.

Kyriacou CP (1990) The molecular ethology of the *period* gene in *Drosophila*. Behav Genet 20:191–211.

Lehman MN, Silver R, Gladstone WR, Kahn RM, Gibson M, Bittman EL (1987) Circadian rhythmicity restored by neural transplant: immunocytochemical characterization of the graft and its integration with the host brain. J Neurosci 7:1626–1638.

Liu C, Weaver DR, Strogatz SH, Reppert SM (1997) Cellular construction of a circadian clock: period determination in the suprachiasmatic nuclei. Cell 91:855–860.

Loudon ASI, Wayne NL, Krieg R, Iranmanesh A, Veldhuis JD, Menaker M (1994) Ultradian endocrine rhythms are altered by a circadian mutation in the Syrian hamster. Endocrinology 135:712–718.

Marchant EG, Mistlberger RE (1996) Entrainment and phase shifting of circadian rhythms in mice by forced treadmill running. Physiol Behav 60:657–663.

Meijer JH, Rietveld WJ (1989) Neurophysiology of the suprachiasmatic circadian pacemaker in rodents. Physiol Rev 69:671–707.

Meijer JH, Schaap J, Watanabe K, Albus H (1997) Multiunit activity recordings in the suprachiasmatic nuclei: in vivo versus in vitro models. Brain Res 753:322–327.

Miller JD, Fuller CA (1992) Isoperiodic neuronal activity in suprachiasmatic nucleus of the rat. Am J Physiol 263:R51–R58.

Moore RY, Eichler VB (1972) Loss of a circadian adrenal corticosterone rhythm following suprachiasmatic nucleus lesions in the rat. Brain Res 42:201–206.

Morin LP, Goodless-Sanchez N, Smale L, Moore RY (1994) Projection of the suprachiasmatic nuclei, subparaventricular zone and retrochiasmatic area in the golden hamster. Neuroscience 61:391–410.

Mrosovsky N (1988) Phase response curves for social entrainment. J Comp Physiol [A] 162:35–46.

Murakami N, Takamure M, Takahashi K, Utunomiya K, Kuroda H, Etoh T (1991) Long-term cultured neurons from rat suprachiasmatic nucleus retain the capacity for circadian oscillation of vasopressin release. Brain Res 545:347–350.

Numan M, Numan M (1996) A lesion and neuroanatomical tract-tracing analysis of the role of the bed nucleus of the stria terminalis in retrieval behavior and other aspects of maternal responsiveness in rats. Dev Psychobiol 29:23–51.

Omata K, Kawamura H (1988) Effect of methamphetamine upon circadian rhythms in multiple unit activity inside and outside the suprachiasmatic nucleus in the golden hamster (*Mesocricetus auratus*). Neurosci Lett 95:218–222.

Prast H, Dietl H, Philippu A (1992) Pulsatile release of histamine in the hypothalamus of conscious rats. J Auton Nerv Syst 39:105–110.

Raitiere MN, Garyfallou VT, Urbanski HF (1995) Lesions in the bed nucleus of the stria terminalis, but not in the lateral septum, inhibit short-photoperiod-induced testicular regression in Syrian hamsters. Brain Res 705:159–167.

Ralph MR, Foster RG, Davis FC, Menaker M (1990) Transplanted suprachiasmatic nucleus determines circadian period. Science 247:975–978.

Reebs SG, Mrosovsky N (1989) Effects of induced wheel running on the circadian activity rhythms of Syrian hamsters: entrainment and phase response curve. J Biol Rhythms 4:39–48.

Rusak B, Zucker I (1979) Neural regulation of circadian rhythms. Physiol Rev 59:449–526.

Sawaki Y, Nihonmatsu I, Kawamura H (1984) Transplantation of the neonatal suprachiasmatic nuclei into rats with complete bilateral suprachiasmatic lesions. Neurosci Res 1:67–72.

Shibata S, Moore RY (1988) Electrical and metabolic activity of suprachiasmatic nucleus neurons in hamster hypothalamic slices. Brain Res 438:374–378.

Shinohara K, Honma S, Katsno Y, Abe H, Honma K (1995) Two distinct oscillators in the rat suprachiasmatic nucleus *in vitro*. Proc Natl Acad Sci USA 92:7396–7400.

Shioiri T, Takahashi K, Yamada N, Takahashi S (1990) Motor activity correlates negatively with free-running period, while positively with serotonin contents in SCN in free-running rats. Physiol Behav 49:779–786.

Silver R, LeSauter J, Tresco PA, Lehman MN (1996) A diffusible coupling signal from the transplanted suprachiasmatic nucleus controlling circadian locomotor rhythms. Nature 382:810–813.

Stephan FK, Zucker I (1972) Circadian rhythms in drinking behavior and locomotor activity of rats are eliminated by hypothalamic lesions. Proc Natl Acad Sci USA 69:1583–1586.

Thomson DJ (1982) Spectrum estimation and harmonic analysis. Proc IEEE 70:1055–1096.

Turek FW (1985) Circadian neural rhythms in mammals. Annu Rev Physiol 47:49–64.

van Reeth O, Losee-Olson S, Turek FW (1987) Phase shifts in the circadian activity rhythm induced by triazolam are not mediated by the eyes or the pineal gland in the hamster. Neurosci Lett 80:185–190.

Vautard R, Yiou P, Ghil M (1992) Singular-spectrum analysis: a toolkit for short, noisy chaotic signals. Physica D 58:95–126.

Vogelbaum MA, Menaker M (1992) Temporal chimeras produced by hypothalamic transplants. J Neurosci 12:3619–3627.

Watanabe K, Koibuchi N, Ohtake H, Yamaoka S (1993) Circadian rhythms of vasopressin release in primary cultures of rat suprachiasmatic nucleus. Brain Res 624:115–120.

Welsh DK, Logothetis DE, Meister M, Reppert SM (1995) Individual neurons dissociated from rat suprachiasmatic nucleus express independently phased circadian firing rhythms. Neuron 14:697–706.

Wichmann T, Vitek JL, DeLong MR (1995) Parkinson's disease and the basal ganglia: lessons from the laboratory and from neurosurgery. The Neuroscientist 1:236–244.

Wood RI, Newman SW (1993) Mating activates androgen receptor-containing neurons in chemosensory pathways of the male Syrian hamster brain. Brain Res 614:65–77.

Yamada N, Shimoda K, Ohi K, Takahashi S, Takahashi K (1988) Free-access to a running wheel shortens the period of free-running rhythm in blinded rats. Physiol Behav 42:87–91.

Yamada N, Shimoda K, Takahashi K, Takahashi S (1990) Relationship between free-running period and motor activity in blinded rats. Brain Res Bull 25:115–119.

Yamazaki S, Ishida Y, Inouye S-IT (1994) Circadian rhythms of adenosine triphosphate contents in the suprachiasmatic nucleus, anterior hypothalamic area and caudate putamen of the rat: negative correlation with electrical activity. Brain Res 664:237–240.

Yamazaki S, Alones VE, Block GD, Menaker M (1997) Functional connection between the circadian and motor systems. Soc Neurosci Abstr 23:790.

Modeling the Dual Pacemaker System of the *tau* Mutant Hamster

Gisele A. Oda, Michael Menaker, and W. Otto Friesen[1]
Department of Biology, NSF Center for Biological Timing, University of Virginia, Charlottesville, VA 22903-2477, USA

Abstract Circadian pacemakers in many animals are compound. In rodents, a two-oscillator model of the pacemaker comprising an evening (*E*) and a morning (*M*) oscillator has been proposed based on the phenomenon of "splitting" and bimodal activity peaks. The authors describe computer simulations of the pacemaker in *tau* mutant hamsters viewed as a system of mutually coupled *E* and *M* oscillators. These mutant animals exhibit normal type 1 PRCs when released into DD but make a transition to a type 0 PRC when held for many weeks in DD. The two-oscillator model describes particularly well some recent behavioral experiments on these hamsters. The authors sought to determine the relationships between oscillator amplitude, period, PRC, and activity duration through computer simulations. Two complementary approaches proved useful for analyzing weakly coupled oscillator systems. The authors adopted a "distinct oscillators" view when considering the component *E* and *M* oscillators and a "system" view when considering the system as a whole. For strongly coupled systems, only the system view is appropriate. The simulations lead the authors to two primary conjectures: (1) the total amplitude of the pacemaker system in *tau* mutant hamsters is less than in the wild-type animals, and (2) the coupling between the unit *E* and *M* oscillators is weakened during continuous exposure of hamsters to DD. As coupling strength decreases, activity duration (α) increases due to a greater phase difference between *E* and *M*. At the same time, the total amplitude of the system decreases, causing an increase in observable PRC amplitudes. Reduced coupling also increases the relative autonomy of the unit oscillators. The relatively autonomous phase shifts of *E* and *M* oscillators can account for both immediate compression and expansion of activity bands in *tau* mutant and wild-type hamsters subjected to light pulses.

Key words circadian rhythm, computer simulation, limit cycles, oscillators, coupling, period mutants

Two properties of the circadian pacemaker play central roles in the mechanism of its entrainment by light-dark cycles: its free-running period (τ) and its phase response curve (PRC). The PRC shape and amplitude define the phase relationship attained by an oscillator of period τ for a given light cycle and also determine its limits of entrainment (Daan and Pittendrigh, 1976). Organisms with τ altered by genetic mutations offer a good opportunity to approach an explanation of the mechanistic interconnections between τ and the PRC (Menaker, 1992; Menaker and Takahashi, 1995).

1. To whom all correspondence should be addressed.

JOURNAL OF BIOLOGICAL RHYTHMS, Vol. 15 No. 3, July 2000 1-19

Comparative PRCs for period mutant organisms were performed first for eclosion rhythms (Konopka, 1979) and later for activity rhythms (Saunders et al., 1994) in *Drosophila* and in *Neurospora* (Dharmananda, 1980). In *Drosophila*, the *per* short mutation led to a change in the PRC from a low-amplitude type 1 to a high-amplitude type 0. In *Neurospora*, different period mutants presented a correlation between period decreases and phase response increases, with the short period mutants presenting type 0 PRCs. Comparative studies of PRCs in wild-type ($\tau \cong 24$ h) and homozygous *tau* mutant ($\tau \cong 20$ h) hamsters were performed by Menaker and his coworkers (Shimomura and Menaker, 1994; Menaker et al., 1994; Menaker and Refinetti, 1992). In these studies, wild-type hamsters were initially maintained on 24-h and *tau* mutants on 20-h light-dark (LD) cycles. The animals were then transferred to constant darkness (DD) and PRCs subsequently measured after 7 days and 49 days. When tested after 7 days in DD, wild-type and *tau* mutant hamsters exhibited identical type 1 PRCs (Fig. 1A). Remarkably, during 49 days in DD, the *tau* mutant PRC amplitude increased progressively, until a transition to type 0 PRC was observed (Fig. 1B). The wild-type PRC, on the other hand, remained largely unchanged after 49 days in DD (data not shown).

The second remarkable behavioral effect of prolonged exposure to DD in hamsters was the gradual lengthening of the activity time (α) observed in both wild-type (S. Yamazaki, data not shown) and *tau* mutant hamsters (Fig. 1C). In another set of experiments, groups of *tau* mutant hamsters were maintained in various T-cycles and then subjected to light pulses. In these experiments, there was a direct correlation between the amplitude of phase shifts for each experimental group and the corresponding α lengths caused by the different T-cycles (Shimomura and Menaker, 1994).

Pittendrigh and Daan (1976b) proposed that the pacemaker in many animals is compound, comprising at least evening (E) and morning (M) oscillators. Two bouts of activity are considered, the first controlled by the *E* oscillator and the second by the *M* oscillator. The resulting activity has duration α; hence, the value of α reflects the phase relationship between *E* and *M*. Their proposition was based on the observation of "splitting" of animal activity into two distinct components and of bimodal activity peaks in some animals. These often-covert components become evident when lighting conditions are altered. This two-oscillator model was explored theoretically by Daan and Berde (1978),

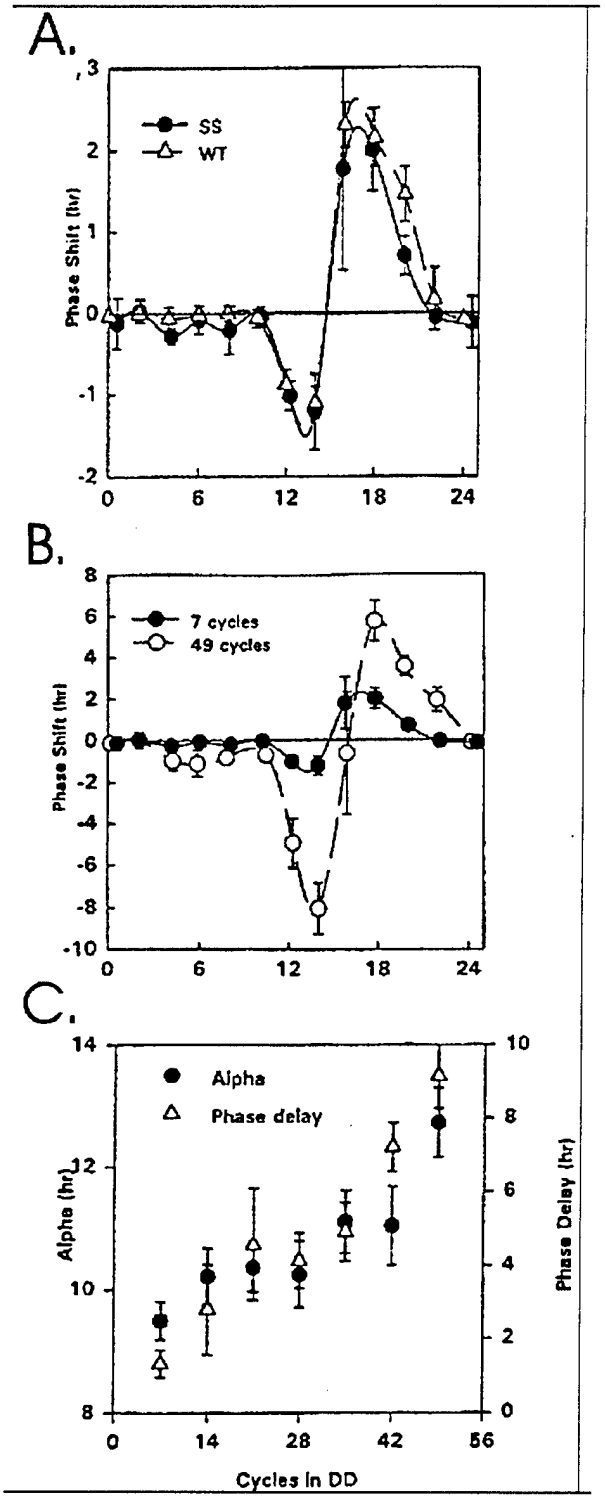

Figure 1. Phase response curves measured at 2-h intervals. (A) PRC of homozygous *tau* mutant hamsters (filled circles, SS) and a wild-type PRC (open triangles, WT) obtained by Takahashi et al. (1984) after 7 days of DD are replotted on equivalent circadian coordinates. Standard errors are indicated by the bars or are within the symbols. (B) PRCs of homozygous *tau* mutant hamsters after 7 (filled circles) and 49 (open circles) days in constant

darkness. (C) Relationship between increase in activity time (filled circles, alpha) and increase in light-induced phase delay (open triangles, phase delay) with increased number of days in constant darkness in homozygous *tau* mutant hamsters. Alpha estimated by naive observers; bars indicate standard errors. From Shimomura and Menaker (1994). ~~[*AUTHOR: PLEASE PROVIDE PERMISSION IF FIGURE WAS TAKEN DIRECTLY FROM THIS SOURCE*]~~

Kawato and Suzuki (1980), Kawato (1985), and Mori et al. (1994). The two-oscillator model explains the results of many experiments on hamsters (Pittendrigh and Daan 1976b; Elliot and Tamarkin, 1994; Gorman et al., 1998), and therefore we employ it here.

The coupling of oscillators adds greatly to the difficulty of understanding the interdependence of τ and PRC shapes because it is necessary to consider the intrinsic properties of the constituent oscillators, the nature of the coupling, and the emergent properties of the coupled system. We describe here our computer simulations of the *tau* mutant hamster pacemaker viewed as a system of mutually coupled *E* and *M* oscillators. Our aim was to determine the relationships between oscillator amplitude, period, PRC, and activity duration. During these analyses, we found that two complementary approaches are useful for analyzing such coupled oscillator systems. When the system is weakly coupled, we can employ either a "distinct oscillators" view in considering the properties of the separate components and a "system" view when considering the emergent properties of the system as a whole. For strongly coupled systems, only the system view is appropriate.

THE MODEL

Our modeling analyses were aimed primarily toward an analysis of the results of experiments on hamsters performed by Shimomura and Menaker (1994).

Our model pacemaker system is based on a set of two identical Pittendrigh-Pavlidis equations to simulate the *E* and *M* oscillators. These equations, developed by Pavlidis, capture many of the formal properties of the *Drosophila* eclosion pacemaker (Pavlidis, 1967) and were examined extensively by Pittendrigh et al. (1991). Each oscillator, *E* or *M*, is described by two first-order nonlinear differential equations. State variables (*R* and *S*, which are the same letters employed by Pittendrigh) are indexed by *E* and *M* to designate the specific oscillator. We assume that evening and morning oscillators are identical; thus, subscripts are omitted when they refer to identical parameter values. The following equations describe the coupled oscillator system:

Evening oscillator (*E*):

$$dR_E/dt = R_E - cS_E - bS_E^2 + (d - L) + K, \quad (1)$$

$$dS_E/dt = R_E - aS_E + C_{ME}S_M. \quad (2)$$

Morning oscillator (*M*):

$$dR_M/dt = R_M - cS_M - bS_M^2 + (d - L) + K, \quad (3)$$

$$dS_M/dt = R_M - aS_M + C_{EM}S_E. \quad (4)$$

Four parameters describe the morning and evening oscillators: *a*, *b*, *c*, and *d*. Each set of equations includes a small nonlinear term, K ($K = k_1/(1 + k_2R^2)$, $k_1 = 1$, $k_2 = 100$), formulated by W. T. Kyner (Pittendrigh and Kyner, personal communication, ***YEAR?***) to make the equations smoother. The effect of light on the system is mediated by the term *L*. Positive values of *L* correspond to light pulses of amplitude *L*. Light-pulse duration is that interval during which *L* is nonzero.

We define A_M and A_E, respectively, as the amplitudes of the *M* and *E* oscillators, with each term computed as follows (see appendix):

$$A_M = A(R_M) + A(S_M) \text{ and } A_E = A(R_E) + A(S_E).$$

The amplitude term, $A(R_M)$, is the peak-to-trough excursion of state variable *R* for the morning oscillator, and $A(S_M)$ is the peak-to-trough excursion of the *S* variable for the morning oscillator. The amplitudes for the evening oscillators have similar nomenclature (Fig. 2A).

The coupling term C_{ME} defines the effect that the *M* has on *E*; equivalently, C_{EM} defines the effect that *E* has on *M*. Coupling is linear, mediated through actions on the *S* variable for each oscillator. For most simulations, coupling strengths between oscillators are of equal amplitude but have opposite sign, with positive C_{ME} and negative C_{EM}. Positive C_{ME} implies that the morning oscillator drives the evening one. Similarly, negative C_{ME} causes the evening oscillator to retard the morning one. The consequence of this coupling scheme is that *E* phase-leads and has smaller amplitude than *M*, even though the equations for the two oscillators are otherwise identical.

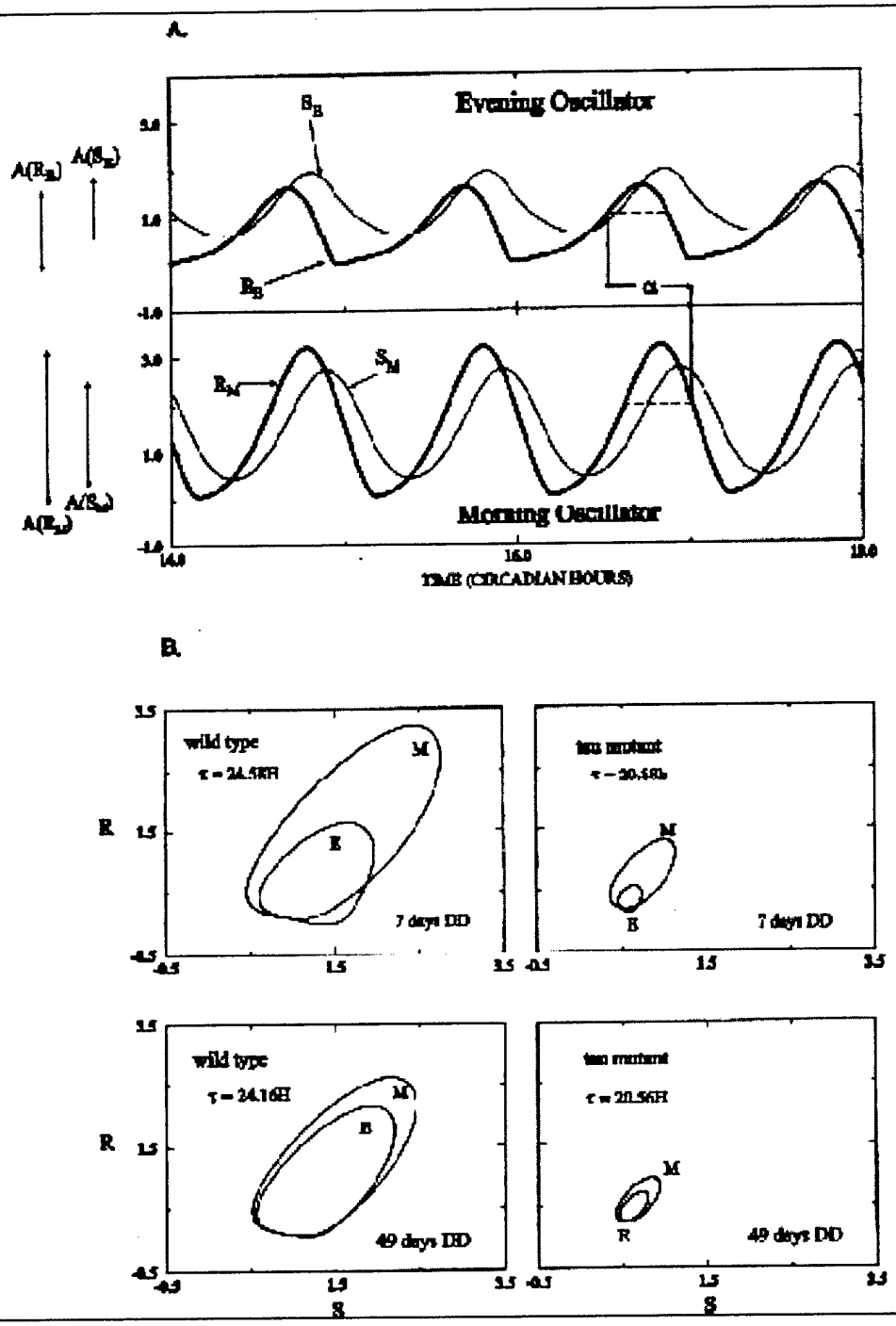

Figure 2. Simulations of the *E* and *M* oscillators. The graphs are of CircadianDynamix-generated plots of the state variables (R_E, S_E, R_M, and S_M) of the *E* and *M* oscillators. (A) Time-series graphs, wild-type, 7 days in DD. The upper and lower traces show the simultaneous and instantaneous values of the four state variables of the pacemaker system. Note that the *E* oscillator has lower amplitude, and phase leads the *M* oscillator. Amplitudes (lengths of bars: $A(R_E)$, $A(S_E)$, $A(R_M)$, and $A(S_M)$) are the peak-to-trough excursions of the respective variables. The duration of simulated hamster running wheel activity, α, is the interval between the beginning of activity set by the evening oscillator (time point at which R_E exceeds 2/3 of its maximum value-dashed line in the upper panel) and the end of the activity set by the *M* oscillator (time point at which R_M exceeds 2/3 of its maximum value-dashed line in the lower panel). (B) Phase plane plots of state variables for wild-type and *tau* mutant hamster simulations. The simulated system comprises two limit cycle oscillators, each defined by *R* and *S* variables. Note the smaller size of the limit cycles in the *tau* mutant simulations. Coupling strengths of the simulations of hamsters after 7 days DD were set to $C_{ME} = 0.2$ and $C_{EM} = -0.2$. For the simulations of hamsters after 49 days DD, they were set to $C_{ME} = 0.05$ and $C_{EM} = -0.05$. Parameter values for the wild type are ($a = 0.85$, $b = 0.3$, $c = 0.8$, $d = 0.5$) and for the *tau* mutant are ($a = 0.85$, $b = 0.3$, $c = 1.5$, $d = 0.5$).

We used Pittendrigh's standard set of parameters, except for the parameter a, as follows: $a = 0.85$, $b = 0.3$, $c = 0.8$, $d = 0.5$ (developed for *Drosophila* eclosion simulations) (Pittendrigh et al., 1991) to generate a 24-h "wild-type" circadian oscillator. The Pittendrigh-Pavlidis equations were used for their great convenience, even though they lead to PRCs that have larger delay than advance regions, opposite to what the hamsters show (Daan and Pittendrigh, 1976; Johnson, 1992). This difference, however, affects only one aspect of our work, as we will indicate later. To obtain simulations of the *tau* mutant hamster pacemaker, we altered only one value in this basic parameter set; namely, we increased the value of c from 0.8 to 1.5 (see appendix). This single change reduces the oscillator period to 20 h and hence mimics the period of the homozygous *tau* mutant hamster. All other parameters are identical for both wild-type and *tau* mutant simulations. Circadian time (CT) is normalized, so that one circadian hour always corresponds to the period τ divided by 24.

In this model, the analog of running wheel activity occurs every time the variable R in either the morning or evening oscillator is above some threshold value, which we set to 2/3 of the amplitude of this variable (Fig. 2A). As a result, we have an activity band whose total duration includes a first subband controlled by E and a second one controlled by M. The length of the total activity (α) thus reflects the phase relationship between E and M oscillators. The onset of activity was assigned as the phase reference point for circadian time 12.00 h. Model assumptions are summarized in the Discussion section.

We explored the properties of the coupled pacemaker system described by these equations with CircadianDynamix, a computer program that is an extension of NeuroDynamix, originally developed to explore the properties of neurons and small neuronal networks (Friesen and Friesen, 1994; Angstadt and Friesen, 1995). (Another variation of this program, CalciumDynamix, helped provide new insights into mechanisms underlying intracellular calcium oscillations [Friesen et al., 1995].) In this program, the responses of oscillators can be simulated under conditions of constant darkness, constant light, and single- or double-pulse light entrainment paradigms. The instantaneous values of state variables are displayed as time-series graphs or as phase plane plots. Simulated animal running wheel activity is shown as actograms, with onset of activity at CT 12. Finally, CircadianDynamix displays instantaneous values for many computed quantities, including amplitude, period, and phase. Two sets of paired oscillators are included in the program. An "experimental" set of oscillators can be manipulated by light sources. A second set of identical oscillators, which are unaffected by such manipulations, serve as controls. Thus, the values of simulated light-induced phase shifts are determined by a comparison between phase reference points on the experimental and control oscillators.

SIMULATIONS

One of our central aims was to provide an explanation for the differences in the PRCs of wild-type and *tau* mutant hamsters assessed 7 days and 49 days in DD after being held under LD 14:10 and LD 11.7:8.3 conditions, respectively (Shimomura and Menaker, 1994). Our central assumption is that prolonged exposure to DD reduces the coupling strength between the morning and evening oscillators in both wild-type and *tau* mutant hamsters. The idea is that after 7 days in DD, hamsters exhibit the aftereffects of their previous light schedules, thus showing a configuration of stronger coupling. After 49 days in DD, on the other hand, they exhibit their new state, that is, weaker coupling. Thus, for simulations of the pacemakers in both hamster strains after 7 days in DD, we set the coupling strengths (C_{ME} and C_{EM}) to relatively large values. To simulate the state of the pacemaker systems after prolonged DD (49 days), we reduced the values of the coupling constants. The resulting limit cycles of wild-type and *tau* mutant hamsters' dual pacemakers are shown in Fig. 2B. In all simulations, the duration of the light pulse was set to 1.0 h with amplitude 1.1—an arbitrary unit of intensity.

For maximum realism, we simulated the effect of long-term exposure to DD by a stepwise decrease in the coupling strength between the E and M oscillators, for both control and experimental oscillator systems. With coupling strength for C_{ME} ranging from 0.2 to 0.05 (correspondingly, C_{EM} ranging from −0.2 to −0.05), we conducted computer experiments to determine the shapes and amplitudes of PRCs in both wild-type and *tau* mutant hamsters. The most striking results of these simulations are that changes in coupling strength hardly altered the shape of the PRC for simulations of wild-type animals (Fig. 3A), whereas the PRC amplitude in *tau* mutant simulations increased progressively as coupling strength was decreased (simulating progressively longer exposure to DD). At the weakest

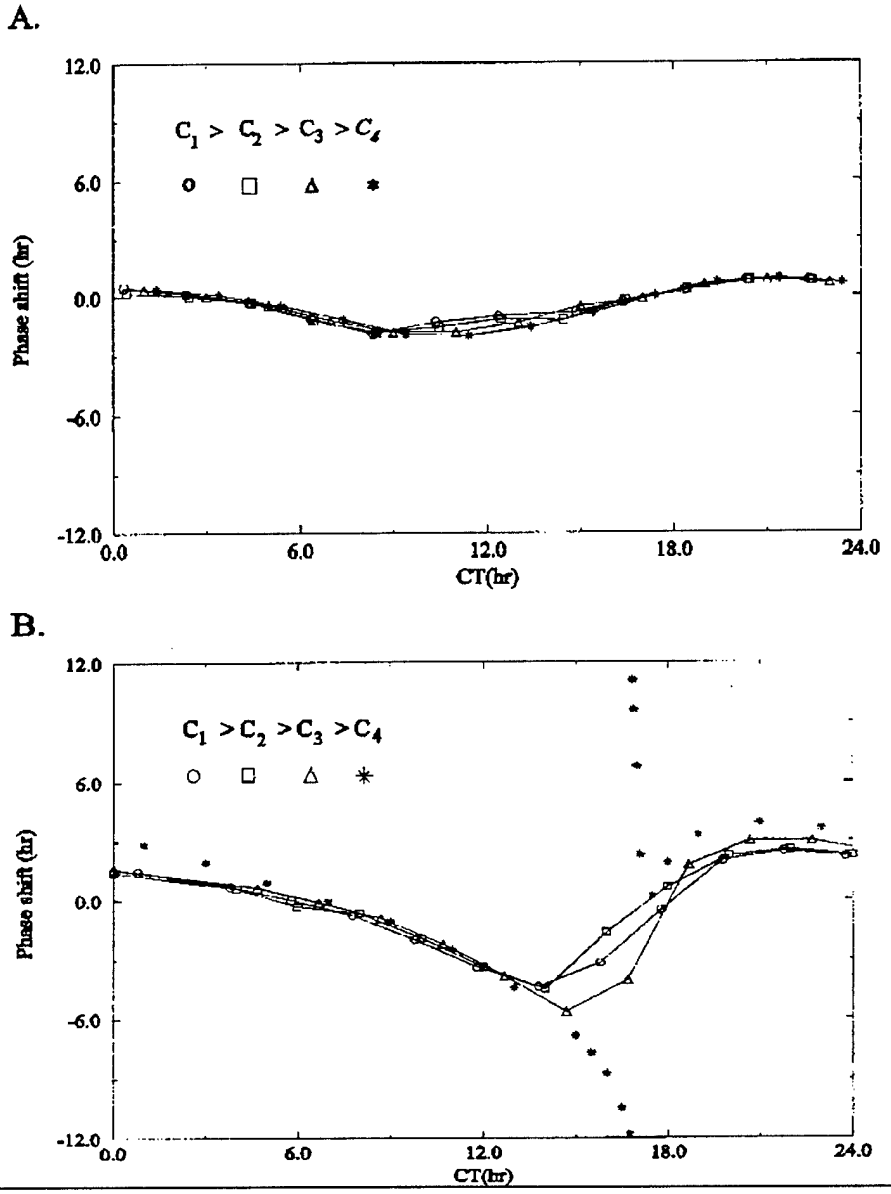

Figure 3. Effect of coupling strength on PRC amplitude. The graphs illustrate PRC alterations during long-term exposure of hamsters to DD simulated as a stepwise decrease in the coupling strength between *E* and *M*. (A) PRC of wild-type pacemaker ($a = 0.85, b = 0.3, c = 0.8, d = 0.5$). Reduction of coupling strengths has little effect on PRC amplitude or shape. (B) PRC of *tau* mutant pacemaker ($a = 0.85, b = 0.3, c = 1.5, d = 0.5$). Note that decreasing coupling strengths causes increases in PRC amplitude. For the weakest coupling, C4, there is a transition to a type 0 PRC. Light-pulse intensity: $L = 1.1$; pulse duration = 1.0 h (clock time, not circadian hours). PRCs were obtained with CircadianDynamix programmed to simulate identical *E* and *M* Pittendrigh-Pavlidis oscillators. Coupling strength [$C_{ME} = C$, $C_{EM} = -C$]: C_1 (open circles) = 0.25; C_2 (open squares) = 0.2; C_3 (open triangles) = 0.1; C_4 (*) = 0.05.

coupling strength employed, the *tau* mutant PRC showed a transition from type 1 to type 0 (Fig. 3B). These results successfully replicate the PRC alterations observed in the experiments on hamsters (Fig. 1). We also found that reduced coupling strength increases the values of α in simulations of the activity rhythms of both systems.

Two Views of Coupled Oscillators

To understand the mathematical basis of the simulated behaviors described above, we first sought to understand the relationship of the PRC of the coupled pacemaker system to those of the constituent oscillators. That is, we asked, "For the hamster, is the system

PRC some average of the intrinsic PRCs of *E* and *M* oscillators?" If so, how is the system PRC amplitude and shape affected by the phase relationship between the unit oscillators? Here we argue that the coupled system should be viewed differently, depending on the strength of coupling between the oscillator units. Most generally, the coupled system has to be considered as a whole unit, and we cannot associate the PRC of the system with the intrinsic PRCs of the components. We call this a "system" view. Nevertheless, weak coupling strength ensures preservation of the intrinsic properties for each oscillator. In this case, we can estimate the PRC of the system from the intrinsic PRC of the components. For such weak coupling, we can adopt a distinct oscillator view for some analytical purposes. We consider the two views in this section. The experiments by Shimomura and Menaker (1994) can only be explained by adopting the system view, but some features of the hamsters' oscillators are better understood by adopting the distinct oscillators view.

The System View

When the coupling is strong, the unit *E* and *M* oscillators begin to lose their original identities, including intrinsic periods, amplitudes, wave shapes, and PRCs. Instead, the properties meld into the corresponding properties of the system. Therefore, we cannot estimate the PRC of the coupled system from the intrinsic PRCs of free oscillators. Instead, the PRC can only be described for the system. Furthermore, with strong coupling, the activity bands controlled by *E* and *M* become cohesive because the phase relationship between them is always maintained. That is, the beginning and end of the activity bands tend to shift equally to the steady-state value when subjected to light pulses.

According to Lakin-Thomas et al. (1991), the phase shift magnitude of an independent oscillator depends on (1) impulse intensity (the greater the impulse, the larger the phase shift) and (2) the amplitude of oscillations (i.e., smaller oscillator amplitudes lead to the larger phase shifts). Here we extend Lakin-Thomas's principle to the coupled oscillator system. We first define the amplitude for a coupled system comprising two unit oscillators and then analyze the interrelationships between systems properties, including coupling strength, α, PRC amplitude, and system amplitude.

We completed a series of three simulations to study the nature of strongly coupled systems using CircadianDynamix. Our principal aim was to understand, systematically, why a direct correlation exists between α (which reflects the phase relationship between *E* and *M*) and phase shift magnitude in *tau* mutant hamsters (Fig. 1C). We show below that this correlation is indeed mediated by the system amplitude changes as follows. Through simulation set 1, we show that phase shift magnitude is determined directly by the component amplitudes of the system, A_E and A_M, and not by α. In simulation set 2, we show that this magnitude is indeed determined by the sum of A_E and A_M, which we call total amplitude (A_T) of the system. Finally, via simulation set 3, we show that the negative correlation between PRC and A_T holds generally; it is independent of specific system parameters.

Table 1. Summary of results from simulation set 1. Arrows indicate changes in parameter values (column 1) and the consequences for the system (columns 2-4).

$a\uparrow$	$\tau\uparrow$	$A_E, A_M\uparrow$	$\alpha\downarrow$
$b\uparrow$	$\tau\downarrow$	$A_E, A_M\downarrow$	$\alpha\downarrow$
$c\uparrow$	$\tau\downarrow$	$A_E, A_M\downarrow$	$\alpha\uparrow$
$d\uparrow$	$\tau\downarrow$	$A_E, A_M\uparrow$	$\alpha\downarrow$

Simulation Set 1: Interrelationships between PRC Amplitude, α, and Oscillator Amplitudes

In these simulations, we determined if phase shift magnitude is affected directly by α or indirectly, via oscillator amplitudes A_E and A_M. Our approach was systematically to vary oscillator parameters while maintaining a constant coupling strength. The four system parameters—*a*, *b*, *c*, and *d*—that define *E* and *M* oscillator properties provide a rich repertoire of possible simulations. Varying these parameters in both *E* and *M* can generate positively and negatively correlated changes in τ, α, A_E, and A_M.

We first set up a basic system configuration defined by the nominal parameter set $a = 0.85$, $b = 0.3$, $c = 0.8$, and $d = 0.5$ with moderately weak coupling strength $C_{ME} = -C_{EM} = 0.05$. After recording the values of τ, α, A_M, and A_E, we changed one parameter at a time, while maintaining all the others fixed, and noted the new values of these four quantities. A sample result is that selectively increasing parameter *a* leads to an increase in τ, increases in both A_E and A_M, and a decrease in α. In Table 1, we present a qualitative overview of our results, demonstrating the interrelationships between changes in system parameters and τ, A_E and A_M, and α.

Table 1 shows that amplitudes A_E and A_M, like α, are negatively correlated with parameter *b*. For changes in

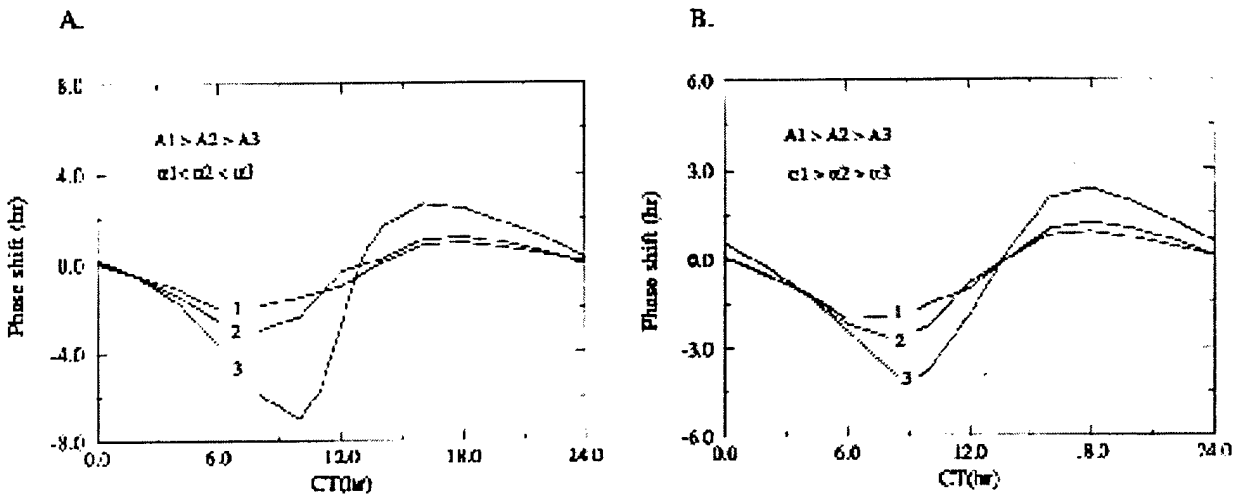

Figure 4. PRCs of coupled oscillators when system parameters are altered, changing amplitudes and phase relationships between E and M oscillators. (A) Series of PRCs generated by decreasing parameter d. These sequential parameter changes (1, 2, and 3) led to increases in PRC amplitude and simultaneous decreases in A_E and A_M, while α increased ($A1 > A2 > A3$; $\alpha1 < \alpha2 < \alpha3$). (B) Series of PRCs generated by increasing parameter b. These parameter changes (1, 2, and 3) led to increases in PRC amplitude and decreases in A_E, A_M, and in α ($A1 > A2 > A3$; $\alpha1 > \alpha2 > \alpha3$). Parameter values in A ($a = 0.85$; $b = 0.3$; $c = 0.8$; $d = 0.5$, 0.3, and 0.1) and in B ($a = 0.85$; $c = 0.8$; $d = 0.5$; $b = 0.3$, 0.5, and 1.0). Coupling strength was constant for all simulations: $C_{ME} = 0.05$; $C_{EM} = -0.05$; pulse intensity = 1.1; pulse duration = 1 h.

parameter d, the quantities have opposite correlations; namely, the amplitudes are positively correlated with d, but for the activity, the correlation is negative. How does the PRC amplitude correlate with b and d? We obtained quantitative measures of PRCs for three decreasing values of parameter d (leading to increasing α and decreasing A_E and A_M). As shown in Fig. 4A, these stepwise decreases in d lead to a progressive increase in PRC amplitude. Similar analysis of the effects of increasing values of b revealed that PRC amplitude increased progressively even with a decreasing α and decreasing A_E and A_M (Fig. 4B). These simulations demonstrate that the PRC amplitude is negatively correlated with oscillator amplitude but is not necessarily positively or negatively correlated with values for α. We generalize this result below.

Simulation Set 2: Interrelationships between Coupling Strength, α, and System Amplitude

In these simulations, we define the total amplitude A_T of the coupled system and show that PRC amplitude is negatively correlated to A_T. Having described the interrelationships of amplitude, activity duration, and PRC amplitude when A_E and A_M covary, we now explore systems showing increasing A_E and decreasing A_M. Such systems are obtained by setting oscillator parameters to a fixed value and then altering only the coupling strength. As in the simulations described above, C_{ME} and C_{EM}, parameters that describe the effect of M on E and of E on M, respectively, always have the same amplitudes but opposite sign, with C_{ME} positive and C_{EM} negative.

We found that decreasing coupling strength always leads to increases in α, that is, to a lengthening of the simulated activity. Stated in other words, decreasing the coupling strength increases the phase difference between E and M. Another consequence of reducing coupling strength is that A_E increases and A_M decreases, a direct consequence of positive C_{ME} and negative C_{EM}. To carry out more quantitative analyses, we defined the total amplitude, A_T, of the coupled system as the sum of the E and M oscillator variable amplitudes:

$$A_T = A_E + A_M = A(R_E) + A(S_E) + A(R_M) + A(S_M).$$

We determined the explicit values assumed by A_E, A_M, and A_T for a wide range of coupling strengths, spanning those we employed to simulate brief and prolonged exposure to DD in wild-type (Fig. 5A) and *tau* mutant hamsters (Fig. 5B). The PRC amplitudes depicted in Fig. 3 can now be understood in light of the relationship between oscillator amplitude and cou-

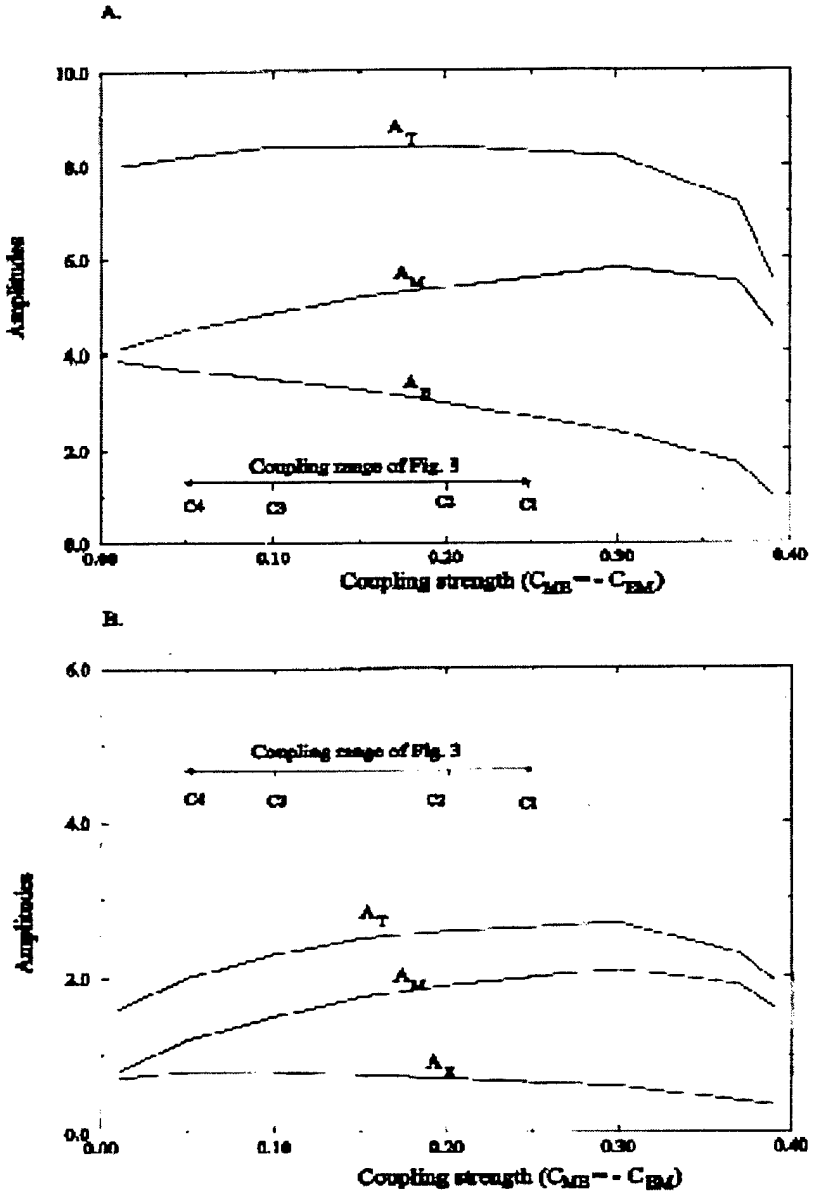

Figure 5. Comparison of amplitude changes in *E* and *M* oscillators with those of the coupled system as coupling strength is decreased. (A) Simulations of the wild-type pacemaker. (B) Simulations of the *tau* mutant pacemaker. The abscissa in each graph is the size of the coupling coefficient—positive for C_{ME} and negative for C_{EM}. The insets describe the values for coupling strength employed for the simulations illustrated in Figure 3. Oscillations damp out, no longer self-sustained, for coupling strengths greater than about 0.39. System parameters were those described in the caption of Figure 3.

pling strength. In simulations of wild-type hamsters (Fig. 5A), we found that as coupling strength decreases, the amplitude of *E* (A_E) increases, the amplitude of *M* (A_M) decreases, and the total amplitude A_T remains nearly constant. Please note again that the PRCs generated for these different coupling strengths (Fig. 3A) are all of nearly equal amplitude. On the other hand, for the *tau* mutant system (Fig. 5B), we found that as coupling strength decreases, the amplitude of *E* increases, the amplitude of *M* decreases, and the total amplitude also decreases. These substantial changes in A_T are reflected in the large changes in PRC amplitude, which are negatively correlated to A_T (cf. Figs. 3B and 5B).

For the wild-type system, A_E and A_M changes have equal absolute values but are of opposite signs. Thus,

their sum, A_T, is nearly unaltered, and consequently PRC amplitudes remain nearly unchanged. On the other hand, in the *tau* mutant system, A_M decreases much more than A_E increases; thus, A_T decreases with exposure to DD. Therefore, the *tau* mutant PRC increases continuously during the decreasing coupling process associated with prolonged exposure to DD. With sufficiently long exposure to DD, the *tau* mutant PRC changes to type 0. The reasons for this transition are described below in the final simulation set.

Simulation Set 3: Transitions between Type 1 and Type 0 PRCs

Correlations between oscillator properties, such as the value of α and system amplitude, usually depend on the choice of the parameter sets. To demonstrate the generality of the behaviors observed in the simulation sets described above, we tested the following proposition: if the phase shift magnitude depends only on A_T, then there must be a threshold value of A_T at which a transition from type 1 to type 0 PRC occurs, independent of α and of the parameter sets used.

We determined PRCs for coupled oscillators defined by a broad range of parameter values (a, b, c, d, C_{EM}, and C_{ME}). Each set of parameters defines a different configuration for the coupled oscillator system and generates a unique pair of values for A_T and α (see Fig. 6). In this illustration, parameter sets that generate type 1 PRCs are represented by open symbols, and those that generate type 0 PRCs are denoted by filled symbols. The plot shows clearly that the zone in which transitions from type 1 (open symbols) to type 0 (filled symbols) occurs is independent of α. Such transitions are confined, moreover, to a very narrow band of values for A_T. Thus, systems characterized by large values of A_T have type 1 PRCs, and those with low total amplitudes have type 0 responses. We also demonstrated that this is true for systems presenting different coupling signs, such as ($+C_{ME}$, $+C_{EM}$) and ($-C_{ME}$, $-C_{EM}$) (data not shown). System configurations displaying equal A_T but very different α values have identical PRCs (data not shown). As is well known, PRC amplitude depends on the intensity of the applied light stimulus light (Winfree 1980); therefore, the zone for type 1 to type 0 transitions is different for every light impulse intensity. In particular, as the intensity of the light pulse is raised, these transitions occur at greater A_T values (data not shown).

Remembering that system configurations are set both by parameters of the unit oscillators and by coupling coefficients, we link systems that have identical component oscillators but with decreasing coupling strengths (arrows, Fig. 6). We also indicate the average range of τ in these linked systems. These data demonstrate that the value of α consistently increases as coupling strength decreases (direction of the arrows) and that A_T can increase or decrease with changes in coupling strength. Thus, for the wild-type pacemaker ($t \cong$ 24 h), decreasing the coupling strength causes only a small decrease in A_T, and these are far from the transition zone. On the other hand, decreasing coupling strength causes larger decreases in A_T of the *tau* mutant hamster system ($t \cong 20$ h), and these values of A_T are near the transition zone. Hence, the *tau* mutant system makes the transition to a type 0 PRC because its amplitude is more sensitive to reductions in coupling strength and because this pacemaker system is adjacent to the type 1 to type 0 transition zone.

Distinct Oscillator View

The system view must be adopted at any coupling strength to analyze interrelationships between τ, α, and amplitudes. As coupling strength is weakened, however, the influence of each component oscillator on the dynamics of the other is weakened, allowing each component to gradually recover its intrinsic properties, even if not completely. In such a weakly coupled system, the properties of the individual oscillators become evident and accessible to analysis. The distinct oscillators view is well suited to explain common phenomena of hamster circadian pacemaker, such as the differential shifts of the beginning and end of the activity bands in response to light pulses.

Light-induced phase shifts of the weakly coupled E and M pacemaker system reflect the combined, intrinsic phase response curves of E and M oscillators (Mori et al., 1994). Two PRCs for a definite light-pulse intensity, PRC_E and PRC_M, generated from simulations of uncoupled wild-type E and M oscillators, are depicted in Fig. 7A. We then applied extremely weak coupling ($C = 0.01$) to this system and generated a third PRC—the system PRC_{EM} (Fig. 7A). In our simulations, we are using two identical E and M oscillators, which are sufficient to describe the following behaviors. In this weakly coupled system, M lagged E by 3.8 h. Hence, in superimposing the three PRCs in Fig. 7A, we shifted the abscissa for PRC_M by +3.8 h. The system

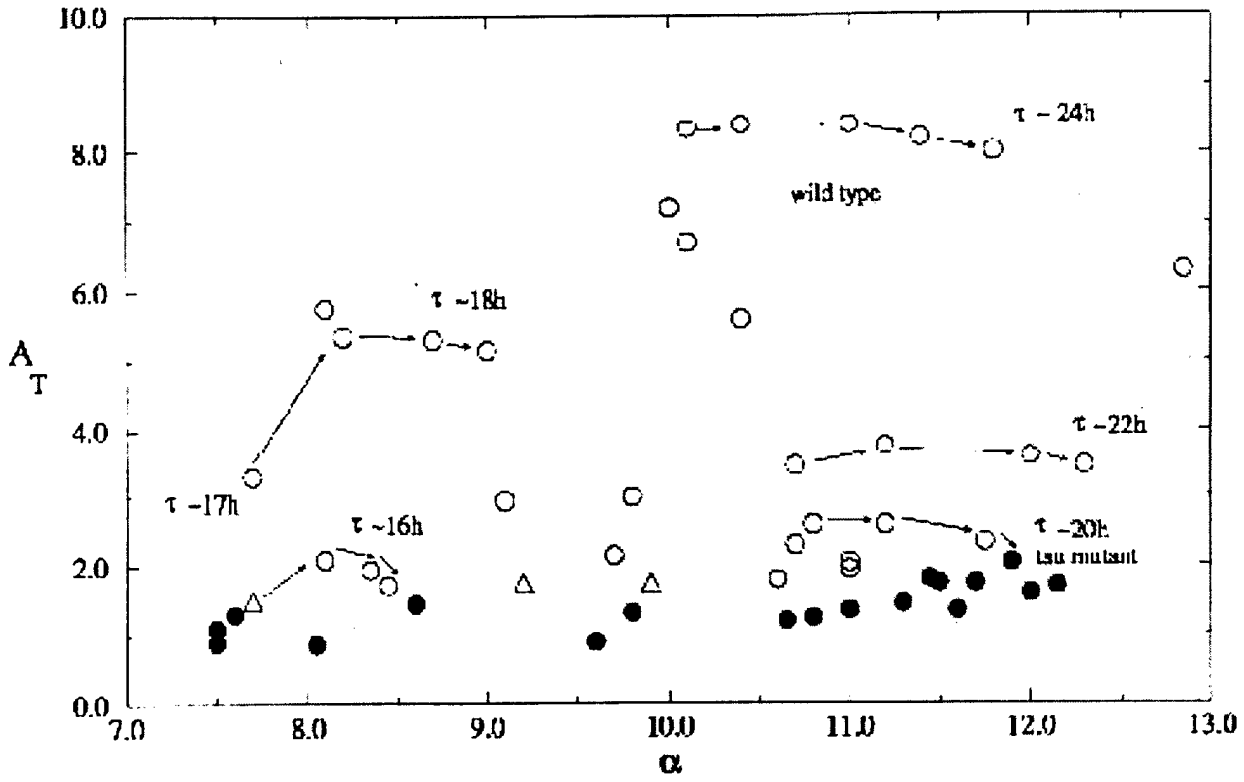

Figure 6. Total amplitude (A_T) and activity length (α) of coupled oscillator configurations generated by a wide range of parameter values. Each point was generated by a different set of values for parameters a, b, c, and d and of the coupling coefficients C_{ME} and C_{EM} and placed on the graph at the system amplitude (A_T) and activity duration (α). Depending on the shape of the system PRC, we represent the configuration as filled circles if the PRC is type 1 or as open circles if the PRC is type 0. The symbol Δ denotes systems that lie exactly on this transition, that is, when the pulse phase-shifts the oscillator to a singularity point. Note that all type 1 systems are in the upper region with high A_T and that the type 0 region is restricted to small values of A_T, independent of the α values. Arrows link systems with identical values of a, b, c, and d but with coupling strength decreasing in the direction of the arrows. As coupling is weakened, α always increases, but A_T can either increase or decrease. Average τ values are indicated for four series of simulations. Note that the *tau* mutant series is at the PRC transition zone, whereas the wild-type series is far above this zone.

PRC_{EM} then lies between those of E and M. We must emphasize that this coupled system PRC estimation from the intrinsic PRCs of the components is only valid for very weak coupling.

By convention, the onset of running wheel activity of hamsters is assigned the phase reference point CT 12. In accordance with this convention, we assigned the phase CT 12 to activity onset in the evening oscillator in our simulations of both coupled and independent oscillators. Thus, CT 12 is the identical reference point for the evening oscillator and for the coupled system. For the specific modeling experiment described here, a response to a light pulse presented at phase Φ for the coupled system is generated by the combined responses of the evening oscillator at phase Φ and of the morning oscillator at phase $\Phi - 3.8$ h. As illustrated in Fig. 7A, there are two system phases, Φ_1 and Φ_2, where there is an intersection of PRC_E and PRC_M. Light pulses presented at these phases cause identical shifts in E and M and hence also in the coupled system. There are two phase ranges, r_1 and r_2, during which PRC_E and PRC_M have the opposite sign; at all other phases, PRC_E and PRC_M have same sign but different amplitudes. As a consequence of weak coupling, there are two primary properties of this pacemaker system.

1. Immediate responses of the E and M oscillators to a pulse of light: the oscillators undergo nearly independent phase shifts (in direction and amplitude). These initial phase shifts correspond to those described by PRC_E and PRC_M (Fig. 7A). If the pulse is given at Φ_1 or Φ_2, both oscillators undergo the same phase shift with no transient change in α. If the pulse falls on ranges r_1 or r_2, one oscillator will advance,

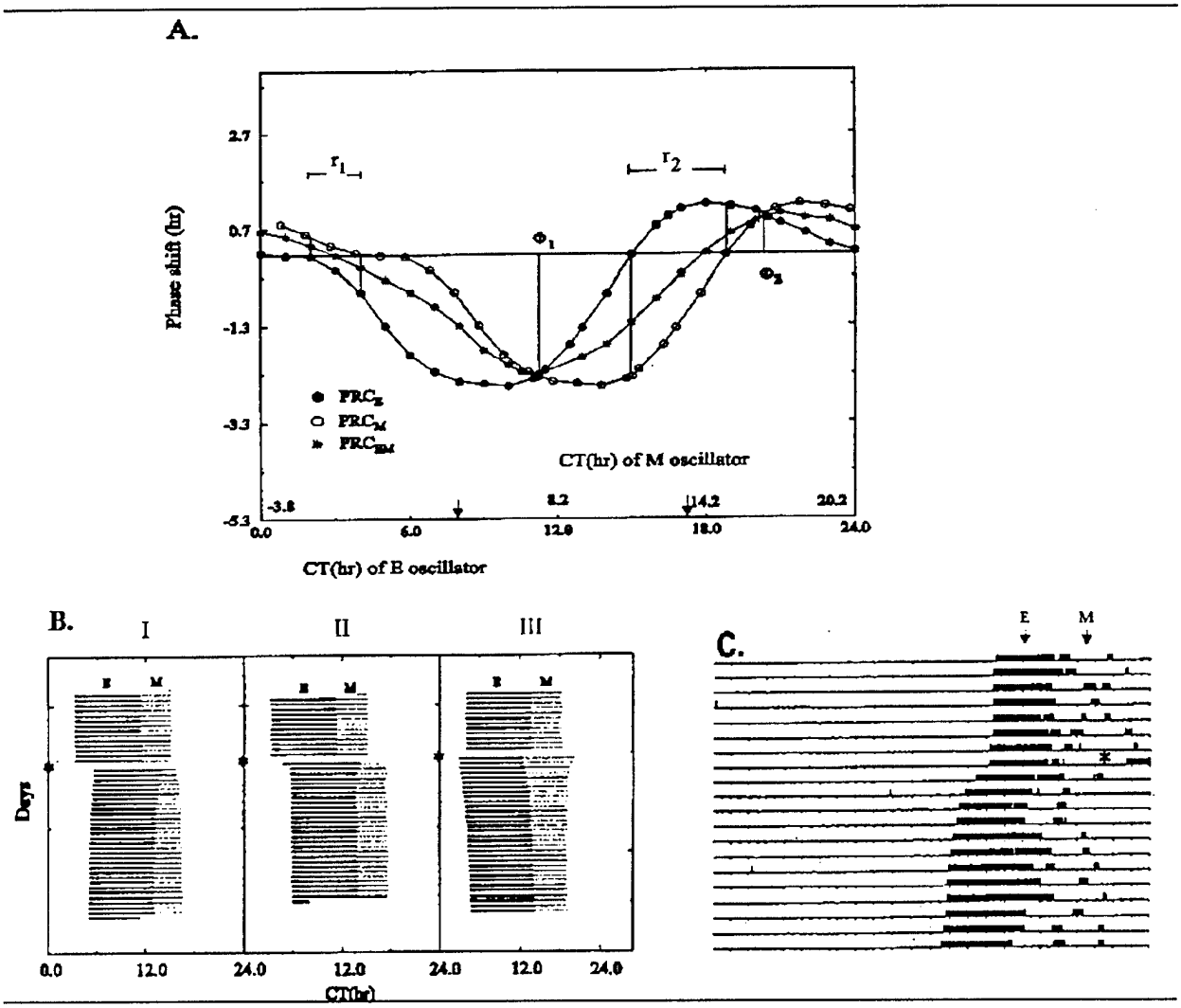

Figure 7. Phase response curves in weakly coupled pacemaker systems: wild type. (A) Computer-generated PRCs for uncoupled independent oscillators, PRC_E (filled circles) and PRC_M (open circles), and for the very weakly coupled system (to simulate prolonged exposure to DD), PRC_{EM} (*). The abscissa for PRC_M is shifted by 3.8 h. The intrinsic PRCs of *E* and *M* intersect at Φ_1 and Φ_2. Phase ranges r_1 and r_2 denote phases for which PRC_E and PRC_M have opposite signs. At all other phases, these curves have the same sign but differing amplitudes. (B) Raster plots showing simulated actograms of hamsters. Light pulses are set by the system on the days indicated by "*" (ordinate) at the following phases: (I) CT 8 (indicated by an arrow in Fig. 7A), (II) CT 11.25 (at Φ_1), and (III) CT 17 (indicated by an arrow in Fig. 7A, during phase range r_1). Because of artifacts generated by the computer program on the "day" that the light pulse is applied, the activity for that day is not shown. At CT 8 (CT relative to the *E* oscillator), both *E* and *M* are immediately delayed, but *E* displays a much larger delay than *M*, causing a transient shortening of α. The *E* oscillator then slowly advances. At Φ_1, both oscillators phase-shift equally (II). At a phase in r_1, *E* initially advances, while *M* initially delays causing a transient increase in α (III). During subsequent cycles, α returns to its previous value and a new, steady-state phase is established. Each line represents 1 day, and the full-scale abscissa is 24 circadian hours. (C) Actogram for hamsters (Shimomura, 1998), showing a transient compression in α due to a pulse given at CT 16, in wild-type hamster. Simulation results were for the wild-type system ($a = 0.85, b = 0.3, c = 0.8, d = 0.5$) with very weak coupling ($C_{ME} = 0.01, C_{EM} = -0.01$). Data were generated by simulating 1-h light pulses with intensity $L = 1.1$ and duration 1.0 h. The PRCs of the intrinsic *E* and *M* oscillators and for the coupled system are type 1.

while the other will be delayed. Finally, if the light pulse occurs at any other phase, both oscillators will phase-shift in the same direction but with differing initial amplitude.

2. Long-term responses of the oscillators: following the initial, transient responses, the phase relationship between *E* and *M* returns to its original value, and the system phase approaches a new steady value. This system shift in phase is described by PRC_{EM} (Fig. 7A). The time interval required for the return to steady state gives rise to transients in phase and α. Depending on the phase of the light pulse, α may be transiently decreased (Fig. 7B-I) or increased (Fig. 7B-III) for several cycles.

Such independent shifts of evening and morning oscillators in response to light pulses were observed during experiments by Elliot and Tamarkin (1994) and Shimomura (1998) (Fig. 7C). Similarly, we found that a light pulse at CT 8 generated a large initial delay in *E* and a smaller delay in *M* (Fig. 7B-I). Subsequently, *E* transiently advances and *M* delays, reestablishing their initial phase relationship. This pattern corresponds to the experimental results obtained for hamsters subjected to light pulses at CT 16 (Fig. 7C). For the animal experiments, however, the behavior was observed in the advance region, rather than in the delay region, of the PRC. To simulate this behavior at CT 16 clearly, we need large advance shifts for *E* and *M*. We were unable to simulate this because our model oscillator (devised for *Drosophila*) displays a PRC with larger delay and smaller advance regions when compared to the PRCs of hamsters. The underlying mechanisms that generate the transient advances and delays are nevertheless identical.

The same relative dynamical independence of *E* and *M* oscillators under weak coupling is even more evident for the *tau* mutant simulations in which both *E* and *M* have type 0 PRCs under standard stimulation (Fig. 8A). Note that PRC_{EM} again lies between PRC_E and PRC_M but not at the midpoint. In this case, PRC_E and PRC_M do not intersect, but there is a phase range, r_3, where they have opposite signs. For this phase range, the activity band controlled by *E* phase-delays, while that controlled by *M* phase-advances; thus, these bands cross (Fig. 8B). Concomitant with these phase shifts, there is a large, transient reduction in α as the activity bands cross. A simulation of the same system with strong coupling is shown in Fig. 8C for comparison. In this case, the activity bands controlled by *E* and *M* shift in the same direction, nearly preserving the phase relationship between them.

The transients in our simulations are conceptually different from those resulting from a master-slave oscillator structure (Pittendrigh, 1967). Double-pulse experiments in *Drosophila* showed that the clock phase-shifts immediately, whereas the overt rhythm shifts slowly. Transients in our simulations correspond to the time interval required by the components within the master clock to reestablish their phase relationship after a light pulse. Elliot and Pittendrigh (abstract from the 1996 SRBR meeting) have shown that in double-pulse experiments with hamsters, the clock takes several cycles to phase-shift. According to our model, although each component *E* and *M* phase-shifts immediately, the whole system takes many cycles to attain its new phase.

Large transients are the hallmark of weakly coupled oscillators. Accordingly, double-pulse experiments on hamsters maintained for different durations in DD can test the hypothesis of weakening the coupling between *E* and *M* under DD. Under this hypothesis, the longer the animal is in DD, the longer the transients within the clock should be.

The distinct oscillators view explains the transient, differential phase shifts of the onset and end of the activity bands in hamsters. These phenomena have strongly supported the two-oscillator model, in which activity onset and end are assumed to be controlled, respectively, by *E* and *M* oscillators.

DISCUSSION

Summary of Results

Physiological experiments provide insights into the properties of specific systems and their responses to perturbations. Modeling studies are valuable because they can provide insights into the mechanistic origins of experimental results. More than that, the many configurations generated during modeling analyses can give insight into the general underlying principles of systems that are independent of any particular configuration. We have presented the results of experiments using computer simulations to analyze the properties that emerge from coupling between two oscillators. Our primary aim was to understand the bases for alterations in the PRC amplitudes observed in wild-type and *tau* mutant hamsters exposed to long-term DD. Our simulation experiments demonstrate the following:

1. A change in a single-system parameter can mimic the reduced period of the *tau* mutation, but a necessary change occurs also in other system properties. In our simulation, the parameter change also decreases the total amplitude of the coupled oscillator system.
2. Incorporating the assumption that the primary effect of exposure to DD is the gradual weakening of the coupling between the *E* and *M* oscillators that comprise the pacemaker led to a large increase in PRC amplitude in our simulated *tau* mutant system but not the wild-type system.
3. Although a direct correlation was shown between α and phase shift magnitude, there is no causal relationship between them. In our simulations, as coupling

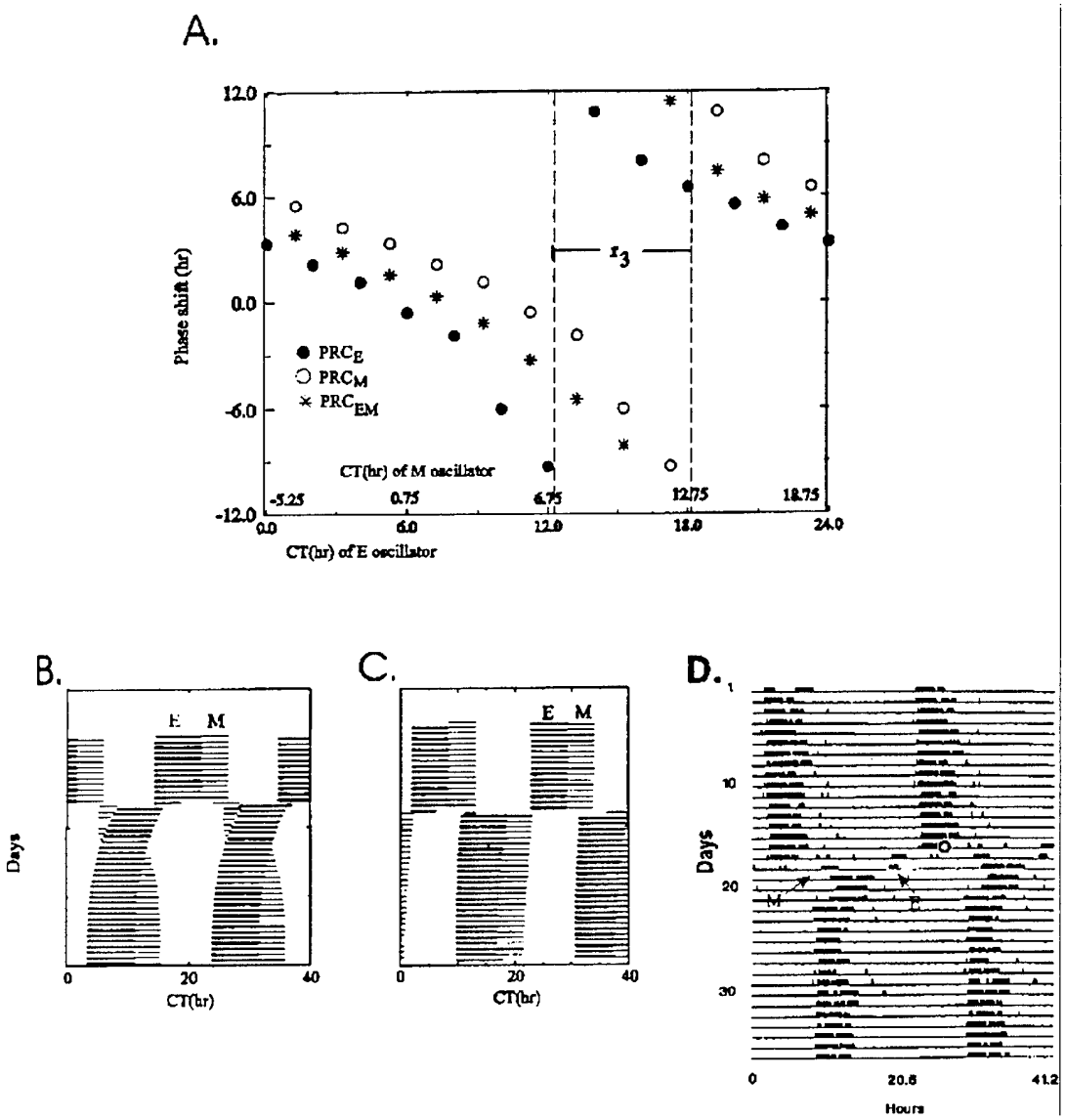

Figure 8. Phase response curves in coupled pacemaker systems: *tau* mutation. (A) Computer-generated PRCs for the uncoupled unit oscillators, PRC_E (filled circles) and PRC_M (open circles), and for the weakly coupled system (to simulate prolonged DD exposure), PRC_{EM} (*). Note that all three PRCs are type 0. In the coupled system, *M* lags *E* by 5.25 h. The PRCs for *E* and *M* never cross, but there is a range of phases, r_3, during which PRC_E and PRC_M have opposite signs. (B) System response to pulse present during range r_3 (CT 17). Note that this stimulus shifts *E* and *M* activity bands strongly in opposite directions so that these bands cross. (C) Phase shifts in strongly coupled systems. Although the simulated light pulse was presented at CT 16.5, during r_3, strong coupling causes *E* and *M* activity bands to shift together as a unit. (D) Comparison with experimental data obtained in a *tau* mutant hamster (from Menaker and Refinetti, 1992), showing the pattern simulated in B. Oscillators parameters for all simulations were set to simulate *tau* mutant values: $a = 0.85$, $b = 0.3$, $c = 1.5$, and $d = 0.5$. The weak coupling in A and B were simulated with $C_{ME} = 0.01$ and $C_{EM} = -0.01$, with light-pulse amplitude = 1.1 and duration = 1 h. In part C, $C_{ME} = 0.38$, and $C_{EM} = -0.38$, with light-pulse amplitude = 1.3 and duration = 1 h.

strength decreases, α increases due to a greater phase difference between *E* and *M*. At the same time, A_T decreases, causing an increase in observable PRC amplitudes.

4. The high sensitivity of the *tau* mutant hamster and low sensitivity of the wild-type hamster to prolonged exposure to DD result from the contrasting location of these systems on the total amplitude scale, shown in Fig. 6; the *tau* mutant system total amplitude lies near the type 1–type 0 transition value, whereas the wild-type system lies far from this value.

Model Assumptions

Several specific assumptions are incorporated into our model. Here we discuss why these assumptions are necessary and how they affect the results of this analysis.

A distinction should be made between the modeling style we use here—namely, the qualitative analysis of formal limit cycle oscillators and the use of differential equations to represent explicitly known cellular processes (Goldbeter, 1996). In the first approach, the state variables (R and S in the case of the Pittendrigh-Pavlidis equation) and parameters (a, b, c, and d) have no physiological meaning. They are simply the components of the formal system of equations. The aim of this formal approach is to explain qualitative features of rhythms in terms of generic limit cycle oscillator properties. In the second approach, state variables and parameters correspond explicitly to concentrations of chemical substances and kinetic constants. They are meant to provide a quantitative view of the limit cycle oscillation generation and dynamic properties of specific, identified circadian pacemakers in cells, plants, or animals. We employed the first approach here because the phenomena we wanted to investigate can be explained in terms of generic limit cycle oscillator properties. In addition, identities of the state variables and of system parameters are unknown in the hamster circadian pacemaker. Either approach seeks to model the system with the smallest set of assumptions to isolate the critical components and to focus on the main features of the phenomena under investigation. Further refinement of the model, with additional assumptions, can be implemented if the initial, simple set of assumptions cannot lead to an explanation of the phenomena. All the assumptions shown below were thus made primarily for the sake of simplicity.

Evening and morning oscillators can be represented by two-dimensional limit cycles. Biochemical processes generating the circadian oscillation probably comprise many more than two proteins and mRNAs whose concentrations are the likely state variables of cellular circadian oscillators (Leloup and Goldbeter, 1998; Sangoram et al., 1998). On the other hand, we are deducing the formal properties of the pacemaker through the direct observation of the output rhythm, which reflects the emergent oscillator properties of the complex biochemical processes. This formal approach allows us to describe the pacemaker by a two-dimensional minimal representation that provides phase and amplitude information of the limit cycle and accounts for both type 1 and type 0 resetting (Winfree, 1980). To simulate the activity controlled by this pacemaker, we define "activity" to occur when the R variable of either evening or morning oscillator is higher than a certain threshold value (2/3 of the amplitude of each variable). Through this choice of simulated activity, α best reflects the phase difference between E and M.

Evening and morning oscillators are identical with identical responses to light pulses. Differences in the properties of evening and morning oscillators in hamsters have been suggested by the differential responses shown by the beginning and end of the activity bands to light pulses (Elliot and Tamarkin, 1994). In Figures 7B and 8B, we showed that these responses could be simulated well by two identical oscillators. Due to the phase difference between them, light hits the oscillators at two different phases, thus evoking distinct phase shifts. Although a more complex system of oscillators might yield similar results, we have shown here that a simple system of weakly coupled, identical oscillators is sufficient to explain these phenomena. We further assumed that the *tau* mutation affected equally the periods of E and M oscillators.

C_{EM} and C_{ME} have identical absolute values and opposite sign. Asymmetry either in the oscillator properties or in the coupling pathways is necessary to generate a coupled system with a stable phase relationship different from 0° or 180°. The choice of two identical oscillators coupled by C_{ME} and C_{EM} with the same absolute values and opposite sign (+,–) was again chosen for simplicity. This asymmetry in the interactions, one excitatory and the other inhibitory, leads to some particular features in the model, such as opposite changes in the amplitudes A_E and A_M when coupling strength is modified (Fig. 5A,B). If the signs of coupling were equal—namely, (+,+) or (–,–)—then both amplitudes would change in the same direction when coupling strength was modified. In all cases, the PRC is negatively correlated to the total amplitude of the system, which is the sum of the amplitudes of E and M oscillators. This is shown unequivocally when the amplitudes of the two oscillators change in opposite directions (Fig. 5A,B).

Aftereffects of a light-dark cycle are simulated by a gradual weakening of the coupling strength. Aftereffects are long-lasting, slowly decaying alterations in pace-

maker properties caused by prior light schedules (Pittendrigh and Daan, 1976a). The phase relationship between *E* and *M* depends on their intrinsic periods and on coupling strength. We assume that the strength of coupling is high in hamsters exposed to LD cycles. When the condition is changed to DD, the coupling strength slowly decays to a low value. Weakening of coupling leads to an increase in the phase difference between *E* and *M*, reflected in the increase of α. We chose not to assume changes in oscillator periods during prolonged exposure to DD, which might also generate changes in α, because many more assumptions would be required. For the purpose of this analysis, our simplest assumption of coupling strength change alone was sufficient to explain the interconnection between τ, α, and PRC amplitude. Our primary result that system amplitude defines the PRC amplitude is independent of the specific model assumptions (Fig. 4).

The Two Views of Coupled Oscillators

Most previous modeling studies on coupled oscillator systems assumed weak coupling and strongly attracting limit cycles, using "phase" oscillators that lack amplitude information (Daan and Berde, 1978; Kawato, 1985; Mori et al., 1994). This is a good approximation when the effects of coupling on the amplitude of the oscillations can be ignored. Amplitude can indeed be neglected in the description of the dynamics of an oscillator if it remains unchanged by experimental manipulations. Amplitude can be ignored, in particular, in the case of strongly attracting limit cycles, which are able to restore the original amplitudes quickly when perturbed by brief external pulses (Ding, 1987) or extremely weakly coupled oscillators (Kuramoto, 1984).

We presented two different views of coupled oscillators, the system view and the distinct oscillators view. The strength of coupling, reflected in these two views, has implications for (1) the degree of the preservation of each oscillator's intrinsic properties, such as free-running period, wave shape, amplitude, and PRC, and (2) the degree to which each oscillator moves independently when submitted to light pulses.

The system view is the more general one, in which the emergent properties of the system as a whole are characterized. Amplitude changes due to strong coupling cannot be neglected because they play primary roles in the behavior of the system. In the limit of weak coupling, the amplitudes as well as other intrinsic properties of the components are assumed unaltered. In this limit, we can see immediate, separate responses of distinct oscillators when a light pulse is given. Moreover, we can estimate the PRC of the system from the intrinsic PRCs of component oscillators and represent these components by phase oscillators.

The pacemaker in hamsters appears to lie at the border between weak and strong coupling, depending on the light regime. On one hand, weak coupling is indicated by the relatively independent phase shifts of the component oscillators to light pulses under prolonged DD. On the other hand, the decrease in A_T after transferring from LD and during long-term exposure to DD (inferred from the increase in PRC amplitude) demonstrates that the strength of the coupling cannot be ignored. No sharp line divides the two views. Either view is useful if the coupling is weak. The choice depends on the specific question that is addressed.

Although the total system amplitude does not change much under prolonged exposure to DD, especially for the wild-type hamster, the amplitude of each component oscillator is changed (Fig. 5A). Thus, care has to be taken when trying to measure the intrinsic properties of *E* and *M*, such as PRC_E, PRC_M, τ_E, and τ_M, during transient dissociation of activity bands and especially when splitting occurs. Although each oscillator appears to be independent under these circumstances, each is in fact altered by the effect of coupling. Therefore, properties measured in the coupled system may not reflect precisely those intrinsic to the oscillators. The stronger the coupling strength, the larger are the modifications of these intrinsic properties.

Pittendrigh et al. (1991) proposed that the photoperiodic time measurement in *Drosophila* would be mediated by its effect on pacemaker amplitude. The two-oscillator system provides a good framework to analyze this proposition since changes in the phase relationship between *E* and *M* clearly occur under different photoperiods. Elliot (personal communication and abstract from the 1999 ICC meeting) has performed PRC experiments in wild-type hamsters exposed to different skeleton photoperiods. Hamsters entrained by short skeleton photoperiods have displayed significant increases in τ, α, and phase shift responses. These findings support the assumption that different light regimes can affect coupling strength (which define the phase relationship between *E* and *M*) and the system total amplitude. System amplitude, in turn, affects the PRC amplitude.

Period Mutant Pacemakers

Because τ and PRC define the phase relationship between the clock and the environmental cycle and because this phase relationship has adaptive value, Daan and Pittendrigh (1976) investigated whether a compensatory mechanism exists between the two. They found indications of an interdependence of τ and PRC shape that provides for a compensation for day-to-day instability of the frequency and the interindividual variation of τ within the rodent species they analyzed. This compensatory mechanism has evolved through natural selection over many generations. Of course, a period mutant organism generated in the laboratory is not adapted to a specific environmental niche, except perhaps by chance. On the other hand, we have shown that physical constraints exist among nonlinear oscillator properties, and these necessarily have to be obeyed by a period mutant. In this sense, if the mutation affects such biochemical parameters as synthesis or degradation rates, it necessarily changes both the period and the pacemaker amplitude, which defines the PRC amplitude. Thus, we have pressure exerted by natural selection for a compensatory mechanism between τ and PRC as well as physical constraints defining the interconnection between τ and PRC. The resulting mechanism reflects a compromise between these two forces; furthermore, this compromise can be modulated by a separate mechanism that changes the sensitivity of the system to light signals.

Model Predictions and Conclusions

The verisimilitude of computer simulations to physiological results can never prove the correctness of a particular model. Nevertheless, the close agreement between our simulations and the available data on hamsters leads us to several proposals. First, we strongly support the proposition—namely, that the pacemaker system in hamsters comprises two oscillators. Second, we propose that the amplitudes of *E* and *M* oscillators in *tau* mutant hamsters are smaller than in the wild-type animals. Third, we propose that weakening of coupling between *E* and *M* during continuous exposure of hamsters to DD is a feasible hypothesis. Finally, we argue that although we used equations devised for the *Drosophila* pacemaker, our analyses do not depend on the specific properties of any system.

APPENDIX

We consider the amplitude of each oscillator as the sum of the amplitudes of both *R* and *S* state variables due to the way the effect of light pulse is incorporated into our equations. In some models, the effect of light is mimicked by an instantaneous change in the level of a specific state variable. In that case, only the amplitude of that variable needs to be considered. In our model, we represent the light effect by a 1-h change in the value of a parameter, affecting all state variables, and consequently we consider all their amplitudes.

The simulation change between wild-type and *tau* mutant hamsters was made by altering a single-system parameter. Wild-type oscillators are represented by the parameter set ($a = 0.85$, $b = 0.3$, $c = 0.8$, $d = 0.5$) and *tau* mutant oscillators by the set ($a = 0.85$, $b = 0.3$, $c = 1.5$, $d = 0.5$). In Figure A1, we show how this parameter change affects τ and the amplitude of the system. Each line in the figure represents the new values assumed by τ and amplitude when one parameter is changed, leaving all the others unaltered. For example, the point indicated by "$d = 1.0$" represents τ and amplitude values of the system when the parameter set is ($a = 0.85$, $b = 0.3$, $c = 0.8$, $d = 1.0$). The wild-type hamster is represented by the right-most star. Similarly, τ and amplitude values of the parameter set defining the *tau* mutant system are indicated by the other star. A change in parameter *b* in the range between 0.5 and 0.7 could also have generated a system with $\tau \cong 20$ h, but the system amplitude would have been too large to provide a type 0 PRC. Two main features shown by this figure are the following: (1) parameter changes that modify τ always modify the amplitude of this nonlinear oscillator, and (2) although most of the PRC experiments on period mutant organisms have shown that mutations that shorten τ also decrease amplitude (since they show increasing PRC amplitude), it is also possible to increase amplitude, as shown by the modifications generated by parameter *d*.

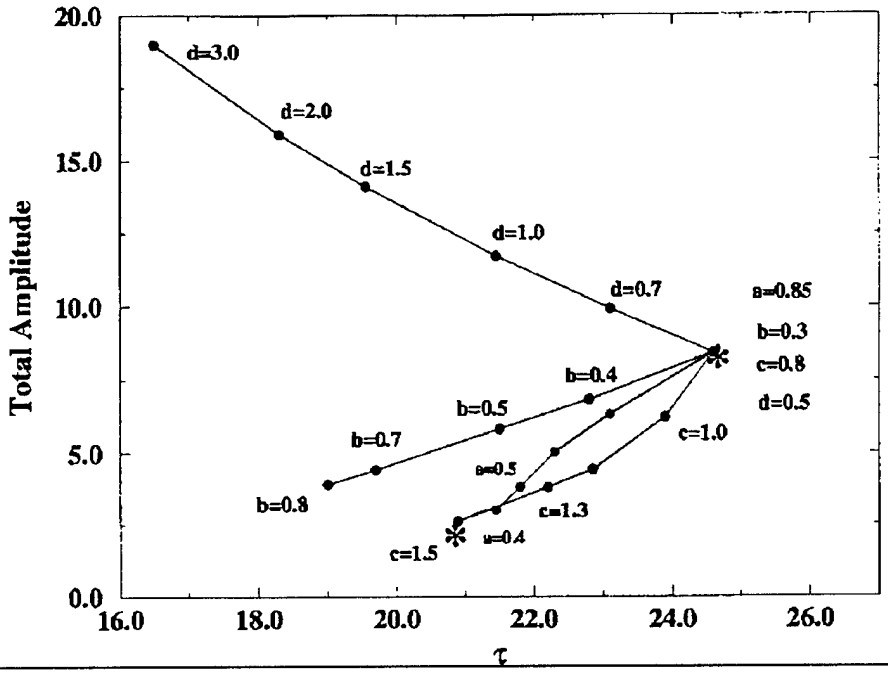

Figure 4 Interdependence of τ and amplitude of coupled Pittendrigh-Pavlidis oscillators. Each parameter set (*a*, *b*, *c*, and *d*) defines a specific τ and amplitude configuration for the system. The wild-type set ($a = 0.85$, $b = 0.3$, $c = 0.8$, $d = 0.5$) generates a system with $\tau \cong 24$ h, indicated by the right-most asterisk. The *tau* mutant set ($a = 0.85$, $b = 0.3$, $c = 1.5$, $d = 0.5$) generates a new configuration with $\tau \cong 20$ h and smaller amplitude, indicated by the left-most asterisk. Each parameter is changed independently; configurations are shown with respective parameter values. $C_{ME} = 0.2$ and $C_{EM} = -0.2$.

ACKNOWLEDGMENTS

We thank Dr. Shin Yamazaki for valuable discussions. We also thank Dr. Mirian Marques for suggestions and careful review of the manuscript and Dr. Erik Herzog for comments at the early stages of the text. G.A.O. was supported by Fundação de Amparo à Pesquisa do Estado de São Paulo (97/13910-0), and W.O.F. was supported by National Science Foundation (IBN 97-23320). The experimental work on *tau* mutant hamsters was supported by grants from the Airforce Office of Scientific Research to M.M. We especially acknowledge support from the NSF Center for Biological Timing.

REFERENCES

Angstadt JD and Friesen WO (1995) Synchronized oscillatory activity in leech neurons induced by calcium channel blockers. J Neurophysiol 66:1858-1873.

Daan S and Berde C (1978) Two coupled oscillators: Simulations of the circadian pacemaker in mammalian activity rhythms. J Theor Biol 70:297-313.

Daan S and Pittendrigh CS (1976) A functional analysis of circadian pacemakers in nocturnal rodents: II. The variability of phase response curves. J Comp Physiol A 106:253-266.

Dharmananda S (1980) *Studies on the Circadian Clock of Neurospora Crassa: Light Induced Phase Shifts*, Ph.D. thesis, University of California, Santa Cruz.

Ding E (1987) Analytical treatment for a driven oscillator with a limit-cycle. Phys Rev A 35 (6): 2669-2683.

Elliot JA and Tamarkin L (1994) Complex circadian regulation of pineal melatonin and wheel-running in Syrian hamsters. J Comp Physiol A 174:469-484.

Friesen WO, Cheek TR, McGuiness OM, Moreton RB, and Berridge MJ (1995) Analysis of calcium fertilization transients in mouse oocytes. Methods in Neuroscience 28:388-423.

Friesen WO and Friesen JA (1994) *NeuroDynamix, a Computer-Based System for Simulating Neuronal Properties*, Oxford University Press, New York.

Goldbeter A (1996) *Biochemical Oscillations and Cellular Rhythms: The Molecular Bases of Periodic and Chaotic Behavior*, Cambridge University Press, Cambridge, UK.

Gorman M, Freeman D, and Zucker I (1998) Photoperiodism in hamsters: Abrupt versus gradual changes in day length differentially entrain M and E circadian oscillators. J Biol Rhythms 12:122-135.

Johnson CH (1992) Phase response curves: What can they tell us about circadian clocks? In *Circadian Clocks from Cell to Human*, Hiroshige T and Honma K, eds, pp 209-249, Hokkaido University Press, Sapporo.

Kawato M (1985) Phase response curves of complex pacemaker. In *Circadian Clocks and Zeitgebers*, Hiroshige T and Honma K, eds, Hokkaido University Press, Sapporo.

Kawato M and Suzuki R (1980) Two coupled neural oscillators as a model of the circadian pacemaker. J Theor Biol 86:547-575.

Konopka RJ (1979) Genetic dissection of the *Drosophila* circadian system. Fed Proc 38:2602-2605.

Kuramoto Y (1984) *Chemical Oscillations, Waves, and Turbulence*, Springer-Verlag, Berlin.

Lakin-Thomas P, Brody S, and Coté G (1991) Amplitude model for the effects of mutations and temperature on period and phase resetting of the *Neurospora* circadian oscillator. J Biol Rhythms 6 (4): 281-297.

Leloup JC and Goldbeter A (1998) A model for circadian rhythms in *Drosophila* incorporating the formation of a complex between the PER and TIM proteins. J Biol Rhythms 13 (1): 70-87.

Menaker M (1992) The use of mutants in the analysis of mammalian circadian organization. Discussions in Neuroscience 8:34-38.

Menaker M and Refinetti R (1992) The *tau* mutation in golden hamsters. In *Molecular Genetics of Biological Rhythms*, Young M, ed, pp 255-270, Marcel Dekker, New York.

Menaker M, Shimomura K, and Ihara NL (1994) The *tau* mutation destabilizes the circadian system of golden hamsters. In *Fifth Sapporo Symposium on Biological Rhythms*, Hokkaido University Press, Sapporo, Japan.

Menaker M and Takahashi J (1995) Genetic analysis of the circadian system of mammals: Properties and prospects. The Neurosciences 7:61-70.

Mori S, Kawato M, and Suzuki R (1994) A quantitative two-oscillator model based on phase-shift data of hamsters. MBE 85-88 (in Japanese).

Pavlidis T (1967) A mathematical model for the light affected system in the *Drosophila* eclosion rhythm. Bull Math Biophys 29:291-310.

Pittendrigh CS (1967) Circadian systems: I. The driving oscillation and its assay in *Drosophila pseudoobscura*. Proc Natl Acad Sci USA 58 (4): 1762-1767.

Pittendrigh CS and Daan S (1976a) A functional analysis of circadian pacemakers in nocturnal rodents: I. The stability and lability of spontaneous frequency. J Comp Physiol A 106:223-252.

Pittendrigh CS and Daan S (1976b) A functional analysis of circadian pacemakers in nocturnal rodents: V. Pacemaker structure: A clock for all seasons. J Comp Physiol A 106:333-355.

Pittendrigh CS, Kyner WT, and Takamura T (1991) The amplitude of circadian oscillations: Temperature dependence, latitudinal clines, and the photoperiodic time measurement. J Biol Rhythms 6 (4): 299-313.

Sangoram A, Saez L, Antoch M, Gekakis M, Staknis D, Whiteley A, Fruechte E, Vitaterna M, Shimomura K, King D, Young M, Weitz C, and Takahashi J (1998) Mammalian circadian autoregulatory loop: A timeless ortholog and mPer1 interact and negatively regulate Clock-BMAL1-induced transcription. Neuron 21:1101-1113.

Saunders DS, Gillanders SW, and Lewis RD (1994) Light-pulse phase response curves for the locomotor activity rhythm in period mutants of *Drosophila melanogaster*. J Insect Physiol 40 (11): 957-968.

Shimomura K and Menaker M (1994) Light-induced phase shifts in *tau* mutant hamsters. J Biol Rhythms 9 (2): 97-110.

Shimomura K (1998) *Analysis of Circadian System of Tau Mutant Hamster*, Ph.D. thesis, University of Virginia.

Takahashi JS, DeCoursey PJ, Bauman L, and Menaker M (1984) Spectral sensitivity of a novel photoreceptive system mediating entrainment of mammalian circadian rhythms. Nature 308:186-188.

Winfree AT (1980) *The Geometry of Biological Time*, Springer-Verlag, New York.